The Role of the Cytoskeleton in the Modulation of the Connexin36 Nexus in N2a Cells

Cherie Brown

A Thesis Submitted to the Faculty of Graduate Studies in Partial Fulfillment of the Requirement for the Degree of Master of Science

Graduate Program in Biology
York University
Toronto, Ontario

August 2015

ABSTRACT

We tested the hypothesis that the interaction of Cx36 with the cytoskeleton is necessary to achieve synaptic plasticity in neurons. In living cells, BioID and FRAP technology was used to demonstrate binding of Cx36 to actin and tubulin. Wild-type and mutant proteins, together with pharmacological blockers or TAT peptides were used to characterize the interaction. Major results of this study are that rCx36 interacts primarily with the neuronal βIII-tubulin isoform to regulate the trafficking and aggregation of connexons at the GJP. Amino acid Lys279 in the CTB domain is critical for this interaction. A potential actin-binding site in the CLB domain of rCx36 was identified, with actin mainly serving as an anchor to stabilize connexons. During a simulation of plasticity *in vitro*, GJPs became more stable; we attribute this to interactions with the cytoskeleton and associating proteins. We conclude that cytoskeletal-dependent interaction is required to modulate the strength of Cx36 synapses.

For my family.

For the few I can call my best friends.

For my sources of inspiration, in loving memory of

Uncle Ray,

Grandma,

Aunty Dorett

ACKNOWLEDGEMENTS

A whole-hearted thank you extended to:

Dr. Georg Zoidl for everything from your playful teasing, to your encouragement and support. You have been so influential in my development over the last two years and I cannot find the right words to thank you enough! Thank you for believing in me, especially in times when I have doubted myself. I could not have found a better supervisor to work with, to grow with, and to eat cake with. Many thanks for your advice, direction and thesis editing skills. I could not have done this without you –"I literally would have passed out". Thank you.

Dr. Logan Donaldson for your advice on everything including science and life! I truly appreciate you as my committee member and lab neighbor. Thank you for being calm and rational during the times you had to deal with me stressing/freaking out. You are always good at lending an ear, not to mention sending me some awesome music which always puts me in a great mood. I cannot thank you enough for reading this thesis and promoting my development as a scientist. Thank you.

Christiane Zoidl for managing the best lab -- I appreciate everything you do for us! Thank you for teaching and refining all the skills I need as a scientist. I can only imagine where I was and how far I've come thanks to you. Thank you for being a great teacher and friend. It's always fun talking with you at lunch, your company is very much enjoyed! Thank you.

Sarah and Stefan Kurtenbach for helping to train me and jump start my research project. You both were such a lovely couple, and always willing to help me when I was too nervous to do things on my own. Thank you for helping me to break out of my shell, and taking the time to make sure I understood key concepts. A special thanks to Sarah for being my daily online shopping buddy and teaching me that eating chocolate in the morning is okay. You both are definitely missed. Thank you. Thank you.

Paige Whyte-Fagundes, where do I start? Oh wait I know… 'Started from the bottom, now we here!' Whaaaaaaat! Whaaaaaaat is cupine!? I don't think Dr. Zoidl could have picked a better match than us two. You are literally my twin, my pumpkin pie, and my best friend. I had no idea I would find a friend like you, let alone someone with a sense of style as great as my own. Thank you for laughing with me, crying with me, freaking out with me and working out with me. I can't imagine how I would get through this degree without you. You keep me in check, up-to-speed, but most of all you motivate me to work harder. Above all things I admire your drive and dedication to everything you love. Thank you.

Ryan Siu my partner in crime. If you ever read Paige's dedication above then it's only appropriate that I say 'Started from the bottom, now my whole team --- here.' I cannot wait to start PhD with you and learn more Mandarin! Thank you so much for your help in the lab, on the computer and for all you have taught me. You are one of the sweetest boys I have ever met and I am so lucky to be working on connexin36 so closely with you. 谢谢.

Mom, Dad, Chris, Michael and Family. Thank you for encouraging my dream since I was old enough to talk. If it wasn't for your encouragement and prayers, I would not have made it this far. Thank you for supporting me so that I would have the tools and the state of mind to overcome my battles and succeed in all I do. You have been the most influential people in my life. My hopes are that I have made you proud. Thank you.

A special tribute to my Uncle Ray, I want you and everyone to know that you first inspired me to pursue research. To my grandmother, thank you for nurturing me as a young girl and through my toughest of times. Last but not least, to my Aunty Dorett. I miss you so very much. I know you would be so proud of how far I've come. I keep you in my thoughts every day, with every dress and pair of heels I wear. You're model niece is almost you're doctor niece! Thank you. May you all Rest in Paradise.

To the few I can truly call my best friends. You've heard me cry and seen my cry. You've listen to me during my lows and celebrated with me during my best. Thank you for being my living de-stressors and diaries. I could not have had a better circle of people surrounding me during this journey. Your support means so much! Just know that if you are reading this, you are one of those people. Thank you.

Matthew 19:26

TABLE OF CONTENTS

LIST OF ABBREVIATIONS

A or Ala	Alanine
A.dest.	distilled water
aa	amino acid
AMPA(R)	α-Amino-3-hydroxy-5-methyl-4-isoxazolepropionic acid (receptor)
APS	Ammonium persulfate
ATP	Adenosine-5'-triphosphate
bp	base pairs
CaM	Calmodulin
CaMKII	Ca^{2+}/calmodulin-dependent kinase II
CIAP	Calf Intestine Alkaline Phosphatase
CL	Cytoplasmic Loop
CLB	Cytoplasmic Loop Binding domain
CLP	Cytoplasmic Loop Phosphorylation domain
Col	Colchicine
CPP	Cell-penetrating peptide
CT	Carboxy Terminus
CTB	Carboxy Terminus Binding domain
CTF	Corrected total fluorescence
CTP	Carboxy Terminus Phosphorylation domain
Ctrl or CTRL	Control
CNS	Central Nervous System
CytoD	Cytochalasin D
Cx	Connexin
DNA	Deoxyribonucleic Acid
E.coli	*Escherichia coli*
EGFP	Enhanced Green Fluorescent Protein
EtBr	Ethidium Bromide
EYFP	Enhanced Yellow Fluorescent Protein
FBS	Fetal Bovine Serum
FRAP	Fluorescence Recovery After Photobleaching
G or Gly	Glycine
GJD2	Gap Juntion Delta 2
GJP	Gap Junction Plaque
H or His	Histidine
I or Ile	Iso-Leucine
Inx	Innexin
Iono	Ionomycin
K or Lys	Lysine
kDa	kilo-Dalton
KO	Knock-Out
L or Leu	Leucine
LTD	Long Term Depression
LTP	Long Term Potentiation
m	mouse

MAP	Microtubule Associating Proteins
MT	Microtubules
N2a	Neuroblastoma 2a or Neuro2a
NEA	Non-Essential Amino acids
NMDA(R)	N-methyl-D-aspartate (receptor)
ns	not significant
O.D.	Optical Density
P or Pro	Proline
Pacl	Paclitaxel
Panx	Pannexin
PBS	Phosphate Buffered Saline
PBS-T	Phosphate Buffered Saline with 0.1% Tween20
PCR	Polymerase Chain Reaction
R or Arg	Arginine
r	rat
ROI	Region of interest
RT	room temperature
S or Ser	Serine
SCN	Suprachiasmatic Nucleus
SDS-PAGE	Sodium Dodecyl Sulphate Polyacrylamine Gel Electrophoresis
TAT	Transactivator of transcription
TEMED	tetranethylethylendiamine
V or Val	Valine
W or Trp	Tryptophan
WT	Wild-type
zf	zebrafish

LIST OF TABLES

LIST OF FIGURES

1 INTRODUCTION

Communication between neurons and glia is vital for the optimization and regulation of brain function in higher organisms. Synapses, the dynamic regions that allow for this cross-talk between neurons, are recognized as protein-dense areas that operate under two main modalities of synaptic transmission referred to as chemical and/or electrical synapses. At the chemical synapse, the release of a neurotransmitter from the presynaptic neuron is detected by receptors of the postsynaptic membrane, allowing for the unidirectional transfer of information and appropriate cellular response. Alternatively, under the electrical transmission model, signaling molecules may be transmitted bi-directionally between directly adjacent neurons through channels known as gap junctions. Although both models of synaptic transmission are often targets for debate, chemical and electrical synapses are now known to co-exist (Pereda, 2014). Evidence to support properties and distributions of these two modalities at mixed synapses is still emerging, yet, allows for the opportunity to identify commonalities in machinery and operation between the two.

Synaptic plasticity, the ability of neuronal synapses to strengthen or weaken over time, serves as the fundamental basis underlying learning, memory and behavior. As such, delineating the mechanism(s) governing synaptic plasticity will drive our fundamental understanding of the regulatory means by which these processes operate. Although research aimed at defining the cellular signaling cascade(s) involved in learning, memory and behavior have largely focused on chemical synapses, emerging evidence supports a significant role of electrical synapses to the contribution of neuronal plasticity.

1.1 THE GAP JUNCTION FAMILY OF PROTEINS

Electrical synapses, the gap junctions of the nervous system, are specialized channels that allow for bidirectional intercellular communication between neurons. Permeability of gap junctions has been attributed to the channel size as the large hydrophobic pore has an estimated diameter of 1.2 nm (M. V. L. Bennett & Zukin, 2004). As such, these structures provide an efficient means of signaling between directly adjacent neurons, allowing for the passage of small molecules (up to 1 kDa) including, but not limited to, second messengers, glucose, ATP, cations and anions (Jabeen & Thirumalai, 2013; Söhl, Maxeiner, & Willecke, 2005). In addition to its involvement in signal transduction pathways and maintenance of cellular homeostasis, gap junctions have also been shown to be involved in the synchronous activity of cardiomyocytes and neuronal networks in electrically excitable cells; consequently, the term "electrical synapse" was derived accordingly (M. V. L. Bennett & Zukin, 2004; Paul, 1995; Revel & Karnovsky, 1967; Weidmann, 1952). Gap junctions differ from most membrane channels in that they exist between two opposing cells rather than function as single membrane units. As determined by electron microscopy, a narrow gap (2-4 nm) exists between the adjoining cells, which in turn lead its designated title as a "gap junction" (Revel & Karnovsky, 1967). Typically, gap junctions are localized in the plasma membrane as aggregates referred to as gap junction plaques, consisting of up to thousands of intercellular channels (Simon & Goodenough, 1998). Although the opening of gap junction channels typically requires a sizeable amount of aggregates (in the order of hundreds) as a prerequisite, in established gap junction plaques meeting this requirement, approximately 1 in 10 remain open at a time (Bukauskas et al., 2000).

From their initial discovery in the crayfish giant motor synapse, gap junctions were later demonstrated to exist in most vertebrate and invertebrate tissues with the exception of spermatozoa, erythrocytes, thrombocytes and adult skeletal muscle cells (Dermietzel & Spray, 1993; Söhl, Odermatt, Maxeiner, Degen, & Willecke, 2004). However, evolutionary divergence of gap junctions lead to the identification of protein families which have similar morphological and physiological properties; in chordates, gap junctions are formed by the family of proteins termed connexins (Cx), whereas the innexin (Inx) protein family is found exclusively in invertebrates. A third family of proteins, termed pannexins (Panx), are found in both invertebrates and chordates, however classification of pannexins as belonging to the gap junction family of proteins is currently

debated (Baranova et al., 2004; Bruzzone, White, & Paul, 1996; Kumar & Gilula, 1996; Pauline Phelan, Bacon, Davies, Stebbings, & Todman, 1998). Although innexins and pannexins will not be described here in detail, it is important to note that all serve to allow for cellular permeability through the formation of hemichannels (Scemes, Spray, & Meda, 2009).

1.1.1 Connexins

The first gap junction proteins were discovered in mouse hepatocytes in 1974 and were classified as belonging to the connexin family. Initially, the names connexin A and B were proposed to coincide with the two identified components of differing molecular weight generated by bulk preparation (Goodenough, 1974). Since then, a number of connexin isoforms have been found. To date, there are 20 known connexin genes in murines, 21 in the human genome and 37 genes in zebrafish; of the 37 genes expressed in zebrafish, 23 are related to 16 mammalian connexins and 14 connexins are completely unique (Eastman, Chen, Falk, Mendelson, & Iovine, 2006; Cruciani and Mikalsen, 2007). Likewise, between the mouse and human genome, 19 genes are orthologs (Söhl & Willecke, 2003). Connexins are identified as the gap junctions of chordates, a phylum consisting of organisms characterized by the presence of a notochord, dorsal neural tube, pharyngeal slits, post-anal tail and an endostyle at some stage throughout development (Holland, 2005).

In vertebrates, each gap junction channel is composed of two docking connexin hemichannels (also referred to as connexons), both formed by six connexin proteins **(Figure 1A)** (M. Bennett, 1977; Kumar & Gilula, 1996). Connexins are tetraspan membrane proteins with two extracellular loops sharing three conserved cysteine residues crucial for docking; both the N-terminal and C-terminal domains are located intracellularly **(Figure 1B)**. Connexons can arrange either homotypically or heterotypically, whereby the composition of the gap junction channel will affect both its localization and conductance properties (voltage dependence, open probability, permeability and gating kinetics), allowing for regulatory variety; mediation of connexon-connexon interaction is achieved through both extracellular loops (M. V. L. Bennett & Zukin, 2004; Cao et al., 1998; Weber, Chang, Spaeth, Nitsche, & Nicholson, 2004). Alternatively, functional hemichannels have been described both *in vivo* and *in vitro* allowing for the passage of molecules between the

intracellular and extracellular space (Kamermans et al., 2001; Paul, Ebihara, Takemoto, Swenson, & Goodenough, 1991). As connexins are named according to their molecular weight (in kDa), variation between connexin isoforms are mainly due to residual differences in the cytoplasmic loop and carboxyl-terminal (Söhl et al., 2005). Additionally, connexins are classified into the alpha (α-), beta (β-), gamma (γ-), delta (δ) or epsilon (ε-) subclasses depending on gene sequence similarity (Söhl & Willecke, 2003).

Properly folded connexin proteins are transferred from the endoplasmic reticulum to the Golgi apparatus prior to transport to the plasma membrane; in the case of Cx26, trafficking to the plasma membrane occurs in a Golgi-independent manner. Connexon assembly may occur in an isoform-specific manner (Sarma, Wang, & Koval, 2002) with evidence supporting assembly at the ER (Ahmad, Diez, George, & Evans, 1999; Falk, Buehler, Kumar, & Gilula, 1997), *trans*-Golgi network (Musil & Goodenough, 1993) or ER-Golgi intermediate (Diez, Ahmad, & Evans, 1999). Upon exiting the *trans*-Golgi network, connexin hemichannels are packaged into vesicles for delivery to the cell surface. Fusion of the vesicles with the phospholipid bilayer allows hemichannels to diffuse laterally and dock with the connexons of the adjacent cell, with the aid of N- and E-cadherins, to form gap junctions (Jongen et al., 1991; Lauf et al., 2002a; Meyer, Laird, Revel, & Johnson, 1992; Thomas et al., 2005; Wei, Francis, Xu, & Lo, 2005). Although upon docking a delay in functional activity typically occurs until coalescence into gap junction plaques, recent studies have confirmed that gap junction channels could acquire an active state in the absence of microscopically identifiable plaques (Essenfelder et al., 2004). Clustering of gap junctions is a continual dynamic event as the turnover rate of connexin-forming gap junctions is typically 1-5 h although longer turnover rates have been recorded (JC Hervé, Derangeon, Bahbouhi, Mesnil, & Sarrouilhe, 2007).

Among the connexin genes identified in mammalian cells, more than half are expressed in the nervous system. As such, several connexins have been identified as significant contributors to neuronal activity such as Cx29 (GJE1), Cx30 (GJB6), Cx30.2 (GJC3), Cx31.1 (GJB5), Cx32 (GJB1), Cx36 (GJD2), Cx43 (GJA1), Cx45 (GJC1), Cx47 (GJC2), and Cx50 (GJA8) (Pereda et al., 2013; Shimizu & Stopfer, 2013; Söhl et al., 2005). Of the known neuronal gap junction proteins,

connexin 36 (Cx36), the focus of this study, was the first isoform to be described as expressed in mammalian neurons (Condorelli et al., 1998).

1.1.2 Innexins

In 1998, analysis of *Drosophila melanogaster* and *Caenorhabditis elegans* lead to the identification of the connexin homologues termed invertebrate connexin analogs, abbreviated as innexins or Inx (P Phelan et al., 1998). In similar topology to connexins, innexins are tetraspan membrane proteins with two extracellular loops sharing two conserved cysteine residues, except in the case of Inx4 containing 3 conserved cysteine residues; both the amino- and carboxy- termini are located intracellularly. Despite being morphologically and physiologically similar to connexins, they lack sequence homology; instead, innexins share sequence identity with another family of proteins named pannexins. However, it is worth noting that the conservation of the cysteine residues of the extracellular loops and surrounding amino acids in innexins may reflect an evolutionary functional significance related to the docking of the hemichannels in a similar fashion to connexins (Bauer et al., 2005).

1.1.3 Pannexins

Pannexins, first discovered in 2000 by Panchina *et al*., were originally described in the human genome as a second family of gap junction proteins (Panchina et al., 2000). Since their discovery, much debate has been focused on the characterization of pannexins where some reports support its classification as a gap junction protein (Sahu, Sukumaran, & Bera, 2014) and others reject it (Sosinsky et al., 2011). Structurally, pannexins are similar to connexins with four transmembrane domains, two extracellular loops sharing two conserved cysteine residues, and both the N- and C-terminal located intracellularly; however, no sequence homology exists between connexins and pannexins. A unique feature of the pannexin family of proteins, not seen in connexins, is the asparagine glycosylation sites located on the extracellular loops responsible for the regulation of localization and intermixing of isoforms (Penuela, Bhalla, Nag, & Laird, 2009), which some argue would prevent formation of gap junctions between cells (Boassa et al., 2007; Boassa, Qiu, Dahl, & Sosinsky, 2008; Penuela et al., 2007). As it is understood to date, pannexins predominantly exist

as single membrane units, allowing for the passage of molecules in and out of cells. As such, these channels are particularly sensitive to changes in the extracellular environment.

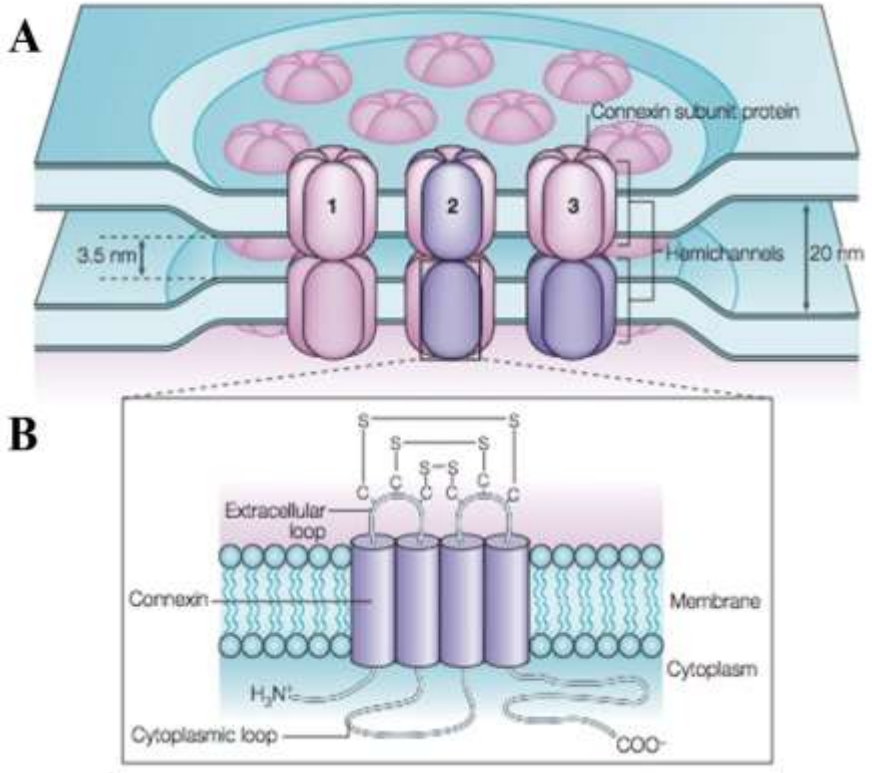

Figure 1| Topology of gap junctions and connexin subunits.
(A) Two docking hemichannels of adjacent cells form a gap junction channel that is either homotypic (1-2) or heterotypic (2-3). Each hemichannel is comprised of 6 connexin proteins to form a channel that allows for the passage of small molecules 1 kDa. (**B)** Connexins are tetraspanning membrane proteins that share three conserved cysteine residues on both extracellular loops crucial for docking. Variations between connexins are mainly due to alterations in the carboxyl terminal and/or cytoplasmic loop. *Modified from Sohl et al., 2005*

1.2 CONNEXIN36, THE MAJOR NEURONAL CONNEXIN OF THE CNS

1.2.1 The Cx36 Gene and Protein

Connexin 36 (Cx36), encoded by the GJD2 gene, is a 321 amino acid protein identified as a major component of neural gap junctions in the CNS. The connexin gene is highly conserved, displaying 98% sequence identity between the rat, mouse and human genomes and 80% identity to its fish ortholog connexin 35 (Belousov & Fontes, 2013). Based on the gene structure, Cx36 is classified as belonging to the gamma (γ) sub-family, determined by the presence of an intron located within its coding region (Abascal & Zardoya, 2012; Condorelli et al., 1998; O'Brien, Al-Ubaidi, & Ripps, 1996; Söhl, Degen, Teubner, & Willecke, 1998). Typically, Cx36 is found between dendro-dendritic and dendro-somatic contacts but has also been described at axon terminals (Hamzei-sichani et al., 2007). In reference to the domains of Cx36, notations were derived from Alev et al. (2008) based on the findings that both the cytoplasmic loop (CL) and cytoplasmic terminal (CT) housed CaMKII binding and phosphorylation sites (Alev et al., 2008). As such, the phosphorylation sites (CLP and CTP) and more specifically the binding domains (CLB and CTB) are referenced in the abbreviated form throughout this thesis.

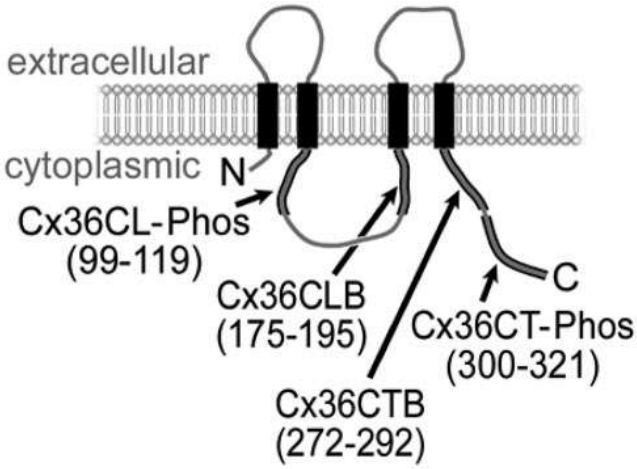

Figure 2| Relevant Connexin36 domains and corresponding nomenclature.
An outline of the Cx36 binding domain nomenclature and corresponding amino acids referenced throughout this thesis. Nomenclature was derived from Alev et al. (2008) based on the binding and phosphorylation sites of CaMKII. *Taken from Alev et al., 2008*

1.2.2 Electrophysiological Properties of Cx36

Relative to other connexin isoforms, Cx36 is described as having one of the lowest voltage sensitivities (half-inactivation voltage ±75 mV) and single channel conductance (10-15 pS). With a low unitary conductance, it is inferred that Cx36 allows for in-depth precision of electrical coupling through the regulation of the number of channels present in the gap junction plaque. Further, during neuronal activity and development, low voltage sensitivity prevents uncoupling in cells that have acquired a high resting potential (Srinivas et al., 1999). Regulation of Cx36 channel gating open probability has been attributed to intracellular [Mg^{2+}] in an ATP-dependent manner (Palacios-Prado et al., 2012) and pH (González-Nieto et al., 2008). Experimental efforts aimed at defining the molecular mechanism of connexin gating have proposed a dual mechanism of "slow V_j-gating" inferring the involvement of the N-terminal domain and "fast V_j-gating" involving the cytoplasmic domain in a connexin-specific manner (Anumonwo et al., 2001; Beyer, Lipkind, Kyle, & Berthoud, 2012; González, Gómez-Hernández, & Barrio, 2007; Moreno et al., 2002; Verselis, Ginter, & Bargiello, 1994). Studies on Cx36 channel gating properties have supported this two-tier mechanism for opening and closing probabilities in a pH-dependent manner (González-Nieto et al., 2008). Additionally, coupling of Cx36 gap junction channels has been shown to be mediated by calcium where high intracellular [Ca^{2+}] results in the uncoupling of junctions (Baux, Simonneau, Tauc, & Segundo, 1978; Rao, Barnes, & McNaughton, 1987).

1.2.3 Implications of Cx36 in Learning, Memory, Behavior and Vision

In the mammalian brain, Cx36 is expressed in a variety of regions including the cerebral cortex and hippocampus (Condorelli et al., 1998). Both the hippocampus and neocortical regions are dictated by the highly regulated synchronous oscillations of neuronal networks and in turn correlate to cognitive and sensory function, attention and memory formation (Buzsaki, Horvath, Urioste, Hetke, & Wise, 1992; Cape, Manns, Alonso, Beaudet, & Jones, 2000; Csicsvari, Hirase, Czurko, Mamiya, & Buzsaki, 1999). The hippocampus, a member of the limbic system, is most notably known for its role in the integration of short-term and long-term memory in addition to spatial navigation. In Cx36 deficient (Cx36 -/-) mice, dendro-dendritic coupling in the hippocampus was nearly abolished. At the behavioral level, Cx36 -/- mice showed impairments in object recognition, displaying an inability to distinguish between new and old objects after short

delays of 15 and 45 minutes. Additionally, the lack of Cx36 expression in mice also resulted in an impairment in short-term spatial memory as determined by their poor performance on a rewarded alternation T-maze task in comparison to wild-type mice (Allen, Fuchs, Jaschonek, Bannerman, & Monyer, 2011; Frisch et al., 2005). Again, the significance of Cx36 at the hippocampus must be elaborated as this demonstrates that Cx36 -/- mice display impairments in learning and memory formation. Furthermore, Cx36 knockout (KO) significantly disrupted synchrony of interneurons in both the cortex and hippocampus, without any signs of a compensatory mechanism (Deans, Gibson, Sellitto, Connors, & Paul, 2001; Hormuzdi et al., 2001; Hormuzdi, Filippov, Mitropoulou, Monyer, & Bruzzone, 2004).

The retina, a light-sensitive tissue, is organized into distinct layers of neuronal cells, interconnected by synapses and responsible for receiving and transmitting visual input through the optic nerve to the brain for visual processing. In the mouse retina, Cx36 is expressed between AII amacrine cells, OFF cone bipolar cells, as well as light sensitive photoreceptors located at the base of the retina. Photoreceptors are divided into two classes known as cones and rods and are responsible for photopic and scoptic vision, respectively. Although Cx36 -/- mice show the normal cellular organization of the retina, coupling between AII amacrine cells and bipolar cells was disrupted. Further, rod-mediated transmission to ganglion cells was impaired in Cx36 KO mice indicating that Cx36 is critical for rod signal propagation and essential for night vision (Deans, Volgyi, Goodenough, Bloomfield, & Paul, 2002; Feigenspan et al., 2004; Güldenagel et al., 2001).

Knockout of Cx36 typically displays a broad range of consequences. In addition to the aforementioned, KO studies have also revealed deficits in the circadian activity, regulated by the suprachiasmatic nucleus (SCN), and behavior as KO mice showed an increase in locomotion and running speed, a reduction in object exploration and displayed more anxiety-like behavior (Long, Jutras, Connors, & Burwell, 2005; Zlomuzica et al., 2012). It is also interesting to acknowledge that in the rat hippocampus and cortex, Cx36 KO resulted in the impairment of long-term potentiation (LTP) of chemical synapses suggesting a close relationship between electrical and chemical synapses (Postma et al., 2011; Wang & Belousov, 2011).

1.3 SYNAPTIC PLASTICITY

As just demonstrated, communication between neurons is critical for optimization and regulation of brain function and synapses allow for this cross-talk between cells. Although the focus of this thesis is on electrical synapses, chemical synapses will be addressed briefly given its developing relationship with electrical synapses and significance in neuronal plasticity. As previously mentioned, synaptic plasticity can involve either the strengthening or weakening of synapses, and in the case of chemical synapses, this is referred to as long-term potentiation (LTP) or long-term depression (LTD) respectively.

1.3.1 LTP of Chemical Synapses

In the chemical synapse model, a release of neurotransmitters from the presynaptic terminal into the synaptic cleft takes place upon a depolarization event. Embedded in the post-synaptic membrane is a combination of both metabotropic and ionotropic receptors capable of binding to neurotransmitters and evoking a response through a defined series of signaling cascades **(Figure 3)** (Sheng, Sabatini, & Sudhof, 2012). Two ionotropic receptors of importance in long-term potentiation (LTP), the underlying basis of the learning, memory and behavior cascades, are N-methyl-D-aspartate receptor (NMDAR) and α-Amino-3-hydroxy-5-methyl-4-isoxazolepropionic acid receptor (AMPAR).

Previous studies have shown that upon release of glutamate from the vesicles of the presynaptic neuron, the post-synaptic membrane responds by depolarizing. In combination with the binding of glutamate to NMDAR, this depolarization event in turn activates NMDARs, relieving the Mg^{2+} blockade. Activated NMDARs allow for the influx of Ca^{2+}, triggering a number of signaling cascades critical for LTP to occur (Collingridge, Isaac, & Wang, 2004; Traynelis et al., 2010). Most notably, the rapid rise in intracellular calcium levels activates Ca^{2+}/calmodulin-dependent kinase II (CaMKII), a protein kinase responsible for phosphorylating a number of targets, upon the initial binding of CaM (Fukunaga, Stoppini, Miyamoto, & Muller, 1993). AMPA receptors, a target of CaMKII, increases in activity levels, trafficking and insertion into the postsynaptic membrane in response to phosphorylation. This is of significance since an abundance of receptors is a crucial regulator in synaptic strength (Sheng & Hoogenraad, 2007). Phosphorylation of

NMDAR by CaMKII increases calcium conductance, thus providing an additional means for controlling synaptic strength **(Figure 4)** (Derkach, Oh, Guire, & Soderling, 2007; Sanhueza et al., 2011; Zhou et al., 2007). These two events are critical for the LTP of chemical synapses and has been widely accepted as a cellular mechanism contributing to learning and memory formation.

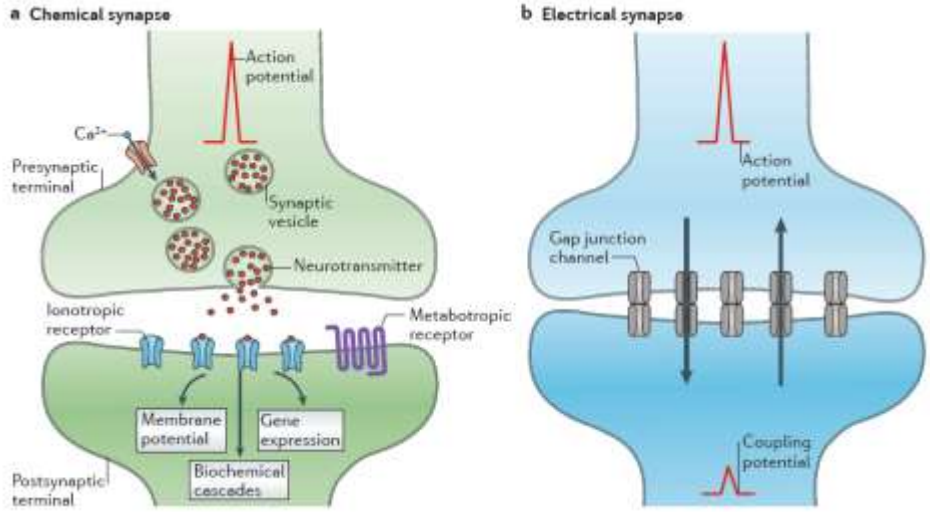

Figure 3| Chemical and electrical models of synaptic transmission.
(A) Upon a depolarizing event, such as an action potential, voltage-gated calcium channels open and allow for an influx of Ca^{2+} ions, mobilizing synaptic vesicles to release neurotransmitters into the synaptic cleft. Neurotransmitters bind to ionotropic receptors on the post-synaptic membrane and in turn influence various signaling cascades. (**B)** Electrically coupled cells allow for the bi-directional transmission of small molecules and ions. *Taken from Pereda, 2014*

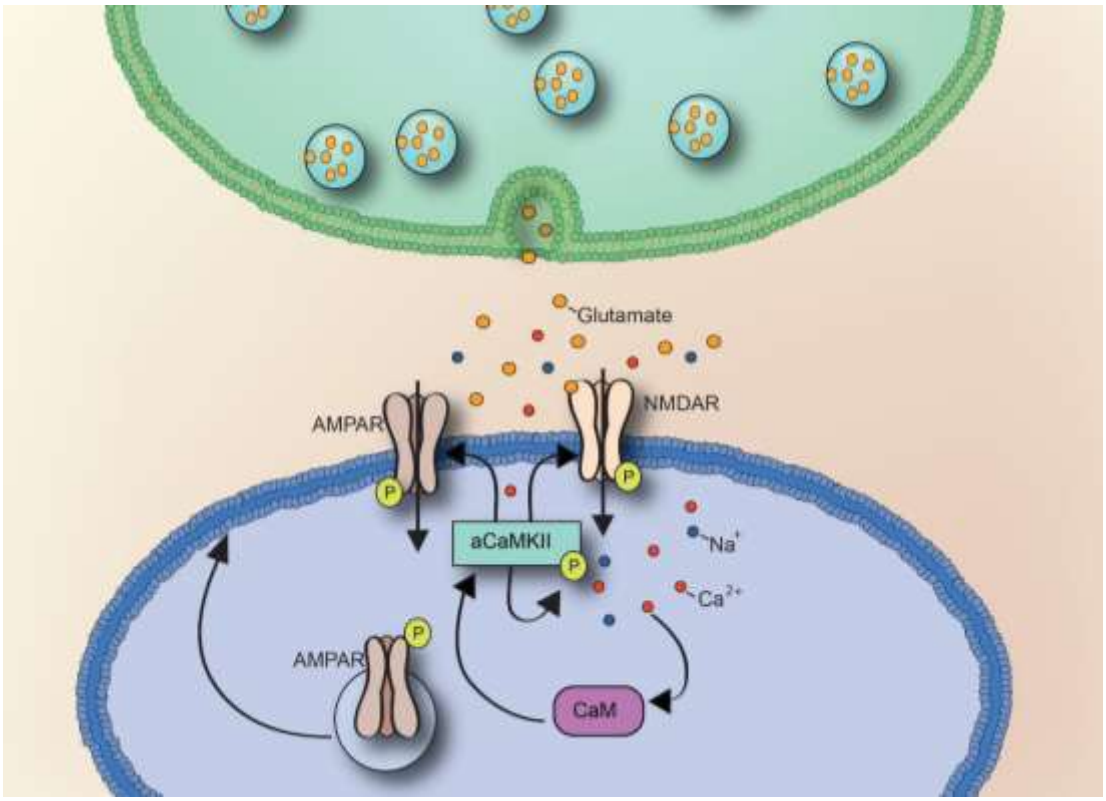

Figure 4| NMDAR-dependent long-term potentiation of chemical synapses.
NMDARs are activated by the binding of glutamate and depolarization of the post-synaptic membrane. Upon activation, calcium levels increase transiently, activating CaM which in turn activates CaMKII. Phosphorylation of AMPAR and NMDAR strengthens synapses by increasing activity, trafficking and insertion of AMPAR in addition to enhancing the calcium conductance of NMDAR.

1.3.2 Role of Gap Junctions in Synaptic Plasticity

Although addressed briefly here, synaptic plasticity (both LTP and LTD) is a well-described phenomenon at chemical synapses in various regions of the brain. However, since there is an emerging role for the contribution of electrical synapses to plasticity, Cx36, the fore-runner of neuronal gap junctions in the CNS, has been of particular interest. The LTP-like "run-up" phenomenon, in which gap junctional conductance increases 10-fold, has been exclusively described at the Cx36 nexus and was found to be CaMKII dependent (Alev et al., 2008; Del Corsso, Iglesias, Zoidl, Dermietzel, & Spray, 2012). This phenomenon resembles phosphorylation of NMDAR by CaMKII to further evoke an influx of Ca^{2+}, a critical mediating step in LTP-based plasticity at chemical synapses, as previously outlined. This demonstrates that electrical and chemical synapses share a common molecular mechanism in modulating synaptic strength.

However, additional critical mediators involved in Cx36-specific plasticity of neurons still remains unclear. Since the transport of Cx36 to the plasma membrane is a prerequisite, we hypothesized that the dynamic delivery, insertion and removal of Cx36 from the Nexus could be a critical mediating step in run-up plasticity. As such, our investigations were directed towards interactions of Cx36 with cytoskeletal proteins.

1.4 THE DYNAMIC CYTOSKELETON

In eukaryotes, the neuronal cytoskeleton is a dynamic network comprised of microtubules, actin microfilaments, and neurofilaments/intermediate filaments **(Figure 5)**. The primary roles of the cytoskeleton include the maintenance of cell structure as well as intracellular trafficking of organelles and cargo-carrying vesicles. As the focus of this thesis is on the interaction of Cx36 with tubulin and actin, the basic unit of microtubules and microfilaments respectively, neurofilaments will not be described.

1.4.1 Actin

Actin in its free monomeric form is a 42 kDa globular protein (G-actin) with 375 amino acids which can polymerizes to form microfilaments (F-actin), a major contributor to the cytoskeleton, particularly at synapses **(Figure 5A)**. Of the three classes of actin that have been described: α, β and γ, the latter two are involved in F-actin polymerization. Both G-actin and F-actin are essential for maintaining cell morphology, motility, cell signaling as well as the trafficking of organelles and vesicles in a highly dynamic manner. Typically, actin localizes beneath the plasma membrane where, in addition to structural support, interacts with membrane proteins to facilitate receptor mobility and anchoring with the aid of scaffolding proteins (Dillon & Goda, 2005). Interestingly, it was recently determined that the actin cytoskeleton and associating proteins, being functionally linked to synaptic receptors, are also necessary entities in memory formation (Bi et al., 2010; Fischer, Sananbenesi, Schrick, Spiess, & Radulovic, 2004; Hou et al., 2009; Nelson, Witty, Williamson, & Daniel, 2012; Young et al., 2014).

1.4.2 Microtubules

Microtubules (MTs) are hollow tubes approximately 25 nm in diameter formed by protofilaments of α-, β-tubulin heterodimers running lengthwise **(Figure 5B)**. During assembly, tubulin heterodimers are typically added to the plus (+) end, giving MTs a characteristic structural polarity, while the minus (-) end grows at a slower rate. Microtubule assembly is a GTP-dependent process with GTP being hydrolyzed to GDP forming a stable GDP-tubulin cap at the plus end. A number of proteins have been shown to interact with MTs including microtubule-associated proteins (MAPs), responsible for stabilizing MTs, and motor proteins dynein and kinesin, essential for microtubule-dependent trafficking (Wade, 2009).

The α- and β-tubulin monomers responsible for the configuration of microtubules are approximately 55kDa in size with 450 amino acids residues. Throughout evolution, the tubulin monomers have remained highly conserved, showing approximately 60% sequence identity across species; between the tubulin monomers themselves, there is approximately 40% conservation (Wade, 2009). Multiple copies of the tubulin gene exist in both human and murine genomes, leading to the identification of 19 isoforms in humans (10 of which belong to the alpha isotype and 9 to the beta) and 16 in murines (8 alpha and 8 beta) (Saillour et al., 2014).

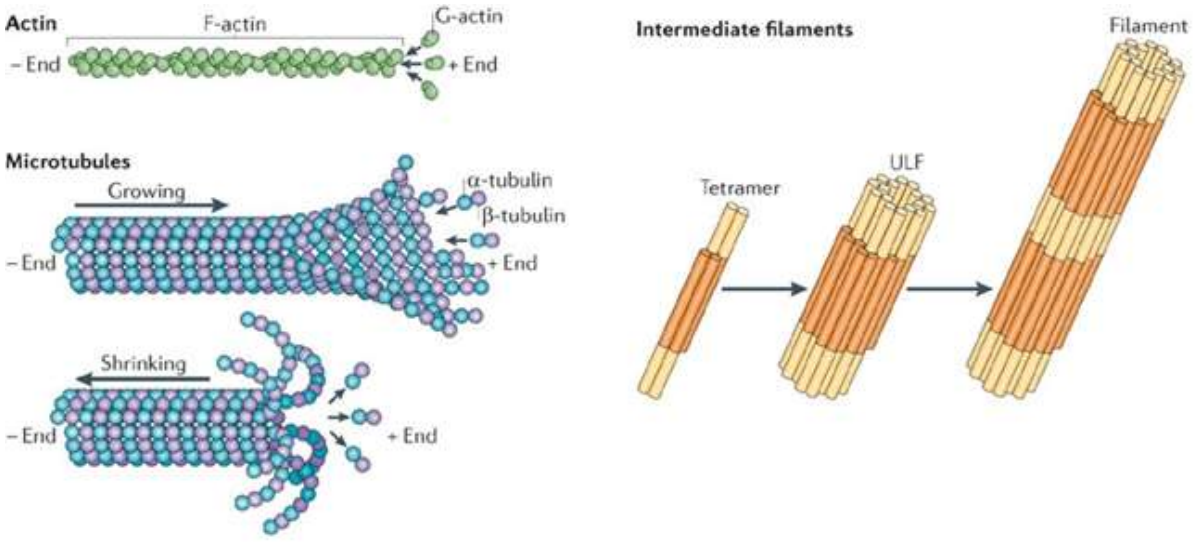

Figure 5| Cytoskeletal components and structure.
(A) Actin microfilaments, about 7 nm in diameter, is formed by the polymerization of G-actin at the plus (+) end to form F-actin. **(B)** Microtubules are hollow tubes, approximately 25 nm in diameter formed by α and β tubulin heterodimers. Polymerization of microtubules occurs typically at the plus (+) end in a GTP-dependent manner. **(C)** Intermediate filaments, the third component of the cytoskeleton. *Adapted from Mostowy & Cossart, 2012.*

1.4.3 The Role of the Cytoskeleton in Gap Junction Trafficking

All three filaments of the cytoskeleton differ in a variety of ways including assembly dynamics, polarity and associating motor proteins (Fletcher & Mullins, 2010). However, most notably is the organization within neuronal cells. Actin, for example, can be found within the dendritic and axon terminal ends, highly concentrated at protein-rich areas known as post-synaptic densities (PSD) beneath the synapse (Hotulainen & Hoogenraad, 2010; Sheng & Hoogenraad, 2007). In contrast, microtubules are excluded from end terminals and are considered to be restricted to the dendritic spine (Gu, Firestein, & Zheng, 2008). As such, transport of proteins destined for the synapse often requires a combination of tubulin- and actin-dependent transport.

Interactions between gap junctions and actin have only recently been described in the past few years. Although Cx30 has been shown to interact directly with actin, more often gap junctions require adaptor proteins to facilitate indirect contact, such in the case of Cx43 (Bhalla-Gehi, Penuela, Churko, Shao, & Laird, 2010; Butkevich et al., 2004; Qu, Gardner, & Schrijver, 2009). Early reports have indicated that actin is involved in turnover and endocytosis of gap junctions,

typically in cells expressing connexins known to interact indirectly with actin, through an invagination event into the cytoplasm prior to degradation (Watanabe, Washioka, & Tonosaki, 1988). However, a more recent study on connexin 30 (Cx30) proposed that actin is likely involved in the anchoring of connexons and short distance transport rather than in the facilitation of internalization (Qu et al., 2009).

As previously mentioned, evidence suggests that upon leaving the Golgi apparatus, connexon are assembled and transported in vesicles to the plasma membrane. In support to this, it was found that Cx43 binds to both α- and β-tubulin with equal affinity and trafficking to the membrane was indeed dependent on microtubules (Giepmans, Verlaan, & Moolenaar, 2001; Giepmans, Verlaan, Hengeveld, et al., 2001). Although microtubules facilitate transport of connexons to the membrane thus improving efficiency, it is thought that under some circumstances, MTs may not be essential (Laird, 2010); however, in the case of Cx43, MT-dependent trafficking is indeed necessary (Giepmans, Verlaan, Hengeveld, et al., 2001; Lauf et al., 2002a). Recent reports have indicated that upon binding of tubulin, the tubulin binding site and surrounding region (encompassing amino acids K243-D259) adopts a helical structure to promote interaction. Furthermore, mediation of interaction between tubulin and Cx43 is achieved by phosphorylation where phosphorylation of Tyr247 by v-Src prevents association with tubulin. The microtubule binding region, located within the C-terminal (CT) domain of Cx43, is enriched in the basic amino acids lysine (K), glycine (G), proline (P), valine (V) and arginine (R), and our group was the first to identify that this region is conserved in the Cx36 CT domain **(Figure 6)**. Furthermore, our research group has successfully confirmed the interaction between rCx36 and tubulin *in vitro* and has provided evidence indicating that tubulin inhibition abolishes the run-up phenomenon previously described. As such, interactions with tubulin were of particular interest in this thesis.

```
                235        243
Cx43 Rat        ---GVKDRVKGR--------------------------------
Cx36 Human      GWRKIKLAVRGAQAKRKSIYEIRNKDLPRVSVPNFGRTQSSDSAYV
Cx36 Rat        GWRKIKLAVRGAQAKRKSVYEIRNKDLPRVSVPNFGRTQSSDSAYV
Cx36 Chicken    GWRKIKMAVRGVQAKRKSIYEIRNKDLPRMSMPNFGRTQSSDSAYV
Cx35 Zebrafish  GWRKIKTAVRGVQARRKSIYEIRNKDLPRMSMPNFGRTQSSDSAYV
              276   :*  *:*                                 321
```

Figure 6| Sequence alignment of the rCx43 tubulin binding region to Cx36 and respective fish ortholog. Protein sequence alignment of the rCx43 binding domain against Cx36 across specifies including the fish ortholog Cx35. Sequence alignment revealed that the tubulin binding domain is conserved in Cx36, encompassing amino acid residues spanning from 279-287.

1.5 RESEARCH DESIGN

Since synaptic plasticity is critically dependent on the trafficking of the protein in/out of the Nexus, determining possible binding partners influencing trafficking of Cx36 is an area of significant interest. As such, the objective of this research study was to confirm the interaction of tubulin and actin with rCx36 in living cells. We hypothesized that both tubulin and actin, the basic unit of microtubules and microfilaments respectively interact with Cx36 to facilitate its transport to the plasma membrane. To approach this research question, the *in vivo* techniques BioID and fluorescence recovery after photobleaching (FRAP) were employed in combination with recombinant DNA technology like Site-Directed Mutagenesis, and pharmacological blocking in a cell culture model.

1.5.1 BioID

Bio-ID is a newly developed technique used for proximity-dependent identification of interacting proteins in eukaryotic cells. Originally, this technique was employed to study the interacting candidates of human lamin A (LaA), an intermediate filament protein associated with the inner nuclear membrane, a component of the nuclear envelope. In this technique, the promiscuous *E. coli* protein ligase BirA is utilized for its ability to attach biotin to close proximity proteins. Since biotinylation is a rare modification, the BirA used in this methodology, denoted as BirA*, has been mutated to achieve is promiscuous characteristic and to prevent self-association. By this technique,

the authors were able to successfully identify a novel interacting partner of LaA (Roux, Kim, Raida, & Burke, 2012).

For the purpose of this thesis, we utilized rCx36-BirA* wild-type and mutant variant (directed against the CLB and CTB) fusion proteins to achieve biotinylation of proximal proteins. The biotin-labeled protein fraction was then enriched using a highly selective purification procedure by Dynabeads MyOne Streptavidin. Upon protein denaturation, biotin affinity capture is achieved using magnetic streptavidin-conjugated beads to which biotin has high affinity. By this technique, interacting proteins can be segregated, screened and identified via mass spectrometry and/or western blot.

1.5.2 Fluorescence Recovery After Photobleaching

Fluorescence recovery after photobleaching (FRAP) is a microscopy based tool that allows for the *in vivo* measurement of molecular dynamics such as diffusion, active transport and protein binding. In this technique, a fluorescently labeled region of interest (ROI) can be selected and bleached with a high power laser. The recovery rate of the ROI is dependent on diffusion and potential interacting partners. Two parameters of particular interest for this thesis were: firstly, the mobile fraction (%), the amount of bleached molecules that are replaced by unbleached molecules and secondly, the half-time of recovery ($t_{½}$), which measures the time taken for fluorescence intensity to recover to half of its initial value (Carisey, Stroud, Tsang, & Ballestrem, 2011).

Previous studies on connexin 43 (Cx43) have successfully confirmed the *in vivo* dynamics of Cx43-YFP gap junction plaques in HeLa cells using FRAP, concluding that Cx43 delivery at the lateral ends of the gap junction plaque occurs in a rapid manner (Shaw et al., 2007). For the purpose of this study, we have selected several ROIs for analysis: (1) intracellular space (2) first lateral end of Cx36 gap junction plaque (3) center of the Cx36 gap junction plaque (4) second lateral end of the Cx36 gap junction plaque (5) plasma membrane and (6) extracellular space **(Figure 7)**. Since it has been reported that connexons are delivered to the plasma membrane singly or in small groups moving laterally to replenish the gap junction plaques from the outer margins, with older channels removed from the center of the plaque (Lauf et al., 2002a), we were interested in determining if

the dynamics of the rCx36 gap junction plaque were consistent with literature and if cytoskeletal dependency existed.

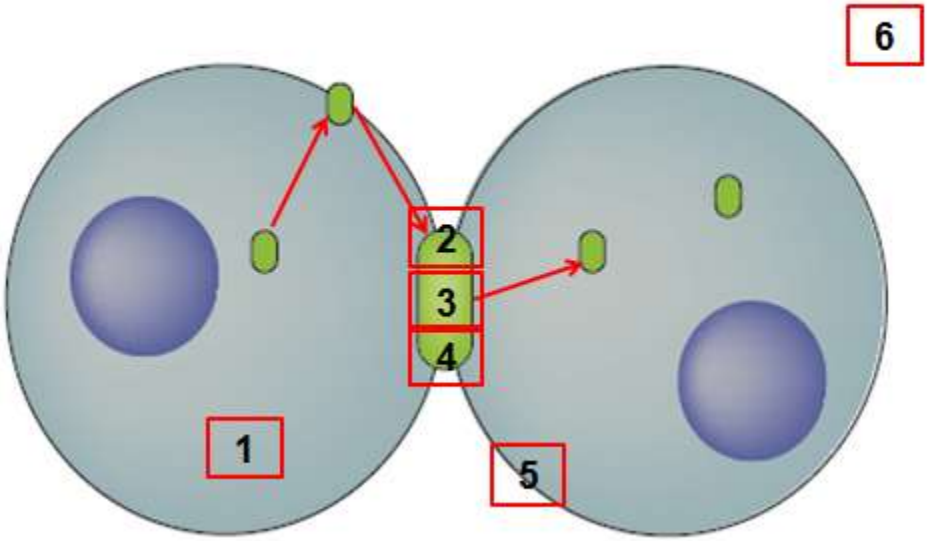

Figure 7| Regions of Interest (ROIs) for FRAP Experiments.
Several ROIs were selected for analysis: (1) intracellular space (2) first lateral end of Cx36 gap junction plaque (3) center of the Cx36 gap junction plaque (4) second lateral end of the Cx36 gap junction plaque (5) plasma membrane and (6) extracellular space. Analyzing the GJP in sub-sections allowed for transport dynamics to be determined under wild-type, mutant or pharmacologically altered conditions. The intracellular space and the plasma membrane were used as comparative references; results were normalized against the extracellular space to improve the signal-to-noise ratio.

1.5.3 Pharmacological Blocking and Site-Directed Mutagenesis

In addition to our wild-type analyzes, we selected a number of reagents directed against tubulin. In particular, both colchicine, which inhibits the polymerization of microtubules, and paclitaxel, which prevents the disassembly of MTs were utilized. Cytochalasin D was selected for is ability to prevent the polymerization of actin filaments. Peptide blocking the tubulin binding site of wild-type rCx36 was achieved with a TAT peptide. The TAT peptide, utilized for its cell-penetrating ability, is derived from the transactivator of transcription (TAT) of human immunodeficiency virus. Cell penetrating peptides (CPPs) have been used to overcome the lipophilic barrier of the cellular membranes to deliver molecules variable in size inside the cell for their specified biological actions.

Here, this property is used to carry the C-terminal binding (CTB) sequence and respective controls into Neuro2a cells as a competitor for tubulin binding. Both, pharmacological and peptide approaches provide a means to test the hypothesis that Cx36 transport to the plasma membrane is tubulin- and/or actin-dependent.

Additionally, mutants carrying deletions in regions of the Cx36 protein considered critical for transport and plasticity were used in this analysis. Site-directed mutagenesis allowed for the generation of point mutations in both the CT binding (CTB) regions and CL binding (CLB) region to determine critical residues in the tubulin- and actin-mediated transport respectively **(Figure 8)**.

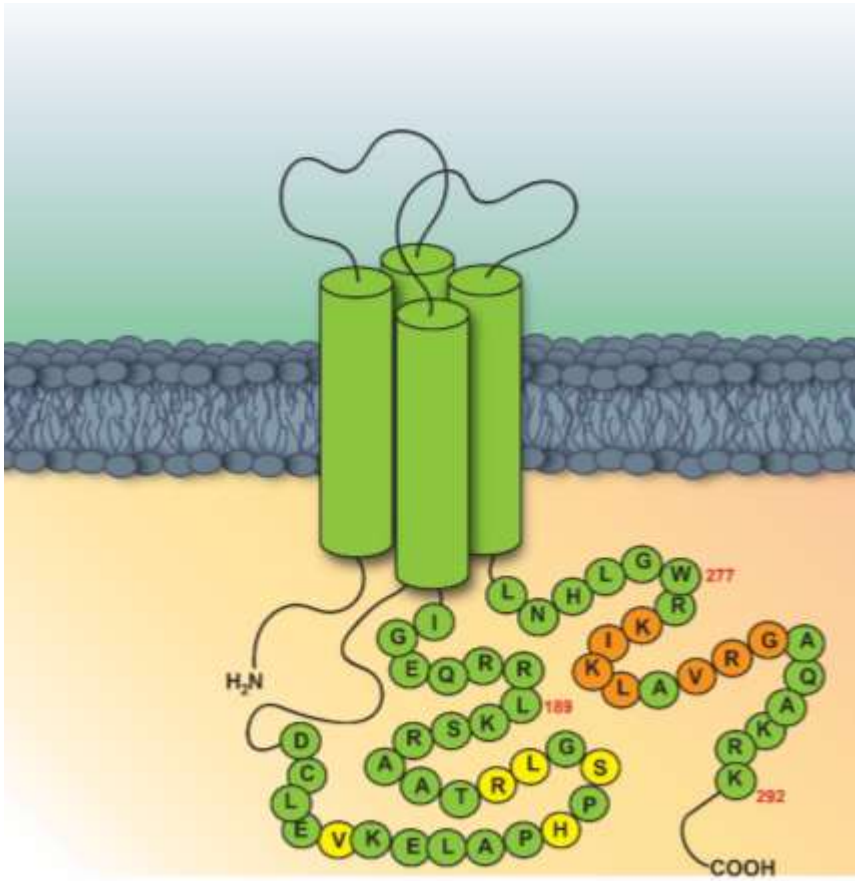

Figure 8| Illustration of Mutants Generated by Site-Directed Mutagenesis.
Highlight of the site-directed mutagenesis targeted residues generated in the CLB (in yellow) and CTB (in orange) region of rCx36. These were specifically directed against the hypothesized actin and tubulin binding domain respectively. All original amino acids, as highlighted, were mutated to alanine (A) to determine effects on rCx36 transport.

2 AIM OF THESIS

The central hypothesis of this thesis is that plasticity of gap junctions formed by Cx36 depends on interaction with the cytoskeleton. In previous studies, the Zoidl group demonstrated interaction of rCx36 with the microtubule protein tubulin *in vitro* (unpublished). The aim of this thesis is to investigate rCx36 interactions with the cytoskeleton *in vivo* and to explore the potential involvement of this interaction in the run-up plasticity mechanism.

To confirm the interaction between cytoskeletal elements and rCx36 in living cells, neuroblastoma cells (N2a) were selected since previous work has been performed in this cell model. At the beginning of this thesis work, investigations were primarily focused on tubulin-specific interactions with rCx36, and BioID was chosen as the methodology to study such interaction. BioID is a newly developed technique for studying proximity dependent protein-protein interactions *in vivo* using a highly selective enrichment and purification procedure developed for eukaryotic systems (Roux, Kim, Raida, & Burke, 2012b). The first aim of this thesis was to confirm the interaction between rCx36 and tubulin *in vivo* while simultaneously assessing the efficiency of the methodology.

The second objective of this thesis was to specifically characterize the involvement of the cytoskeleton in rCx36 trafficking, focusing on transport and insertion into the gap junction plaque. For the purpose of this study, the *in vivo* technique termed fluorescence recovery after photobleaching (FRAP) was utilized for its ability to measure molecular dynamics specific to diffusion and protein-protein interaction as it relates to trafficking. A series of experiments using rCx36 wild-type and deletion mutant constructs in addition to pharmacological blocking of cytoskeletal dynamics was utilized to characterize wild-type conditions and determine the specific contributions of actin and tubulin interaction.

Using the same technique, the third aim of this thesis was carried out to determine the critical binding sites involved in rCx36-cytoskeletal interaction. Specifically, this thesis addresses critical amino acid residues pertaining to the rCx36-tubulin interaction.

The final aim of this thesis was to assess the involvement of the cytoskeleton in the run-up phenomenon, first described by Zoidl et al. (2002). In this phenomenon, rCx36 is described to

undergo an LTP-like behavior in which gap junctional conductance increases 10-fold in a CaMKII dependent manner (Del Corsso et al., 2012; Zoidl et al., 2002). However, the mechanism by which this occurs is unknown. As such, in the finals parts of this thesis, cytoskeletal-dependent trafficking is assessed as a potential contender in the mediation of the run-up phenomenon.

3 MATERIALS

3.1 ORGANISMS

All handling, manipulation and storage of bacterial and eukaryotic cell lines were performed in a licensed CL2 laboratory located in the Department of Biology, Life Science Building, York University in compliance with federal, provincial and institutional bylaws.

3.1.1 Bacterial Strains

Escherichia coli (*E.coli*) DH5α (Invitrogen, Burlington, Canada)

Genotype: F^- Φ80*lac*ZΔM15 Δ(*lac*ZYA-*arg*F) U169 *rec*A1 *end*A1 *hsd*R17 (r_k^-, m_k^+) *pho*A *sup*E44 *thi*-1 *gyr*A96 *rel*A1 λ^-

E.coli NEB 5-alpha competent (New England Biolabs, Whitby, Canada)

Genotype: *fhuA2 Δ(argF-lacZ) U169 phoA glnV44 Φ80 Δ(lacZ)M15 gyrA96 recA1 relA1 endA1 thi-1 hsdR17*

3.1.2 Eukaryotic Cell Lines

Neuroblastoma 2a cells (Neuro 2a or N2a cells) were derived from *Mus musculus* from a spontaneous tumor in a strain A albino mouse (Klebe & Ruddle, 1969). N2a cells were purchased from ATCC®.

3.2 MEDIA AND SOLUTIONS

3.2.1 Solutions and Media for Cell Culture

Phosphate buffered saline (PBS -/-)	130 mM NaCl, 2.8 mM KCl, 10 mM Na_2HPO_4, 1.8 mM KH_2PO_4, pH 7.4
Trypsin-EDTA solution	0.05% trypsin, 0.02% EDTA (1x) in D-PBS (PAA)
Dulbecco's Modified Eagle Medium (DMEM)	+ 10% Fetal Bovine Serum (FBS) + 1% non-essential amino acids (NEA) +1% penicillin/streptomycin (10,000 U/ml/10mg/ml)

3.2.2 Solutions and Media for Microscopic Analyses

Clear DMEM	+1% L-glutamine - phenol red
PBS +/+	+ 0.0133% calcium chloride dihydrate + 0.01% magnesium chloride hexahydrate

3.2.3 Solutions and Media for Bacterial Cultivation

LB media	1% bacto tryptone, 0.5% yeast extract, 0.5% NaCl 50µg/ml kanamycin or 100µg/ml ampicillin
LB agar plates	LB medium containing 1% agar 50µg/ml kanamycin or 100µg/ml ampicillin
SOC medium	2% bacto tryptone, 0.5% bacto yeast extract, 10 mM NaCl, 2.5 mM KCl, 10 mM $MgCl_2$, 10 mM $MgSO_4$, 20 mM glucose

3.2.4 Solutions for Molecular Biology

Tris-acetate-EDTA (TAE)	1 mM EDTA, 40 mM Tris-acetate
6x DNA Loading Dye (Fermentas)	10 mM Tris-HCl (pH 7.6), 0.03% bromophenol blue, 0.03% xylene cyanol FF, 60% glycerol 60 mM EDTA

3.2.5 Solutions for Protein Biochemistry

Laemmli sample buffer	2% SDS, 10% glycerol, 5% β-meraptoethanol, 0.1% Orange G, 50 mM Tris-HCl, pH 6.8
Laemmli running buffer	192 mM glycine, 0.1% SDS, 25 mM Tris-HCl, pH 8.3
Transfer buffer	20% methanol, 48 mM Tris. 39 mM glycine, 0.037% SDS, storage at 4°C
Blocking solution	Odyssey Blocking Buffer (LI-COR)
iBind™ Solution	1% iBind 100X Additive

20% iBind 5X buffer

3.2.6 Solutions for BioID Protein Purification

NP40 Lysis buffer*	1% Nonidet P40 50 mM Tris-HCl, pH 7.4 250 mM NaCl 5 mM EDTA 50 mM NaF 1 mM Na_3VO_4 0.02% NaN_3

*used with 1% Protease Inhibitor Cocktail (Thermo Scientific)

Wash buffer 1	2% SDS
Wash buffer 2	0.1% deoxycholate, 1% Triton X-100, 500 mM NaCl, 1mM EDTA, 50 mM Hepes, pH 7.5
Wash buffer 3	250 mM LiCl, 0.5% NP-40, 0.5% deoxycholate, 1 mM EDTA, 10 mM Tris, pH 8.1
Wash buffer 4	50 mM Tris, pH 7.4, 50 mM NaCl

3.3 ANTIBODIES

Table 1: List of primary antibodies.

Name	Species (Type)	Origin	Specification	Used Dilution*
anti-β-actin	Mouse IgG	Sigma-Aldrich	β-actin	1:10000
anti-GFP	Rabbit IgG	Santa Cruz	EGFP, EYFP	1:1000
anti-HA	Mouse IgG	Sigma-Aldrich	HA-tag	1:10000
anti-β-tubulin	Mouse IgG	Sigma-Aldrich	β-tubulin	1:1000

*for the use of the iBind protocol, antibodies were concentrated to 5X of the listed dilutions

Table 2: List of secondary antibodies.

Name	Species (Type)	Origin	Specification	Used Dilution*
anti-mouse IRDye800	Goat	Li-Cor Biosciences	Against mouse IgG with IRDye800 tag	1:10000
Anti-rabbit IRDye680	Donkey	Li-Cor Bioscience	Against mouse IgG with IRDye680 tag	1:15000

*for the use of the iBind protocol, antibodies were concentrated to 5X of the listed dilutions

Table 3: List of enzyme conjugates.

Name	Origin	Specification	Used Dilution*
Streptavidin-HRP	Invitrogen	Biotin	1:2500

3.4 CHEMICALS, ENZYMES, AND KITS

3.4.1 Chemicals

Acetic Acid Glacial (Bioshop), Acrylamide (Bioshop), agar (Bioshop), agarose (Fisher), ammonium persulphate (Bioshop), bacto tryptone (Fisher), bacto yeast extract (Fisher), bromphenol blue (Bioshop), $CaCl_2$ (Bioshop), colchicine (Sigma), cytochalasin D (Sigma), D-Biotin (Bioshop), EDTA (Bioshop), ethanol (Commercial ALC.), ethidium bromide (Bioshop), ethylenediaminetetraacetic acid (EDTA) (Bioshop), fetal bovine serum (FBS) (Life Technologies), formaldehyde solution (formalin) (Sigma), Glucose (Fisher), L—glutamine (100x) (Life technologies), glycerol (Bioshop), glycine (Bioshop), Hepes (Sigma), immersion oil (Zeiss), HCl (Fisher), ionomycin calcium salt (Sigma), Isopropyl alcohol (Bioshop), KCl (Fisher), KH_2PO_4 (Sigma), LiCl (Bioshop), 2-Mercaptoethanol (Bioshop), methanol (Bioshop), MgCl2 (Fisher), MgSO4 (Fisher), NaCl (Bioshop), Na-deoxycholate (Sigma), Na_2HPO_4 (Sigma), non-essential amino acids (100x) (Sigma), odyssey blocking buffer, Orange G (Sigma), paclitaxel (Sigma), protease inhibitor cocktail (Thermo Scientific), SDS (Bioshop), TAT peptides (United Biosystems), tetramethylethylenediamine (TEMED) (Bioshop), tris(hydroxymethyl) aminomethane (Tris) (Bioshop), Triton X-100 (Sigma), Trypsin-EDTA (Sigma), Tween 20 (Sigma), water (ultrapure Distilled Water DNAse RNAse free) (CellGrow), Xylene Cyanol FF (Bioshop)

3.4.2 Enzymes

Calf intestine alkaline phosphatase (CIAP) (Invitrogen), FastDigest restriction endonucleases (Fermentas), T4 DNA ligase (Thermo Scientific), Phusion High-Fidelity DNA Polymerase (NEB)

3.4.3 Kits

Polymerase Chain Reaction (PCR)	Phusion High Fidelity PCR Kit (Thermo Scientific)
Purification of PCR and DNA fragments	NucleoSpin® Gel and PCR Cleanup Kit (Clontech)
DNA gel elution	QIAquick Gel Extraction Kit (Qiagen)
Cloning of DNA fragments	CloneJET PCR Cloning Kit (Thermo Scientific) Rapid DNA Ligation Kit (Thermo Scientific)
Plasmid Purification	QIAPrep Spin Miniprep Kit (Qiagen)
Subcloning of DNA fragments	Rapid DNA Ligation Kit (Thermo Scientific)
DNA Restriction Digest	Fast Digestion Top Fermentas Kit (Thermo Scientific)
DNA Transfection	Effectene Transfection Reagent (Qiagen)
Site-Directed Mutagenesis	Q5® Site-Directed Mutagenesis Kit (New England Biolabs)
iBind Western Blot	iBind™ Solution Kit (Life technologies)
Protease Inhibition	Protease Inhibitor Cocktail Kit (Thermo Scientific)

3.5 ANTIBIOTICS

Ampicillin (Bioshop), kanamycin (Bioshop), penicillin/streptomycin (Life Technologies)

3.6 PLASMIDS AND OLIGONUCLEOTIDES

3.6.1 Plasmids

Table 4: List of commercially available plasmids used.

Name	Description	Sources
pcDNA 3.1 MCS-BirA(R118G)-HA	Eukaryotic expression vector used for the generation of BirA-tagged C-terminal fusion proteins, ampicillin resistance	Addgene
pEGFP-N1	Eukaryotic expression vector used for the generation of EGFP-tagged C-terminal fusion proteins, kanamycin resistance	Clontech
pEYFP-N1	Eukaryotic expression vector used for the generation of EYFP-tagged C-terminal fusion proteins, kanamycin resistance	Clontech
pJET 1.2	Blunt end cloning vector, ampicillin resistance	Thermo-Fisher

Table 5: List of plasmid constructs generated by in vitro recombination.*

Vector	Insert	Description of usage
pcDNA 3.1 MCS-BirA(R118G)-HA	rCx36	For the *in vivo* detection of tubulin interaction via BioID
	rCx36 Δ279-292	" "
	rCx36 Δ175-196	" "
pEYFP-N1	rCx36	For the *in vivo* determination of cytoskeletal interaction and respective dynamics at the Cx36 nexus using confocal microscopy imaging and FRAP
	rCx36 Δ175-196	" "
	rCx36 Δ182-198	" "

	rCx36 Δ279-292	“ ”
	rCx36 Δ182-198, 279-292	“ ”
pEGFP-N1	rCx36	“ ”
	rCx36 Δ279-292	“ ”
	rCx36 Δ182-198, 279-292	“ ”
pDsRed-monomer	CaM	For the *in vivo* assessment of cytoskeletal involvement in the run-up using FRAP

*All plasmids were made readily available by Dr. Georg Zoidl, Dept. of Biology. *See Appendix A.*

Table 6: List of plasmid constructs generated by site-directed mutagenesis.

Vector	Insert	Description of usage
pEGFP-N1	rCx36 V171A	For the determination of critical binding residues in the Cx36-actin interaction
	rCx36 H177A	“ ”
	rCx36 S179A	“ ”
	rCx36 L181A	“ ”
	rCx36 R182A	“ ”
	rCx36 K279A	For the determination of critical binding residues in the Cx36-tubulin interaction
	rCx36 I280A	“ ”
	rCx36 K281A	“ ”
	rCx36 L282A	“ ”
	rCx36 V284A	“ ”
	rCx36 R285A	“ ”
	rCx36 G286A	“ ”

3.6.2 Oligonucleotides

Table 7: List of oligonucleotides used for cloning.*

Name	Sequence 5'→3' (Description)
rCx36 s rCx36 as	**GAATTC**ATGGGGGAATGGACCATCTTGGAGAG **GAATTC**CACATAGGCGGAGTCACTGGACTGA Introduces EcoRI restriction site at the 5' end used for the cloning of rCx36 into pcDNA 3.1 BirA expression vector

*Restriction enzyme site bolded and underlined.

Table 8: List of oligonucleotides used for site-directed mutagenesis and sequencing.*

Name	Sequence 5'→3'
rCx36 V171A	
F1:	CTTAGAGGTT**CAT**GAGCTGGCTC
R1:	CAATCTGGTTCTGTCTCC
rCx36 H177A	
F1:	GCTGGCTCCA**GCT**CCATCTGGGC
R1:	TCTTTAACCTCTAAGCAATC
rCx36 S179A	
F1:	TCCACATCCA**GCT**GGGCTGCGCA
R1:	GCCAGCTCTTTAACCTCTAAGCAATCTGG
rCx36 L181A	
F1:	TCCATCTGGG**GCG**CGCACAGCAG
R1:	TGTGGAGCCAGCTCTTTAAC
rCx36 R182A	
F1:	ATCTGGGCTG**GCC**ACAGCAGCAAGGTC
R1:	GGATGTGGAGCCAGCTCT
rCx36 K279A	
F1:	GGGATGGCGGGCGATCAAACTGG
R1:	AGATGGTTAAGTTCAGCC
rCx36 I280A	
F1:	ATGGCGGAAG**GCC**AAACTGGCTG
R1:	CCCAGATGGTTAAGTTCAG
rCx36 K281A	
F1:	GCGGAAGATCGCACTGGCTGTCC
R1:	CATCCCAGATGGTTAAGTTC
rCx36 L282A	
F1:	GAAGATCAAAGCGGCTGTCCGGGG
R1:	CGCCATCCCAGATGGTTA

rCx36 V284A	
F1:	CAAACTGGCTGCGCGGGGAGCCC
R1:	ATCTTCCGCCATCCCAGATG
rCx36 R285A	
F1:	ACTGGCTGTCGCGGGAGCCCAGG
R1:	TTGATCTTCCGCCATCCC
rCx36 G286A	
F1:	GGCTGTCCGGGCGGCCCAGGCCA
R1:	AGTTTGATCTTCCGCCATCCCAG
pEGFP-N1	
R1:	GTCCAGCTCGACCAGGATG
	Sequencing of EGFP-N1 constructs

* Mutated sites underlines and bolded

3.7 PEPTIDES

Table 9: List of peptides used for rCx36 specific tubulin interference.

Name	Sequence (Description)
TAT CT-ON	GRKKRRQRRRPQGWRKIKLAVRGAQAKRK (Used for competitive binding of the tubulin binding site of Cx36. Targets residues:276-292)
TAT CT-OFF	GRKKRRQRRRPQKDLPRVSVPNFGRTQSSDSAYV (Used as a control for competitive binding of the CT domain, outside of the tubulin region. Targets residues: 300-321)
TAT CT-ON (Scrambled)	GRKKRRQRRRPQQARWKLKVRRGGIKKAA (Control sequence of CT-ON in a scrambled orientation)
TAT CT-OFF (Scrambled)	GRKKRRQRRRPQDRVVSSSVLSPNGYKARDFTQP (Control sequence of CT-OFF in a scrambled orientation)

*TAT sequence denoted in red

3.8 SIZE STANDARDS

3.8.1 DNA Size Standard

GeneRuler 1kb Plus DNA Ladder	Fermentas

3.8.2 Protein Size Standard

Spectra™ Multicolor Broad Range Protein Ladder	Thermo Scientific

3.9 CONSUMABLES

Serological pipettes (5ml, 10ml, 25ml)	Fisher Scientific
Culture dishes (6cm, 10cm)	Falcon, Thermo Scientific
24-well plates	Falcon
MatTek plate	MatTek Corp
Petri dish	Fisher Scientific
Plastic consumables (pipette tips, eppendorf tubes, etc.)	Fisher Scientific, Sarstedt, Qiagen, Neptune
Syringe filters (0.20µm²)	HSW

3.10 EQUIPMENT

3.10.1 Cell Culture Equipment

Incubator	Formula Steri-Cycle CO_2 Incubator; Thermo-Scientific
Laminar flow unit	1300 Series A2; Thermo Scientific
Lab centrifuge and rotor	CL10 Centrifuge (Thermo Scientific)
Water bath	VWR
Hemocytometer	La fontaine

3.10.2 Molecular Biology Equipment

Bacterial shaker	(Innova40)
	MaxQ4450 (Thermo Scientific)
Rocking Platform	Model 100 (VWR)
Water bath	Isotemp 205 (Fisher Scientific)
Scale	Navigator XT (OHAUS)
	AB104-S/FACT (Mettler Toledo)
Magnetic Stirrer and Hot Plate	Isotemp® (Fisher Scientific)
Electrophoresis Chamber System	(Bio-Rad)
Incubator	HERA THERM (Thermo Scientific)
Nucleic Acid Purification Systerm	Qiacube (Qiagen)
Centrifuge	Sorval Legend Micro 21R
	(Thermo Scientific)
PCR machine	Mastercycler Nexus
	(Eppendorf)
Vortex Mixer	(Fisher)
UV Transilluminator	High Performance UV Transilluminator (UVP)
UV Gel Documentation System	Alpha Imager HP System
	(Fisher Scientific)
Nanodrop 2000 Photospectrometer	(Thermo Scientific)
Agarose gel electrophoresis	Mini-sub cell GT (Biorad)
pH Meter	Five Easy FE20 (Mettler Toledo)
Programmable rotator-mixer	Multi Bio RS-24 (Peqlab)

3.10.3 Protein Biochemistry Equipment

Sodium dodecyl sulphate polyacrylamide gel electrophoresis (SDS-PAGE)	Mini-PROTEAN tetra System (BioRad)

Blotting chamber	Trans-Blot® Turbo transfer system (BioRad)
Infrared western blot scanning system	Odyssey Infrared Imaging System; (Licor)
Nitrocellulose membrane	Tran-blot Turbo Transfer Pack; (BioRad)
Thermomixer	(Eppendorf)

3.10.4 Microscopic Analysis Equipment

Light Microscope	CKX41 (Olympus)
Confocal Microscope	LSM 700 (Zeiss)
Coverslips	(Fisher Scientific)
Mounting slides	(Fisher Scientific)

3.11 SOFTWARE

DNA Concentration	Nanodrop 2000
Gel Documentation	AlphaImager
Image processing	Image J, Photoshop and Illustrator CC 2015 (Adobe)
Primer design	NEBaseChanger (New England Biolabs)
Analysis of DNA sequences	SnapGene Viewer
Protein Sequence alignments	ClustalW2
Image acquisition and processing	ZEN 2010 software (Zeiss)
Spreadsheet analyses	Excel 2010 (Microsoft)
Text processing	Word 2013 (Microsoft)

4 METHODS

4.1 MOLECULAR BIOLOGICAL METHODS

4.1.1 Cloning of DNA Fragments

4.1.1.1 Cultivation of bacteria

Recombinant bacteria was cultured on LB-agar plates supplemented with the appropriate selection antibiotic, as determined by the expression vector, and incubated at 37ºC overnight. Single colonies were obtained and grown in 5mL of antibiotic supplemented LB medium for overnight incubation at 37ºC. To achieve optimal growth conditions, bacterial cells were placed on a tilted rack in a horizontal shaker at 200 rpm for the duration of incubation.

4.1.1.2 Determination of nucleic acid concentration

DNA concentration was measured using the NanoDrop 2000 and Nanodrop2000 software under the nucleic acid program, at an absorbance of 280 nm (A_{280}). Simultaneously, samples were assessed for purity as indicated by the quotient A_{260}/A_{280}. As pure DNA typically reads as a value of 1.8, residual chemical contamination was recognized as a significant deviation from this value; an increase ≥2.0 or decrease ≤1.6 is indicative of RNA or protein contamination respectively. EB buffer (Qiagen), the final DNA elution buffer, was used as a blank prior to concentration measurements.

4.1.1.3 Plasmid DNA preparation

To obtain highly purified DNA for further applications, such in the case of DNA sequencing or transient transfection, small-scale plasmid purification from DH5α *E.coli* was performed. Plasmid purification was carried out using the Qiacube and with respective QIAPrep Spin Miniprep Kit as per the manufacturer's guidelines. From a 5mL overnight culture, approximately 9-12µg of plasmid DNA was purified by this method. The DNA concentration was subsequently determined by measurement of the A_{280} (see section 4.1.1.2).

4.1.1.4 Agarose Gel electrophoresis and DNA gel elution.

Agarose gel electrophoresis was performed for the confirmation of inserts through test restriction digests with type II restriction endonucleases or as prerequisite for DNA purification. In preparation of either PCR or general purification, DNA samples were mixed 5:1 with the 6x DNA loading dye as loading buffer (see 4.1.1.6 for DNA preparation for restriction digest). 1% agarose

gels were supplemented with 0.1g/mL ethidium bromide for DNA staining. A horizontal Mini-Sub® Cell GT electrophoresis chamber (BioRad) was used in operation with PowerPac™ Basic power supply. Gel electrophoresis was achieved using consistent voltages ranging from 90-100 V and operated in 1x TAE buffer solution. DNA was visualized and digitally documented with the Alpha Imager HP system (Fisher Scientific). The GeneRuler 1kb Plus DNA Ladder was used as the size standard. The DNA of interest was excised rapidly from the agarose gels under UV light supplied by the UV Transilluminator TFM-20V (UVP) using a sharp scalpel. Elution and purification was performed using the NucleoSpin®gel and PCR Clean-up kit in the case of PCR (for details see section 4.1.1.5) or Qiaquick gel extraction kit for general purification as per the manufacturer's protocols.

4.1.1.5 Amplification of DNA fragments by PCR

For the amplification of specific DNA fragments, the polymerase chain reaction (PCR) was carried out using the Mastercycler® Nexus. The assembly of the PCR reaction and program listed in Table 9. Amplicons were fractionated on a 1% agarose gel and purified using the NucleoSpin®gel and PCR Clean-up kit. Modifications to the manufacturer's protocols were as follows: (i) washing of the silica membrane with NT3 buffer was repeated twice and (ii) for DNA elution, 15µl of NE buffer was added to the amplicons and incubated at room temperature (RT) for 1 minute and repeated twice for a total elution flow-through of 30µl. For DNA concentration measurements, NE buffer was used as a blank.

Table 10: Assembly of PCR reaction and PCR program.

	PCR Reaction
Primer (s/as) (10µM)	1.0 µl
dNTPs	1.0 µl
10x buffer	10.0 µl
(Phusion High-Fidelity) DNA polymerase	0.5 µl
template DNA (10 ng/µl)	1.0 µl
A. dest.	35 µl
PCR program	
initial denaturation	1. 94ºC, 3 min
denaturation	2. 94ºC, 30 s
hybridization	3. 52ºC or 63ºC, 30s
elongation	4. 72ºC, 1 min
	5. 25 cycles of steps 2-4
elongation	6. 72ºC, 10 min
	7. 4ºC ∞

4.1.1.6 DNA restriction digest

Restriction digests of DNA were performed with type II restriction endonucleases with the Fast Digestion Top Fermentas Kit (Thermo Scientific) as per the manufacturer's guidelines. For analysis of recombinant plasmids, digest reactions were set up with 0.2-0.4µg DNA and incubated for 5 min at 37ºC. Prior to the ligation, vector DNA was dephosphorylated with calf intestine alkaline phosphatase (CIAP), preventing the vector from re-ligating on itself and producing false-positive clones. Under the dephosphorylation protocol, 1 µl of CIAP was added to the digest reaction and incubated at 37ºC for 30 min. Upon completion, CIAP was inactivated by an incubation step carried out at 65ºC for 10 min. Restriction digests to be used further in cloning were electrophoresed, excised and eluted from the gel with the QiaCube in combination with the QiaQuick gel extraction kit as per the manufacturer's guidelines. Test restriction digests, such in the case of positive clone confirmation, were imaged upon completion of gel electrophoresis.

4.1.1.7 Ligation of DNA fragments

Initial ligation of DNA to pJET1.2, chosen for its high efficiency cloning of PCR products, was performed using the CloneJET PCR Cloning Kit as per manufacturer's guidelines for the blunt end cloning protocol. Ligation reactions were incubated at RT for 30 minutes prior to transformation. Listed below is the corresponding reactants of the ligation mixture.

T4 DNA Ligase	1.0 µl
2X Reaction Buffer	10.0 µl
pJET1.2/blunt Cloning Vector (50ng/µl)	1.0 µl
purified PCR product	50 ng (3:1 molar ratio to pJET1.2/blunt)
Water, nuclease-free	up to 19 µl for a total reaction volume of 20µl

For sub-cloning, such in the case of obtaining pcDNA 3.1 MCS-BirA(R118G)-HA-rCx36 (abbreviated as pcDNA 3.1 BirA*-rCx36) wild-type and mutant constructs, ligation was achieved using the Rapid DNA Ligation Kit as per the manufacturers guidelines. A base pair ratio of 1:6.4 (insert:vector) was used. Ligation reactions were incubated at RT for 5 minutes prior to transformation. Listed below is the corresponding reactants of the ligation mixture:

T4 DNA Ligase (5u/µl)	1.0 µl
5X Rapid Ligation Buffer	4.0 µl
Linearized Vector DNA	80-90 ng
purified PCR product	40-50 ng
Water, nuclease-free	up to 19 µl for a total reaction volume of 20µl

4.1.1.8 Transformation of plasmid DNA into competent bacteria via heat-shock

For the preparative production of recombinant plasmid DNA, 100µl of competent DH5α *E. coli* bacteria was added to 2-5 µl of previously prepared ligation mixture (see section 4.1.1.7 for details) and incubated on ice for 30 minutes. Following incubation, the bacterial/ligation mixture was briefly heat shocked at 42ºC for 30 s and recovered in 800 µl of pre-warmed SOC medium. Post-heat-shock, bacteria was incubated at 37ºC in a bacterial shaker for 1h at 200 rpm. Upon completion, 200 µl of the bacterial suspension was plated on LB-agar plates containing the appropriate selection antibiotic and incubated overnight at 37ºC for the production of single isolated colonies.

4.1.2 Site-Directed Mutagenesis

Prior to start, primers were designed to introduce alanine point mutations at selected residues of rCx36 cytoplasmic loop and carboxyl terminal domain. Primers were generated using the NEBaseChanger™ online program and were ordered from Integrated DNA Technologies, Iowa. Mutant pEGFP-rCx36 plasmids were generated using Q5® Site-Directed Mutagenesis Kit (New England Biolabs, Canada) as per manufacturer's protocol with pEGFP-rCx36 as the template. Transformed NEB 5-alpha competent *E. coli* cells were plated onto LB-KAN plates to isolate single bacterial colonies which were subsequently grown in LB-KAN media overnight. Small-scale plasmid purification (starting from 5ml bacterial cultures) was carried out via the QiaCube and respective QIAPrep Spin Miniprep Kit as per manufacturer's protocols. A list of the used mutagenic primers is provided in **Table 8**.

4.1.3 Sequencing of Plasmid DNA

Purified pEGFP-rCx36 mutant plasmid DNA generated from the Q5® Site-Directed Mutagenesis Kit was sent to Eurofins Genomics, USA, for sequencing.

4.1.4 Bioinformatics

Protein and DNA sequences were obtained from the National Center for Biotechnology Information (NCBI; http://www.ncbi.nlm.nih.gov) under the protein and nucleotide database engine respectively. DNA sequences were analyzed using ClustalW2, for the generation of sequence alignments with the multiple sequence alignment tool and SnapGene Viewer to confirm mutated constructs and generate DNA restriction maps. ImageJ software was used to generated image montages and to measure gap junction plaque area and fluorescence (CTF_{cell} and CTF_{GJP}) with the free-hand trace tool. Predicted models of the rCx36 structure were generated using the online I-TASSER tool.

4.2 CELL CULTURE

4.2.1 Culture of N2a

Mouse neuroblastoma 2a (N2a) cells were grown in Dulbecco's Modified Eagle Medium (DMEM) supplemented with 10% fetal bovine serum (FBS), 1% non-essential amino acids (NEA) and 1% penicillin/streptomycin. Cells were maintained in a Forma Steri-cycle CO_2 Incubator at 37ºC and 5% CO_2 in a humidified atmosphere. Cells were passaged routinely twice a week, allowing cells to grow to confluence over a three to four day time period. For passaging purposes, cells were initially washed with pre-warmed PBS (- calcium chloride/- magnesium chloride; -/-) and subsequently treated with pre-warmed trypsin-EDTA for 30-60 seconds to relieve cell adherence. Upon addition of 10ml pre-warmed DMEM, trypsin-EDTA was rendered inactive. Cells were collected and resuspended in solution to produce a homogenous mixture. Finally, 1 ml of the cell suspension was added to 9 mL of fresh DMEM in a 10 cm dish.

4.2.2 Transient Transfection

Transient transfection of N2a cells was achieved using the Effectene Transfection Reagent Kit (Qiagen) as per the manufacturer's protocols. For localization studies of fixed cells, 10000 cells were seeded onto coverslips in a 24-well plate. For a small scale production of whole cell protein lysates to be used in western blot and/or SDS-PAGE gel staining analyses, 30000 cells were seeded into a 24-well plate. For utilization in the biotinylation assay (BioID), 900000 cells were plated on a 6 cm dish. For live cell imaging and fluorescence recovery after photobleaching (FRAP) studies, 10000 cells were seeded onto a 14 mm microwell of a 35 mm MatTek dish. Transient transfected was performed 24h after seeding using 0.2-2.0 µg of DNA depending on the appropriate protocol. Cells were used 48 h post-transfection in the analyses as outlined.

4.2.3 Preparation for BioID Pull-Down

For use in the biotinylation assay, media was exchanged 24h post-transfection and supplemented with 50 µM of biotin.

4.2.4 Preparation for Confocal Analyses

For use in live cell imaging analyses, N2a cells were washed with pre-warmed PBS (+/+) and cultured in 2mL of DMEM (without phenol red) 48 h post-transfection. N2a cells were incubated under normal conditions for a minimum of 10 minutes prior to live cell studies. In the case of drug treatment, cytochalasin D (3µM), colchicine (0.1µg/ml) or paclitaxel (2.5µg/ml) was added additionally and cells were incubated at 37°C for 10 min prior to use. For the purpose of this study, cytochalasin D was used to inhibit the polymerization of microfilaments (Sigma-Aldrich, USA). Paclitaxel (Sigma-Aldrich, USA) and Colchicine (Sigma-Aldrich, USA) were used for tubulin-specific interference ***(See Appendix B)***.

Cells destined for fixation were washed with RT PBS (+/+) and subsequently treated with 500 µl of 10% formalin for 15 min at RT. Upon completion of the incubation period, cells were washed with RT PBS (+/+), distilled water and subsequently mounted onto a microscope slide (Fisherbrand) using 10 µl of Fluoroshield™ with DAPI (Sigma). Slides were stored at 4ºC until ready for use.

4.3 PROTEIN BIOCHEMICAL METHODS

4.3.1 Determination of Protein Concentration

Refer to section 4.1.1.2 with the following exceptions: (i) the nanodrop 2000 software was used under the Protein A280 program (ii) purified protein was indicated by the A_{260}/A_{280} value of approximately 1.6.

4.3.2 SDS-Polyacrylamide Gel Electrophoresis (SDS-PAGE)

Whole cell lysates for SDS-PAGE and western blots were prepared by aspirating the culturing media and scraping the cells into 1x Laemmli sample buffer. Preparation of cell lysates used in the biotinylation assay (BioID) is detailed in section 4.3.4. Protein samples were denatured at 95ºC for 5 min prior to electrophoresis using a vertical Mini-PROTEAN® Tetra System used in operation with PowerPac™ Basic power supply. Spectra™ Multicolour Broad Range Protein Ladder was used as the size standard. Typically, 10-20 µg of protein was loaded per lane, equally across

experiments. Gel electrophoresis was achieved using consistent voltages ranging from 100-150 V until complete protein separation was achieved; the operation was in 1x Laemmeli running buffer solution. Denaturing SDS-polyacrylamide gels were prepared with the following compositions:

Separation gel:	10% acrylamide 380 mM Tris-HCl, pH 8.8 0.1% SDS 0.08% tetramethylethylenediamine TEMED 0.8% ammonium persulphate (APS)
Comb gel:	5% acrylamide 125 mM Tris-HCl, pH 8.8 0.1% SDS 0.08% tetramethylethylenediamine TEMED 0.8% ammonium persulphate (APS)

Gels were stained with PageBlue Protein Staining solution (post-transfer if destined for western blot) for 30 min before overnight destaining commenced. Protein stained gels were visualized and digitally documented with the Alpha Imager HP system (Fisher Scientific).

4.3.3 Western Blot

Post-SDS-PAGE, proteins were transferred onto a nitrocellulose membrane in accordance with the semi-dry blot system. The Trans-Blot® Turbo™ Transfer Pack used contained equilibrated nitrocellulose membranes prepackaged with filter paper and buffer. Proteins were transferred using the Trans-Blot® Turbo™ Transfer System (Bio-Rad) at 5A, 25V, for 10 min under the high molecular weight protocol.

4.3.3.1 Traditional

Nitrocellulose-bound immobilized proteins were washed with PBS and blocked with Odyssey Blocking Buffer for 1 h at RT to minimize nonspecific interactions thus enhancing detection sensitivity. Primary antibodies directed against the protein(s) of interest were applied in blocking buffer overnight at 4ºC (see Table 1 for primary antibodies and dilutions). To remove unbound primary antibodies and further reduce unspecific binding, membranes were washed with PBS supplemented with 0.1% Tween 20 (PBS-T). Membranes were incubated with IRDye coupled

secondary antibodies in blocking buffer for 1h at RT in the dark (see Table 2 for secondary antibodies and dilutions). Upon completion, membranes were washed 4 times in PBS-T and once in PBS for removal of Tween 20. Membranes were kept in the dark until imaged; fluorescent signals were detected using the Odyssey Infrared Imaging System.

4.3.3.2 iBind

As an alternative to the traditional method, nitrocellulose-bound immobilized proteins were immersed in 5 ml 1x iBind™ solution. Membrane blocking and antibody application was achieved using the iBind™ Western System in combination with the iBind™ Solution Kit and iBind™ Cards as per manufacturer's guidelines. Upon completion, membranes were stored in distilled water kept in the dark. Fluorescent signals were detected using the Odyssey Infrared Imaging System.

4.3.4 Biotinylation Pull-Down (BioID)

For preparation of cell lysates used in the biotinylation pull-down (BioID), N2a cells were washed with cold PBS (-/-) upon removal of the culturing media. Cells were collected into 2 ml of PBS (-/-) and centrifuged at 400 rpm for 5 min at RT. Supernatant was discarded, and the pellet was washed by resuspension in PBS (-/-) following by centrifugation under the same conditions; washing step was repeated twice. Cells were lysed with 200 µl of NP40 Cell Lysis Buffer supplemented with 1% protease inhibitor cocktail and transferred into a Protein LoBinding Tube (Eppendorf). Lysate(s) was incubated on ice for 30 minutes with periodic vortexing every 10 minutes. For protein separation, lysates were centrifuged at 13,000 rpm for 10 min at 4ºC. The supernatant was transferred into a new Protein LoBinding Tube and subjected to further experiments; a small aliquot was retained for western blot analysis as pre-incubation lysate (pre-lysate).

Dynabeads®MyOne™ Streptavidin C1 were prepared by vortexing to re-suspend the beads. 90 µl of the resuspension was transferred into a Protein LoBinding Tube and washed 3 times with 1 ml of PBS; bead capture was achieved using a magnetic rack. Pre-lysate was incubated with the beads

overnight at 4ºC on a rotating platform. Upon completion of incubation, beads were collected on the magnetic rod, and supernatant was stored as the lysate post-incubation (post-lysate). Collected beads were washed twice for 8 min at RT with 1 mL of wash buffer 1 (2% SDS in dH_2O), once with wash buffer 2 (0.1% deoxycholate, 1% Triton X-100, 500 mM NaCl, 1 mM EDTA and 50 mM Hepes, pH 7.5), once with wash buffer 3 (250 mM LiCl, 0.5% NP-40, 0.5% deoxycholate, 1 mM EDTA and 10 mM Tris, pH 8.1) and twice with wash buffer 4 (50 mM Tris, pH 7.4, and 50 mM NaCl); a small aliquot of the last wash fraction was reserved for western blot analysis as the "wash." Bound proteins were eluted from the bead in 50 µl of 1x Laemmeli sample buffer at 95ºC for 5 minutes; a total of two elutions were performed.

4.3.5 Protein Identification by Mass Spectrometry

Proteins eluted from the streptavidin beads were fractionated by SDS-PAGE and stained with PageBlue Protein Staining solution. After destaining, whole gel lanes were cut into 6 equal-sized gel bands, and mass spectrometry was performed at the in house facility of the Dept. of Chemistry, York University.

4.4 MICROSCOPIC METHODS

4.4.1 Confocal Laser Scanning Microscopy

Confocal imaging was performed using the Zeiss LSM 700 confocal microscope in operation with the ZEN 2010 software program for data analysis. The microscope was equipped with the 405, 445, 488, 555 and 639 nm laser lines of which the 405 and 555 lasers were used in conjunction with this thesis for the detection of EGFP, EYFP, DAPI and DsRed fluorescence. Images were taken with a resolution of 512 x 512 pixels and exported as TIFF files to be used for documentation in Image J, Adobe Photoshop and/or Illustrator. Tables generated from FRAP studies were exported as .txt files and transferred into Microsoft Excel 2013 for data analysis and preparation of graphs.

4.4.2 Localization Studies of N2a Cells

Confocal laser scanning microscopy was used to analyze the cellular localization of EYFP- or EGFP-tagged rCx36 variants in transfected N2a cells. Images were taken with either living or fixed cells using the Plan-Apochromat 63x/1.4 Oil DIC M27 objective at a resolution of 512 x 512 pixels. Scanning repetitions were set to an averaging of 4 in the single or double track mode depending on fluorophores used for detection. A combination of single plane and z-stacked images were taken for the compilation of localization studies. In the case of time-lapse observations, averaging was set to 1, and single track mode was utilized for observations made in the single plane.

4.4.3 Fluorescence Recovery After Photobleaching (FRAP)

To analyze the dynamics of rCx36 and variant gap junction plaques, fluorescence recovery after photobleaching (FRAP) was utilized. Specifically, rCx36 GJ plaques (center and lateral ends), plasma membrane, intracellular space and extracellular space were photobleached using Zeiss LSM 700 confocal microscope system under Zeiss 63X (Plan-Apochromat, DIC M27 1.4) oil immersion lens, with the 405 nm laser, 48h post-transfection. Samples were placed in an incubating chamber and maintained at a temperature of 37ºC. Acquisition mode was set at a speed of 10 and 8 bit depth. Mobile fraction (%) and half-time of recovery ($t_{½}$) in seconds, was recorded for each ROI of the GJP and respective controls; ROIs were manually drawn using the rectangle tool. Bleaching was achieved with a single event of 40 iterations at a laser intensity of 70% after 10 cycles of 1.0-sec; total recording event was observed over 200 cycles. Observations were recorded with a pinhole of 1.0 airy units (AU) with a scan area of 31.1µm x 31.1µm and resolution of 512x512 pixels. Consistent parameters were used in all experiments. Experiments with considerable fluctuations in fluorescence intensity or frame-shifts were not included in the analyses. Results were normalized against the extracellular space to improve the signal-to-noise ratio and averaged amongst the population, represented as the mean ± the standard error of the mean (SEM). Sample sizes ranged based on the efficiency of plaque formation, however, typically a minimum of n=5 was used for analysis (***see Appendix C***). The data was exported from Zen 2010 for statistical analysis and graphing (see section 4.5).

4.5 ANALYSIS OF DATA

For the analysis of corrected total fluorescence (CTF) and gap junction plaque area, select regions were traced with the ImageJ free-hand tool. Fluorescence measurements were subtracted from background fluorescence to obtain the corrected value; the mean fluorescence of the background was averaged across a sample size of three. In the case of gap junction plaque area, tracings were made along the axis that yielded the largest surface area (***see Appendix C*** for sample size). Values obtained for CTF_{cell} (Relative fluorescence units or RFU), CTF_{GJP} (RFU), gap junction plaque area (μm^2), mobile fraction (%) and half-time of recovery (s) were averaged across samples and represented as the mean± the standard error of the mean (SEM). To determine statistical significance, the student t-test was performed; significance was arbitrarily determined at a 99% confidence interval where significance (or lack thereof) was denoted as:

ns	$p > 0.01$
**	$p \leq 0.01$
***	$p \leq 0.001$
****	$p \leq 0.0001$

where 'ns' represents no statistical significance. Data analysis and generation of respective figures were completed in Microsoft Excel 2013.

5 RESULTS

5.1 INVESTIGATION OF CX36-TUBULIN INTERACTION VIA BIOID

The first aim of this thesis was to confirm the interaction between rCx36 and tubulin in Neuro2a cells while simultaneously testing a new method for identifying protein interacting partners termed BioID. In this technique, we utilized a C-terminal fusion protein with rCx36 and the promiscuous bacterial ligase BirA* capable of covalently attaching biotin to proteins in close proximity. The biotin labeled protein fraction was then enriched using a highly selective enrichment and purification procedure to identify potential interacting partners **(Figure 9)**. Results generated were to serve as the *in vivo* complement to pre-existing *in vitro* data demonstrating rCx36-tubulin interaction with the CTB region.

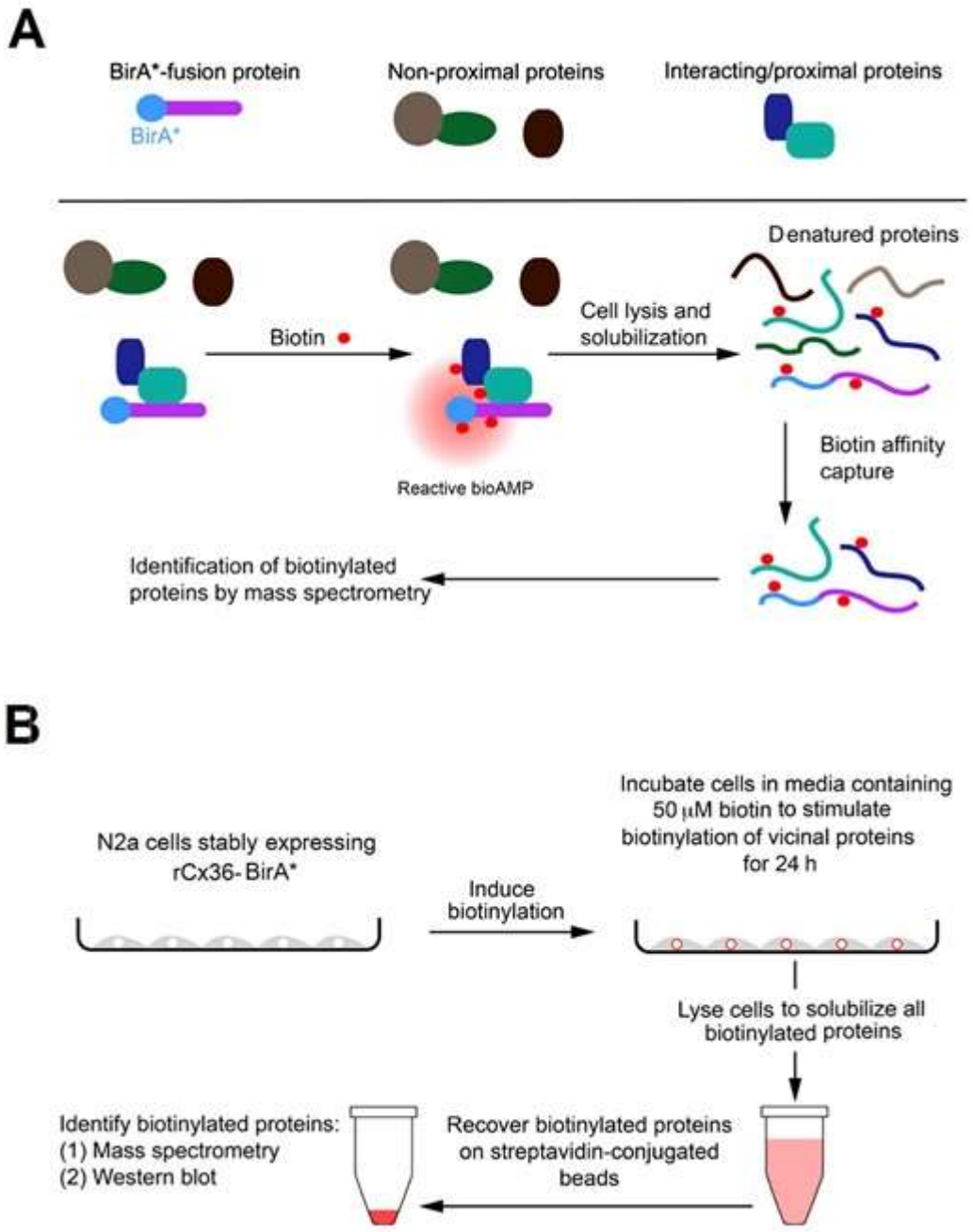

Figure 9: Schematic diagram of the BioID method.
(A) The promiscuous bacterial ligase BirA* is fused to the bait protein of interest and is responsible for the selective biotinylation of proximal proteins once expressed in eukaryotic cell lines. Upon cell lysis and protein denaturation, biotinylated proteins are isolated via biotin affinity capture and identified by mass spectrometry and/or western blot analysis. **(B)** For use in this thesis, N2a cells were transfected with rCx36-BirA* and treated with 50 µM biotin 24 h post-transfection. Biotinylation was carried out over a time span of 24 h. Upon cell lysis, the biotin-labelled fraction was recovered on streptavidin-conjugated Dynabeads in accordance to the Dynabead MyOne Streptavidin purification procedure. Protein(s) of interest were identified via mass spectrometry and/or western blot analysis. *Modified from Roux, Kim, Raida, & Burke, 2012*

5.1.1 Cloning and Confirmation of rCx36-BirA Wild-type and Mutant Constructs

For the generation of the C-terminal fusion protein(s) used in the BioID methodology, PCR was performed for the amplification of the full-length rCx36 gene (*Rattus norvegicus*, 321 amino acids). Previously, full-length rCx36 was cloned into the pEGFP-N1 expression vector to generate pEGFP-rCx36, which served as the template DNA for amplification; all constructs were made readily available by the Dr. Georg Zoidl lab, Department of Biology, York University. PCR was carried out at an annealing temperature of either 52°C or 63°C. The rCx36 amplicons generated from PCR were confirmed via fractionation on a 1% agarose gel and identified by the presence of a band 975bp in length **(Figure 10)**. Since the annealing temperature of 52°C yielded unspecific bands, amplicons of rCx36 annealed at 63°C was chosen for subsequent purification.

PCR purified amplicons of rCx36 were ligated into the pJET 1.2 vector, chosen for its ability to clone quickly with high efficiency. The ligated products were transformed into *E.coli* DH5α competent cells and plated onto LB-AMP plates overnight for selection. Four single bacterial colonies were isolated and grown in LB-AMP media overnight and subjected to small-scale plasmid purification. To confirm positive clones as well as to excise rCx36 DNA from pJET 1.2, a restriction digest with EcoRI was performed. For re-ligation purposes, the vector plasmid pcDNA 3.1 MCS-BirA(R118G)-HA (abbreviated as pcDNA 3.1 BirA*) was also digested with EcoRI and treated with calf intestine alkaline phosphatase (CIAP) to prevent re-ligation of the vector; digest was confirmed by the presence of a band 6382bp in length **(Figure 11A)**. Upon the identification of positive clones, rCx36 was re-ligated to pcDNA 3.1 BirA* and subsequently transformed into DH5α *E.coli* for plating. Similarly, four single colonies were selected and grown overnight in LB-AMP followed by plasmid purification. Three pcDNA 3.1 BirA*-rCx36 positive clones were identified via restriction digest with EcoRI by the presence of a band 969 bp **(Figure 11B)**. A second restriction digest with BamHI confirmed one clone in the correct orientation by the presence of a band 899bp in length **(Figure 11C)**.

Using this method we were able to successfully generate pcDNA 3.1 BirA*- rCx36 Δ175-196 and Δ279-292 and fusion constructs, which contained deletions in the CLB and CTB domains respectively, to be used for further studies. The pEGFP-N1 expression vector with the rCx36 Δ279-292- and rCx36 Δ175-196 genes were used as template DNA for PCR amplification; constructs

were made readily available by the Dr. Georg Zoidl lab. Amplification of the mutant rCx36 by PCR was carried out at an annealing temperature of 52°C to account for the reduction in DNA base pair length. Upon confirmation of mutant amplicons, the DNA was purified and cloned into pcDNA 3.1 BirA* as previously described. Restriction digest with BamHI revealed one positive clone in the correct orientation for pcDNA 3.1 BirA*-rCx36 Δ175-196 **(Figure 12A)** and three clones for pcDNA 3.1 BirA*-rCx36 Δ279-292 as indicated by a band 833bp and 857bp respectively **(Figure 12B)**.

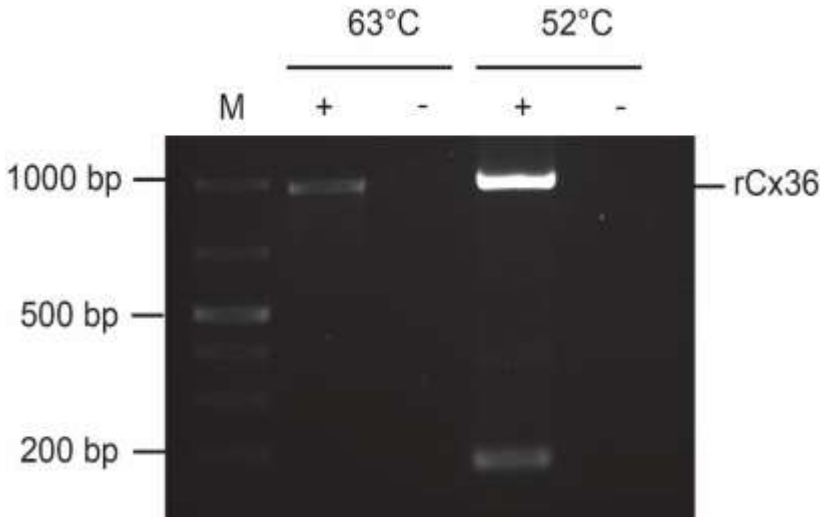

Figure 10| Amplification of the rCx36 gene from pEGFP-rCx36 template DNA.
Amplicons of the rCx36 gene generated from pEGFP-N1-rCx36 template DNA via PCR with annealing temperatures of either 63°C or 52°C. "+" indicates the presence of the template whereas "-" indicates the absence of the template DNA; in the latter case nuclease-free water served as the negative control. Full length rCx36 protein coding region was identified by the presence of a band 975bp. 1% agarose gel with ethidium bromide (EtBr); M: marker, bp: base pairs.

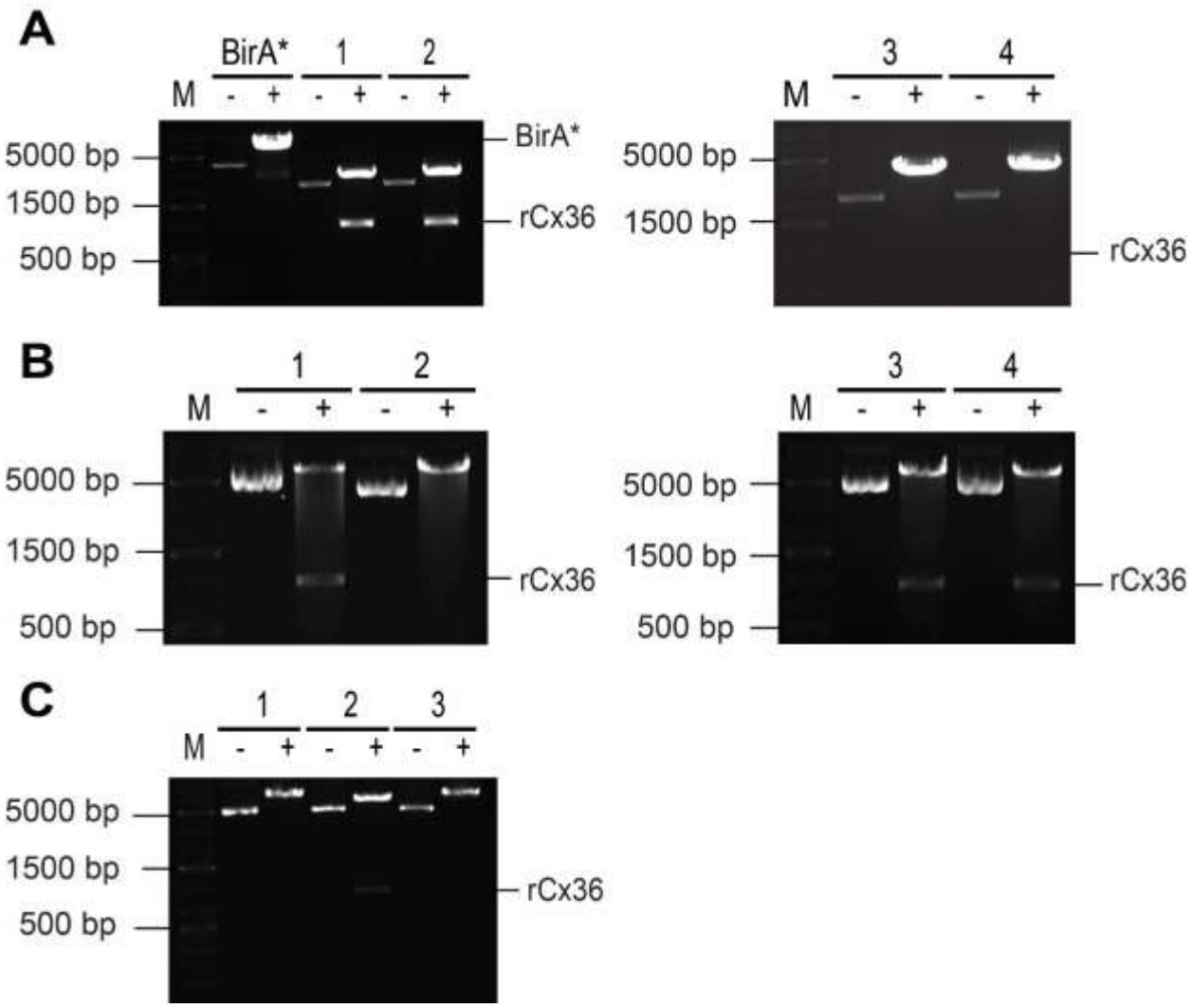

Figure 11| Confirmation of pcDNA 3.1 BirA*-rCx36 fusion constructs.
(A) Restriction digest of the pcDNA 3.1 BirA* plasmid vector and four clones post pJET1.2-rCx36 ligation and transformation with *E. coli*; restriction digest was achieved with EcoRI. Two positive clones for rCx36 were identified (#1 and #2) by the presence of a band 969bp; similarly pcDNA 3.1 BirA* was confirmed by a band 6382bp. **(B)** Positive clones previously identified were excised, purified and re-ligated to the pcDNA 3.1 BirA* vector plasmid. Four clones were selected for DNA extraction and subsequently digested with EcoRI. Clones #1, 3 and #4 were identified as positive for the insertion of full length rCx36 gene by the presence of a band 969bp in length as indicated. **(C)** Restriction digest of pcDNA 3.1 BirA*-rCx36 DNA purified from the three previously identified positive clones was achieved with BamHI to confirm orientation. Correct orientation of rCx36 is denoted by a band approximately 899bp whereas the incorrect orientation is denoted by a band approximately 100bp. One clone (#2) was identified as possessing the full length rCx36 gene in the correct orientation, housed within the pcDNA 3.1 BirA* vector. 1% agarose gel with ethidium bromide (EtBr); M: marker, bp: base pairs. "+" indicated presence of respective restriction enzyme; "-" indicates absence of restriction enzyme where water served as the control.

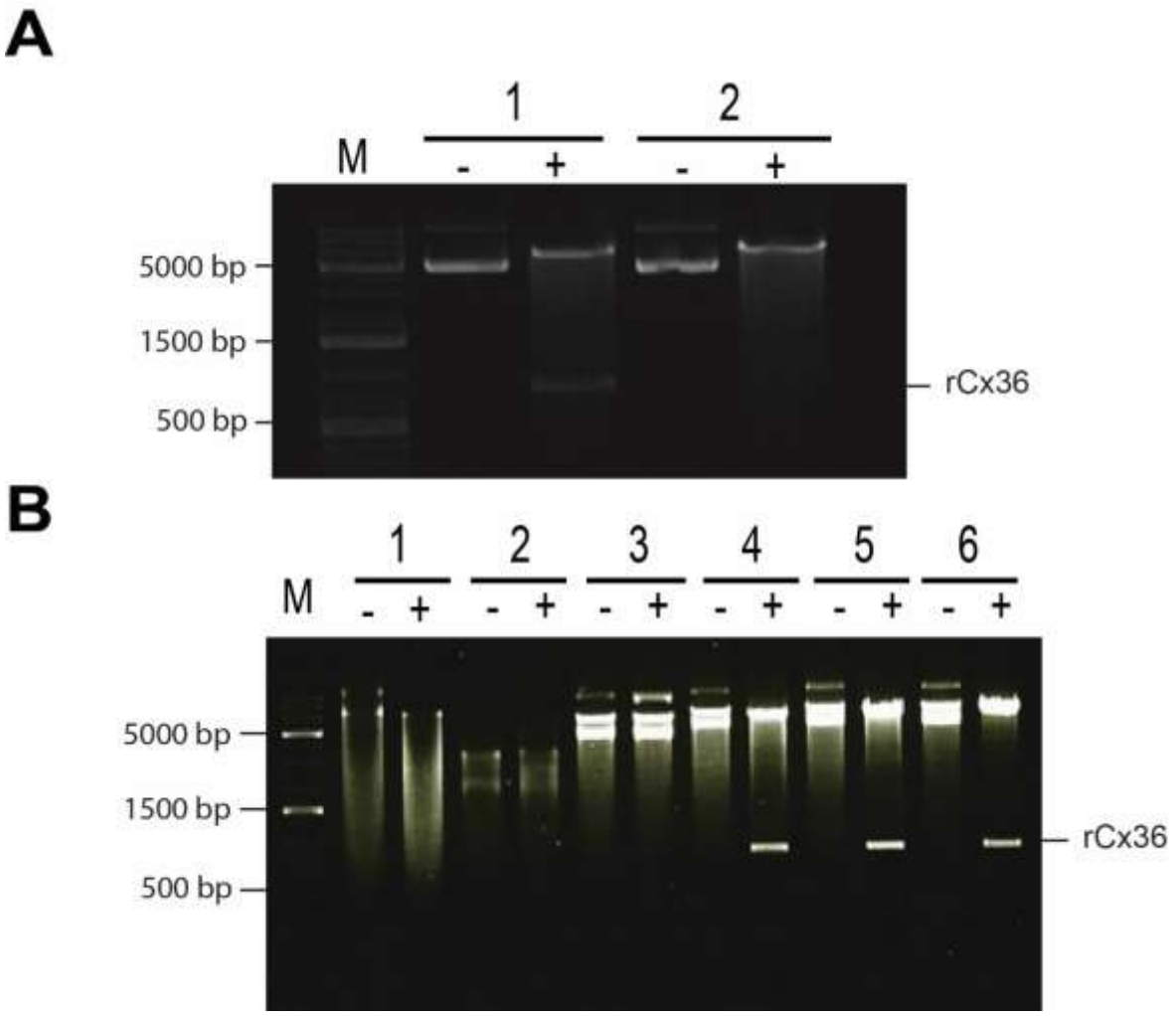

Figure 12| Confirmation of the pcDNA BirA*-rCx36 Δ279-292 and -Δ175-196 fusion constructs.
(A) Following ligation of rCx36 Δ175-196 to pJET 1.2 and re-ligation to the pcDNA 3.1 BirA* vector, two clones were identified as positive for the insertion of the rCx36 Δ175-196 gene. Clones were digested with HindIII to confirm orientation; correct orientation of pcDNA 3.1 BirA-rCx36 Δ175-196 is denoted by a band 833bp whereas the incorrect orientation is denoted by a band approximately 100bp. Clone #1 was identified as possessing the rCx36 Δ175-196 gene in the correct orientation. (**B)** Similarly, post-ligation to the pcDNA 3.1 BirA* vector, clones for rCx36 Δ279-292 were digested with BamHI to confirm orientation. By this, three positive clones were identified by the presence of an 857bp band. 1% agarose gel with ethidium bromide (EtBr); M: marker, bp: base pairs. "+" indicated presence of respective restriction enzyme; "-" indicates absence of restriction enzyme where distilled water served as the control.

5.1.2 Confirmation of BirA* Fusion Protein Expression

To confirm the expression of our target protein(s), N2a cells were transfected with pcDNA 3.1 BirA* -rCx36 WT, -Δ175-196, or -Δ279-292. Since three clones were generated for the pcDNA 3.1 BirA*-rCx36 Δ279-292 construct, all were tested to determine if differences in expression quality existed. Small scale whole cell protein lysates were prepared and subsequently fractionated on a 10% SDS-PAGE gel. Proteins were transferred onto a nitrocellulose membrane for western blotting and the anti-HA primary antibody was applied for validation of protein expression. Expression of BirA* was confirmed by the presence of a 30kDa band whereas all rCx36-BirA* fusion proteins (abbreviated as WT, Δ175-196 and Δ279-292) were confirmed by the presence of a band approximately 60kDa **(Figure 13)**. Although detection of rCx36 Δ279-292-BirA* was observed, fluorescence intensity in all three samples was lesser than that of the wild-type indicating that this mutant was poorly expressed in our cell model; therefore suggesting that this may be a region of interest in mediating expression. As such, this result was taken into consideration for the BioID pull-down experiments to follow. Furthermore, since the first sample of rCx36 Δ279-292-BirA* had the least amount of protein expression, it was not used for further studies.

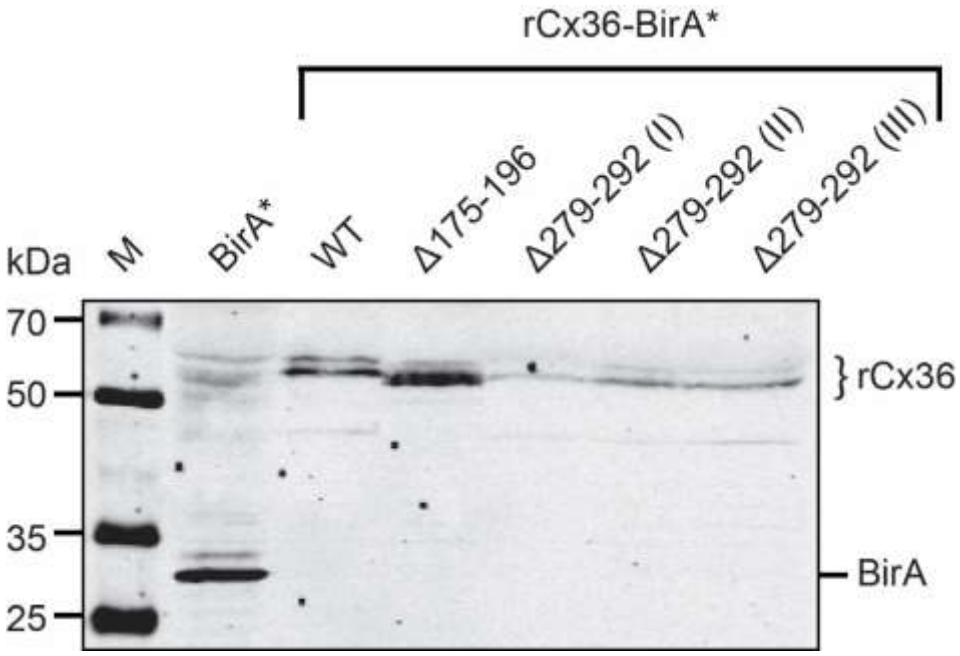

Figure 13| Western blot analysis of rCx36 -WT, -Δ279-292- and -Δ175-196-BirA* fusion proteins.
N2a cells transfected with pcDNA 3.1 BirA*-rCx36 WT, -Δ175-196 or -Δ279-292 were lysed 48h post-transfection. Lysates were fractionated on a 10% SDS-PAGE gel and subsequently used for western blot analysis with the anti-HA and anti-mouse IRDye800 primary and secondary antibodies respectively. BirA* was confirmed by the presence of a band 30kDa and showed strong protein expression. Similarly, strong protein expression was shown for wild-type rCx36-BirA* and rCx36 Δ175-196-BirA* as confirmed by a band approximately 60kDa. Poor protein expression was noted for all three samples of rCx36 Δ279-292-BirA*; the first sample in particular displayed minimal expression and was not used in future analysis.

5.1.3 Confirmation of Eluted Wild-type rCx36-BirA* Fusion Protein Expression

To confirm the expression of the BirA* fusion protein throughout the biotinylation assay, the neuroblastoma cell line Neuro2a (N2a) was transfected with wild-type rCx36 (pcDNA 3.1 BirA*-rCx36). Approximately 900,000 N2a cells were seeded and cultured in supplemented DMEM overnight. Cells were transfected with 2.0 µg of DNA and 50µM biotin was applied 24h post-transfection. Cells were lysed 24h post-biotin application and samples were collected throughout the biotinylation assay for western blot assessment (see 4.3.4 for details). Protein lysates were fractionated on a 10% SDS/PAGE gel and transferred to a nitrocellulose membrane for western blotting. The primary antibody anti-HA was applied for the detection of the wild-type rCx36-BirA* fusion protein. Additionally, for the detection of biotinylated proteins, the conjugate enzyme streptavidin-HRP was also applied. The following sample fractions were collected for analysis:

N2a pellet, lysate prior to Dynabead incubation (pre-lysate), lysate post-incubation (post-lysate), last wash fraction (wash) and two elution fractions.

Western blot analysis revealed modest levels of biotinylated protein in N2a cells expressing wild-type rCx36-BirA* in the pellet and pre-lysate fractions. Absence of biotinylated proteins in the post-lysate fraction indicated that streptavidin-conjugated beads were able to successfully capture and isolate biotin-labeled proteins. Elution from the beads resulted in a highly enriched fraction of biotinylated proteins, most of which were successfully eluted in the initial fraction. Furthermore, biotinylated proteins were not detected in the last wash fraction confirming that elutions were strictly comprised of biotinylated proteins that had bound to the streptavidin-conjugated beads **(Figure 14A)**. As predicted, rCx36-BirA* detection was most notable in the first elution fraction and negligible in the pellet fraction. Additionally, due to low protein:solvent ratio, detection of rCx36-BirA* was minimal in the pre-lysate fraction **(Figure 14B)**. Taken together, these results served as an indication that BirA* was capable of biotinylating proximal proteins including wild-type rCx36 to which it is fused. By this it was concluded that rCx36-BirA* was successfully expressed and eluted during the affinity capture of biotinylated proteins.

To identify potential interacting partners of rCx36, the first elution sample was again fractionated on a 10% SDS/PAGE gel in parallel with the first elution fraction of a control biotinylation pull-down performed with BirA* and subsequently stained with PageBlue™ Protein Staining Solution. Mass spectrometry was performed to identify interacting partners that were unique to rCx36 in comparison to the BirA* control. Among the candidates yielded, the tubulin beta-3 chain (βIII-tubulin) was identified as being unique to rCx36, confirming *in vivo* that tubulin is an interaction candidate of rCx36 either directly or indirectly **(*See Appendix D*)**. Furthermore interaction between rCx36 may occur at a region of βIII-tubulin that is not conserved across tubulin heterodimer monomers and isotypes.

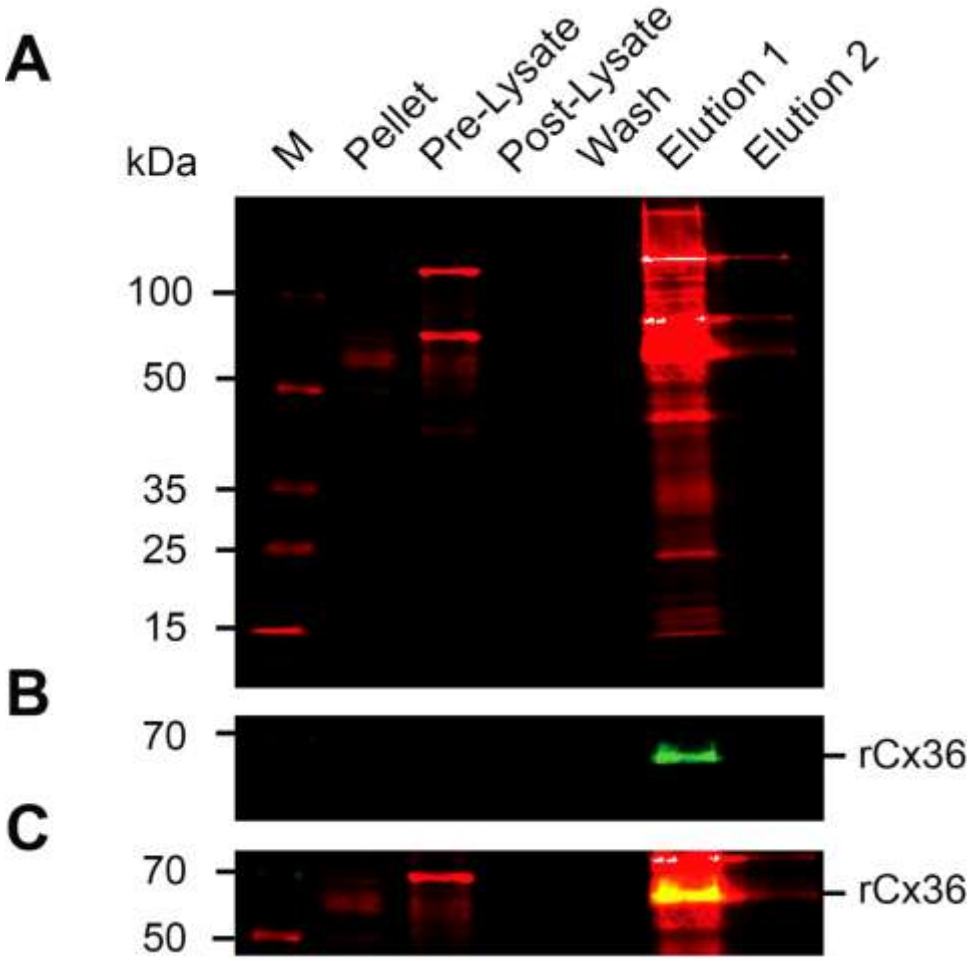

Figure 14| Western blot analysis of biotinylated proteins captured via BioID confirms the presence of rCx36-BirA*.

(A) Western blot analysis of protein fractions collected throughout the BioID methodology. Samples were prepared post-transfection of N2a cells with wild-type rCx36-BirA* and fractionated on a 10% SDS-PAGE for western blotting with the anti-HA primary antibody and anti-mouse IRDye800 secondary antibody; conjugate enzyme Streptavidin-HRP was also applied for the detection of biotinylated proteins. Biotinylated proteins, as shown in red, were detected modestly in the pellet and pre-lysate and second elution fractions and highly concentrated in the first elution. Absence of biotinylated protein in the post-lysate and wash fractions indicates that the biotin affinity capture was successful. **(B)** Wild-type rCx36-BirA* was shown to be detected modestly in the pellet and pre-lysate fractions and heavily concentrated in the first elution fraction. Presence of a band approximately 60kDa indicated that wild-type rCx36-BirA was amongst proteins tagged with biotin. **(C)** Overlay of biotinylated proteins and rCx36-BirA* detection.

5.1.4 Detection of Tubulin via Biotin Affinity Capture

For the detection of tubulin via BioID, sample preparation remained as previously mentioned (also see 4.3.4) and the anti-β-tubulin primary antibody was utilized for the detection of tubulin across the various fractions. We hypothesized that if rCx36 and tubulin were interacting partners *in vivo*, tubulin would follow a similar detection pattern as previously observed with wild-type rCx36-BirA*. Western blot analysis revealed that tubulin was modestly detected in the pellet fraction and prominent in the pre-lysate and post-lysate fractions, likely due to the naturally high abundance of protein. However, it was noted that the fluorescence signal in the post-lysate was lesser than that of the pre-lysate which served as a preliminary indication that a small subset of the total cell tubulin protein had interacted with wild-type rCx36-BirA*, and was successfully isolated during the biotin affinity capture procedure. In support of this, a reduced amount of tubulin was detected in the first elution fraction in comparison to the pre- and post-lysates. Absence of tubulin detection in the wash fraction further confirmed that eluted protein was representative of only that which had been biotinylated by wild-type rCx36-BirA* **(Figure 15)**. These results indicated that rCx36 was capable of interacting with tubulin; however, whether the interactions was direct or indirect *in vivo* had yet to be established.

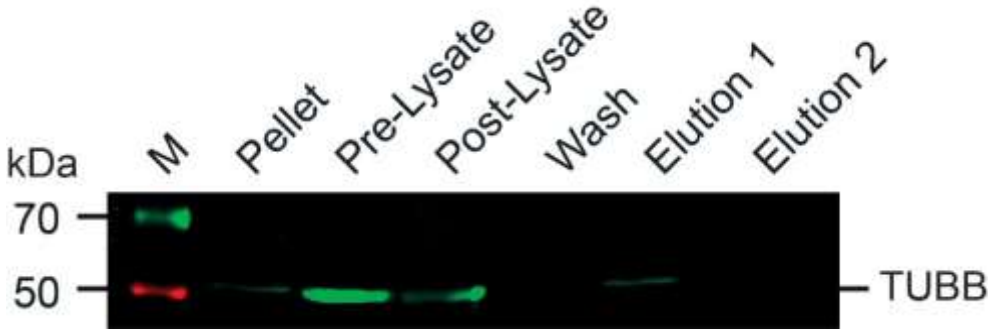

Figure 15| Biotin affinity capture of tubulin with wild-type rCx36-BirA*.
Western blot analysis of protein fractions collected throughout the BioID methodology. Samples were prepared post-transfection of N2a cells with wild-type rCx36-BirA* and fractionated on a 10% SDS-PAGE for western blotting with anti-β-tubulin and anti-mouse IRDye800 primary and secondary antibodies respectively. Tubulin (approx. 50kDa seen in green) was detected in all fractions with the exception of the wash and second elution. The low intensity band in the 1st elution is representative of the small fraction of tubulin that interacted with the rCx36-BirA fusion in comparison to total tubulin available in the N2a cells.

5.1.5 BirA* Interaction with Tubulin Indicates Non-Mutuality

To assess whether the BioID methodology was subject to false-positive results, a control experiment was designed to determine if BirA* was capable of interacting with tubulin in the absence of rCx36. We hypothesized that if the relationship between rCx36 and tubulin was mutually exclusive, tubulin would not be detected in the eluted fractions of the control sample. N2a cells were transfected with either pcDNA 3.1 BirA*-rCx36 or pcDNA 3.1 BirA* for the production of rCx36-BirA* and BirA* respectively; samples were prepared as previously described (see section 4.3.3 for details). For analysis purposes, the pre-lysate, wash and first elution fractions were used in the confirmation of BirA* and rCx36-BirA* expression and detection of tubulin. As predicted, biotinylated proteins in N2a cells expressing BirA* alone were present in the same fractions as with rCx36-BirA*. However, less biotinylated protein was eluted in the elution fraction of BirA* in comparison to rCx36-BirA* suggesting that BirA* alone interacts with a minimal amount of proteins; fusion to rCx36 allowed for a broader range of interactions. Additionally, rCx36-BirA* was exclusively detected in the pre-lysate and elution fraction indicating that it had been biotinylated by BirA*; BirA* was not present in the respective elution fraction indicating the inability to self-associate **(Figure 16A)**.

In addition to the pre-lysate fractions, tubulin was also detected in the elution fractions of both rCx36-BirA* and BirA* expressing cells **(Figure 16B)**. This result indicated that BirA* alone was sufficient to facilitate interaction with tubulin. As determined by the fluorescence intensity, BirA* interaction with tubulin (0.103±0.002 relative fluorescence units, RFU) was 29% greater than that of the wild-type (0.073±0.001 RFU), exposing a quantitative limit to the amount of tubulin rCx36 is capable of interacting with **(Figure 16C)**. Since the BioID methodology was not able to discriminate between tubulin interaction with the BirA* control, we could not conclude that the rCx36-tubulin relationship was mutually exclusive and therefore rejected our hypothesis.

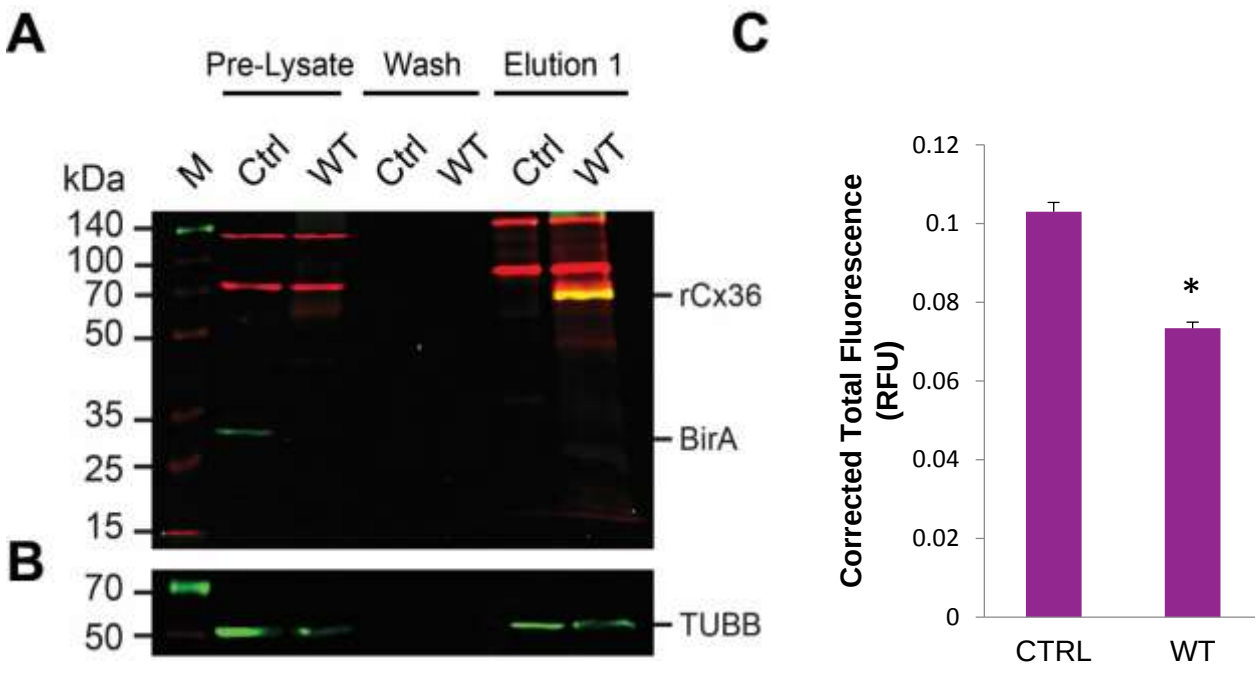

Figure 16| Western blot and fluorescence analysis of the biotin affinity capture of tubulin with rCx36-BirA* and BirA*.

(A) Western blot analysis of the pre-lysate, wash and first elution protein fractions collected throughout the BioID methodology. N2a cells were transfected to express either wild-type rCx36-BirA* (WT) or the control BirA* (Ctrl) and fractionated on a 10% SDS-PAGE for western blotting with anti-HA and Streptavidin-HRP primary antibodies and anti-mouse IRDye800 secondary antibody. Biotinylated proteins, shown in red, were detected in the pre-lysate and first elution fractions. BirA*, confirmed by the detection of a band 30kDa (shown in green), was shown not to self-associate since it was not detected in the respective elution fraction. Wild-type rCx36-BirA was confirmed by a band approximately 60kDa (shown in yellow). **(B)** Samples, prepared as previously described, were tested for the detection of tubulin with the anti-β-tubulin and anti-mouse IRDye800 primary and secondary antibodies respectively. Tubulin was detected in the pre-lysate and first elution fraction of both the WT and Ctrl as confirmed by the presence of a band approximately 50kDa (shown in green). **(C)** Corrected Total Fluorescence of the WT and CTRL elution bands were averaged across three measurements. The BirA* control displayed a significantly higher fluorescence intensity (RFU) in comparison to wild-type rCx36-BirA indicating that BirA* interaction with tubulin was more accessible.

5.1.6 Deletion of the rCx36 Tubulin Binding Region

Since it was previously determined that BirA* was capable of interacting with tubulin, a second control experiment was performed in parallel, designed to find rCx36-specific interactions. In addition to wild-type rCx36-BirA*, two mutants were utilized; rCx36 Δ175-196-BirA*, which housed a deletion in the cytoplasmic loop, served as a positive control and rCx36 Δ279-292-BirA*, which lacked the predicted tubulin binding region in the cytoplasmic terminal domain, as the negative control. We hypothesized that if the rCx36 interaction with tubulin was abolished with

the expression of the C-terminal mutant rCx36 Δ279-292-BirA*, a significantly reduced fluorescence signal would be detected in the respective elution fraction in comparison to wild-type rCx36-BirA*. As such, the signal detected in the rCx36 Δ279-292-BirA* elution would account specifically for the interaction between tubulin and BirA*. Similarly, by this notion we predicted that tubulin would be detected in the eluted fraction of the positive control rCx36 Δ175-196-BirA* and this would be comparable to its wild-type counterpart. For comparative purposes, each control experiment was done in parallel with wild-type rCx36-BirA* with the pre-lysate, post-lysate, wash and first elution fractions chosen for detection against tubulin, and confirmation of BirA* fusion variants and biotinylated proteins.

The pattern of detection for biotinylated proteins were consistent between wild-type and positive and/or negative controls; biotinylated proteins were present in the pre-lysate and elution fractions and absent in the post-lysate and wash fractions indicating successful affinity capture of biotinylated proteins. Additionally, the amount of biotinylated proteins detected in these fractions were comparable between wild-type and respective controls suggesting that the rCx36 mutant proteins were still sufficient to allow for protein-protein interactions despite the partial deletion of the cytoplasmic loop region (Δ175-196) and the cytoplasmic-terminal domain (Δ279-292). As expected, the fusion proteins were highly concentrated in the elution fractions; wild-type rCx36-BirA* was confirmed by the presence of a band approximately 60kDa where as both rCx36 Δ175-196-BirA* and rCx36 Δ279-292-BirA* displayed a slight shift in molecular weight, indicative of the smaller protein size due to the partial deletions **(Figure 17A-B)**.

Due to its high abundance, tubulin was detected in the pre-lysate and post-lysate fractions of the wild-type rCx36-BirA*, positive control rCx36 Δ175-196-BirA* and negative control rCx36 Δ279-292-BirA*. Again, absence of tubulin detection in the wash fractions indicated that eluted the tubulin were interacting partners of the respective fusion protein. However, a significant reduction in the detection of tubulin was observed for both the positive control and negative control elution fractions in comparison to the respective wild-type **(Figure 17C-D)**. Corrected total fluorescence of rCx36 Δ175-196-BirA* (0.0155±0.0003 RFU) displayed a 36% reduction with respect to the wild-type (0.0242±0.0003 RFU). Similarly, corrected total fluorescence of rCx36 Δ279-292-BirA* (0.0038±0.0002 RFU) was reduced by 74% in comparison to the respective wild-

type (0.0148±0.00006 RFU) **(Figure 17E-F)**. These results suggested that tubulin was still capable of close proximity interaction with rCx36 without the requirement of the hypothesized protein binding domain, likely attributed to interactions with BirA*. However, a significant reduction in tubulin detection signal was observed with the rCx36 Δ279-292 mutant variant suggests that tubulin interaction is at least in part rCx36-specific. Since the positive control rCx36 Δ175-196-BirA* also showed a reduction in fluorescence intensity, we concluded that the BioID method was not suitable to determine the tubulin binding region by *in vivo* affinity capture.

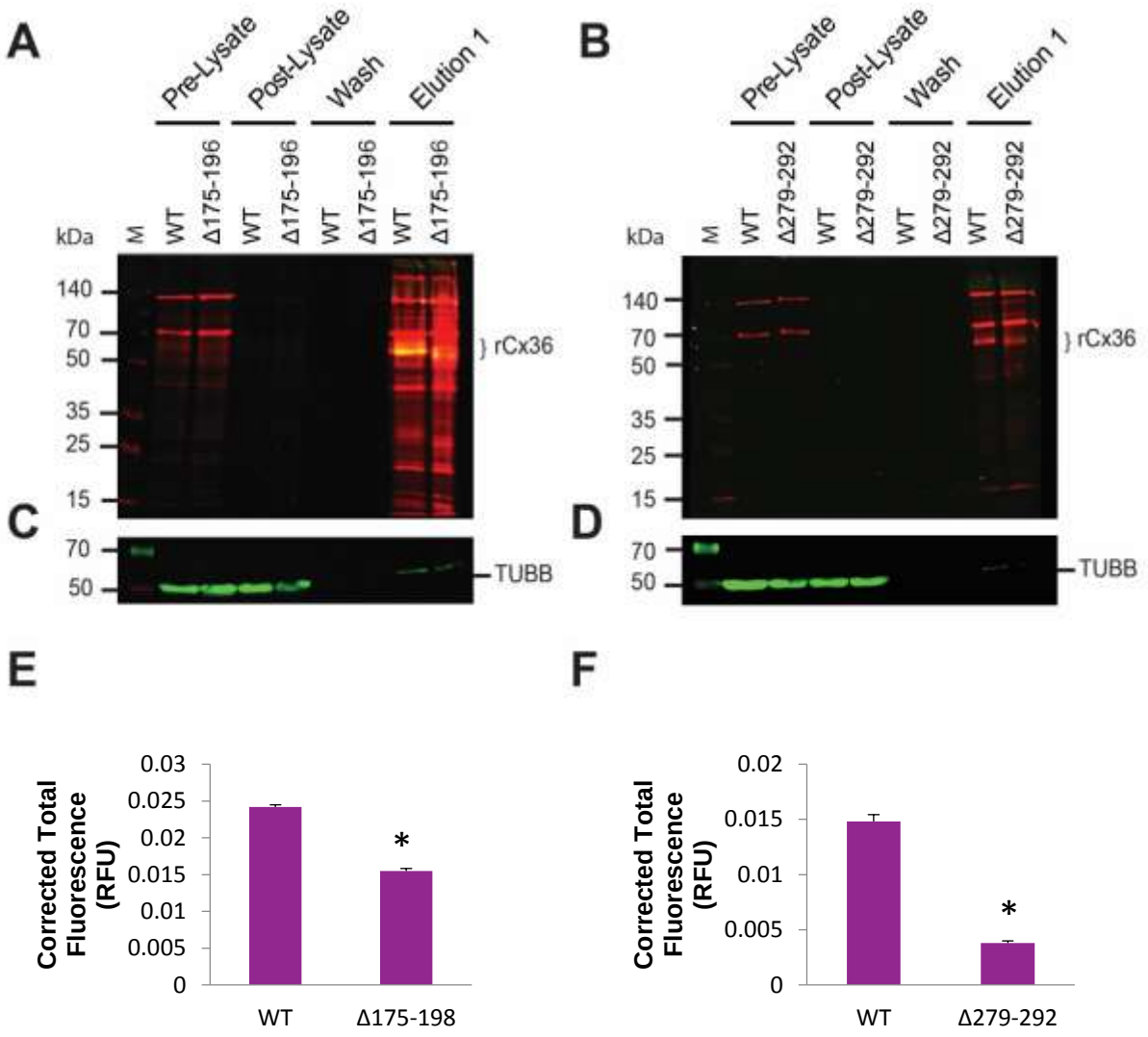

Figure 17| Biotin affinity capture and tubulin detection achieved with rCx36 Δ175-196-BirA* and -Δ279-292-BirA* fusion proteins.

(A-B) Western blot analysis of the pre-lysate, post-lysate, wash and first elution protein fractions collected throughout the BioID methodology. Samples were prepared post-transfection of N2a cells with wild-type rCx36-BirA* (WT) in parallel with either (A) rCx36 Δ175-196-BirA* as a positive control or (B) rCx36 Δ279-292-BirA*. Samples were fractionated on a 10% SDS-PAGE for western blotting with anti-HA and Streptavidin-HRP primary antibodies and anti-mouse IRDye800 secondary antibody. Biotinylated proteins, shown in red, were detected in the pre-lysate and first elution fractions. Wild-type rCx36-BirA* (A and B) was confirmed by the presence of a band approximately 60kDa in the first elution fraction. Similarly, (A) Cx36 Δ175-196-BirA* and (B) rCx36 Δ279-292-BirA* was also confirmed, displaying a small shift in molecular weight respective to the reduction in protein size. **(C-D)** Samples, were tested for the detection of tubulin with the anti-β-tubulin and anti-mouse IRDye800 primary and secondary antibodies respectively. Tubulin was detected in the pre-lysate, post-lysate and first elution fractions of both the WT (C and D), (C) positive and (D) negative controls as confirmed by the presence of a band approximately 50kDa (shown in green). **(E-F)** Corrected total fluorescence of the WT (E and F), positive control (E) and negative control (F) elution bands were averaged across three measurements. Cells expressing rCx36 Δ175-196-BirA* displayed a 36% reduction in fluorescence intensity of tubulin in comparison to wild-type rCx36-BirA* indicating a decrease in interaction with tubulin. Similarly, a 74% reduction in fluorescence intensity of rCx36 Δ279-292-BirA* was found in comparison to the control indicating that tubulin interaction was severely impacted.

5.2 DETECTION OF CYTOSKELETAL INTERACTION AT THE CX36 NEXUS USING FRAP

Since it was concluded that the BioID methodology was not selective enough to confirm amino acids Lys279-Ala287 as the rCx36 tubulin binding region in vivo, we continued our investigations using an alternative *in vivo* technique termed fluorescence recovery after photobleaching (FRAP) to complement existing *in vitro* data. Since this technique utilizes fluorescent signals, EYFP- and/or EGFP-tagged fusion proteins were selected for use in the following studies.

5.2.1 Confirmation of Fluorescently-tagged rCx36 WT and CLB/CTB Deletion Mutant Expression

Previously, full-length rCx36 WT (*Rattus norvegicus*, 321 amino acids) and mutants, Δ182-198, 279-292, Δ182-198, Δ279-292 and Δ175-196, were cloned into the pEYFP-N1 expression vectors to generate EYFP C-terminally tagged fusion proteins; all constructs were made readily available by the Dr. Georg Zoidl lab, Department of Biology, York University. These four mutants: (1) rCx36 Δ182-198, 279-292, (2) rCx36 Δ182-198, (3) rCx36 Δ279-292 and (4) rCx36 Δ175-196, carry deletions in the regions of the rCx36 protein considered critical for transport and plasticity (Alev et al., 2008).

To verify the expression of the fusion proteins, N2a cells were transfected with 200ng of the respective DNA and subsequently lysed with 1x laemmeli sample buffer, 48h post-transfection. Whole cell protein lysates were fractionated on a 10% SDS/PAGE gel and transferred to a nitrocellulose membrane for western blotting; anti-GFP primary antibody was utilized for the detection and validation of the rCx36-EYFP wild-type and mutant expression. **(Figure 18)**. As determined by the results of the western blot, we were successfully able to detect wild-type rCx36-EYFP (approx. 62kDa) and mutant variants with the anti-GFP antibody; β-actin served as a loading control. A reduction in molecular weight was observed in all mutants in comparison to the wild-type due to the partial deletion of protein sequence(s). Both wild-type and mutant rCx36 variants showed similar levels of expression and were used for further studies.

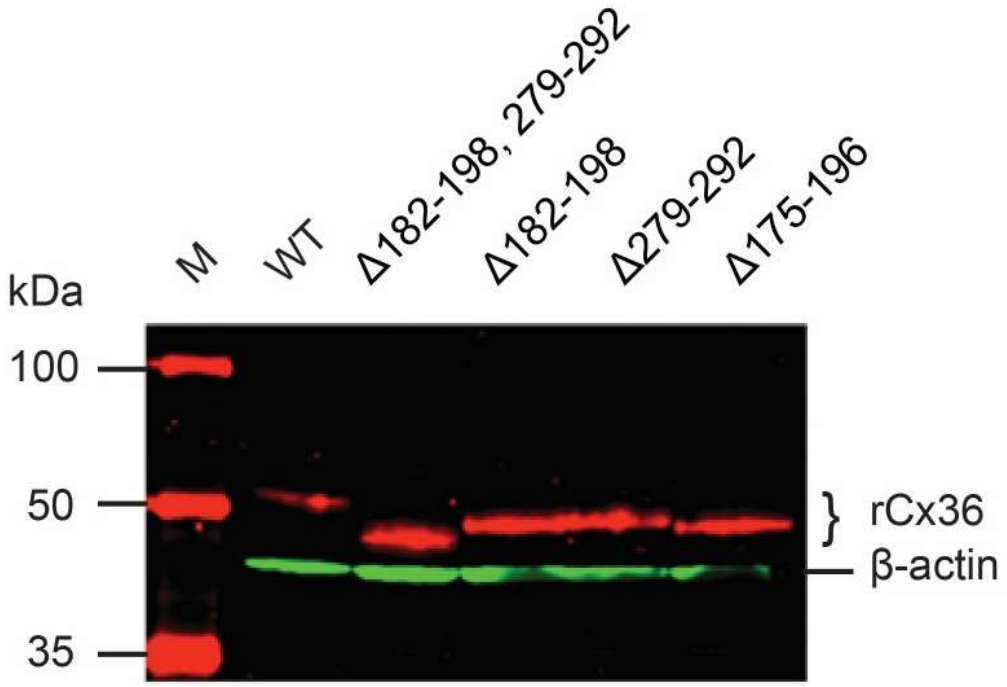

Figure 18| Expression confirmation of EYFP-tagged rCx36 wild-type and deletion mutant variants in N2a cells. N2a cells transfected with pEYFP-rCx36 WT, -Δ182-198, 279-292, -Δ182-198, -Δ279-292 or -Δ175-196 were lysed 48h post-transfection. Lysates were fractionated on a 10% SDS-PAGE gel and subsequently used for western blot analysis with the anti-GFP (denoted in red) and anti-β-tubulin primary antibodies; anti-mouse IRDye800 and anti-rabbit IRDye 680 were the secondary antibodies applied. Expression of rCx36-EYFP was confirmed by the presence of a band approximately 62kDa. Additionally, rCx36 mutant expression was confirmed, displaying a shift in molecular weight respective to the reduction in protein size due to the partial deletion of protein sequence(s).

5.2.2 Localization and Quantitative Analysis of Wild-type rCx36-EYFP and Mutants

To start, localization studies were performed to confirm typical gap junction plaque formation with the rCx36 wild-type and deletion variants previously mentioned. N2a cells were transfected with the respective pEYFP-rCx36 DNA (WT, -Δ182-198, 279-292, -Δ182-198, -Δ279-292 or -Δ175-196) and imaged using Zeiss LSM 700 confocal microscope system, 48h post-transfection. Cells were assessed qualitatively for the ability of GJP formation and presence of intracellular deposits. Qualitative assessments were complimented quantitatively with measurements of mean corrected total fluorescence of the gap junction plaque (CTF_{GJP}), corrected total cell fluorescence (CTF_{cell}) and mean gap junction plaque area (μm^2). Wild-type rCx36-EYFP was used as a comparative reference throughout these analyses to identify deviances in the aforementioned parameters.

Through these studies we have confirmed that rCx36 wild-type and mutant variants were capable of localizing into gap junction plaques at the plasma membrane of two adjoining cells **(Figure 19A-E)**. Interestingly, rCx36 Δ175-196 (1.25±0.21 μm^2) showed a significant reduction in gap junction plaque area in comparison to the wild-type (2.22± 0.19μm2, p=0.002). However, the mean gap junction plaque areas of cells expressing rCx36 Δ182-198, 279-292 (2.33±0.37 μm^2), -Δ182-198 (1.38±0.23 μm^2), and -Δ175-196 (1.75±0.19 μm^2) were indistinguishable from the wild-type **(Figure 19F)**. Localization studies also revealed that the presence of intracellular aggregates was variable across rCx36 mutant variants in comparison to the wild-type. This effect was most pronounced in rCx36 Δ175-196 expressing cells, which showed an increase in intracellular deposits and decrease in observable puncta. To quantify the amount of rCx36 protein at the plaque, the corrected total GJP fluorescence (CTF_{GJP}) was measured and averaged across the population of wild-type and mutant transfected cells. In doing so, the averaged CTF_{GJP} of N2a cells expressing rCx36 mutant variants were shown to be significantly reduced in comparison to the wild-type expressing cells (58335.13±8949.49 RFU) **(Table 10)**.

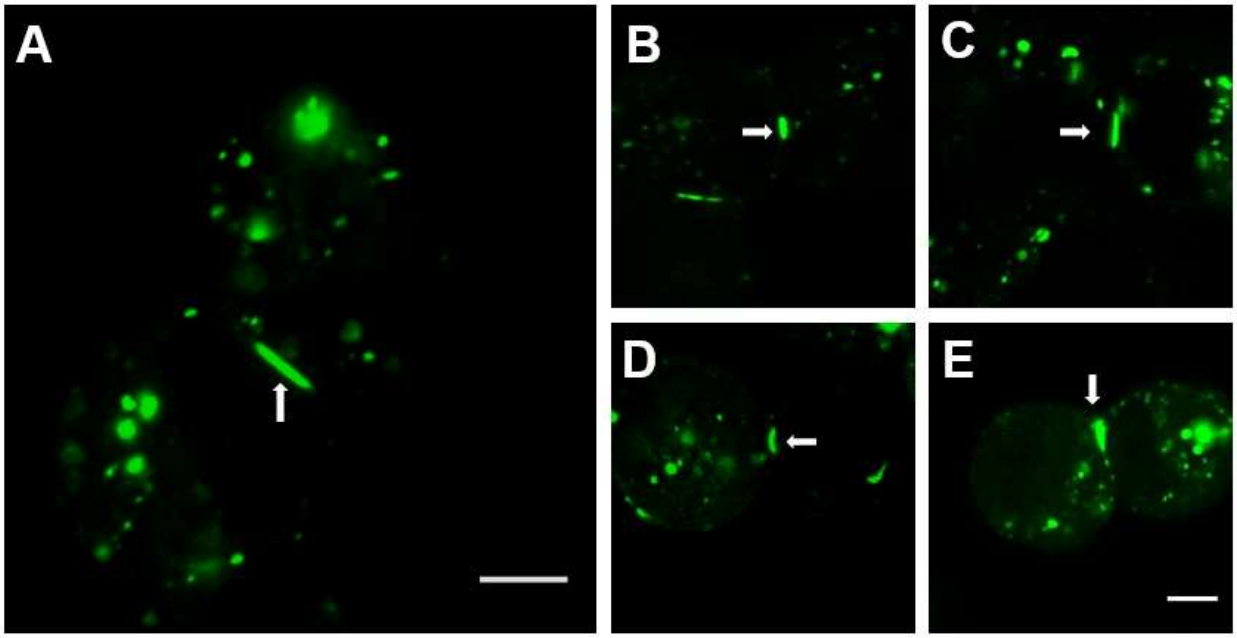

F

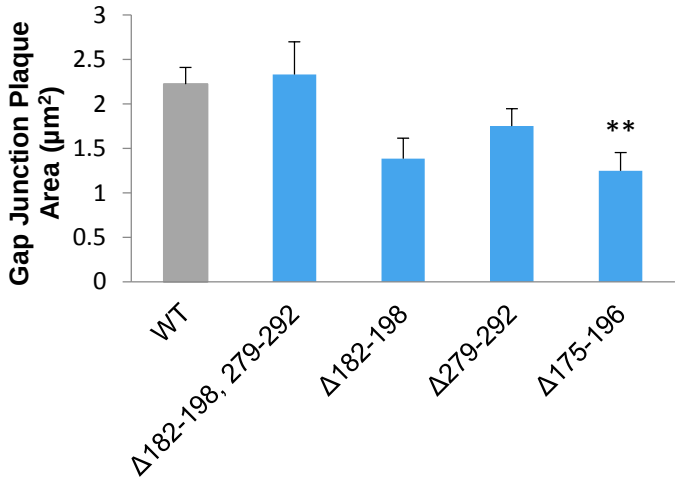

Figure 19| Localization and GJP area of rCx36-EYFP WT and mutant variants in N2a cells.
N2a cells were transfected with pEYFP-rCx36 WT, -Δ182-198, 279-292, -Δ182-198, -Δ279-292 or -Δ175-196 vector constructs to determine localization. Confocal images were obtained 48h post transfection. rCx36-EYFP **(A)** -WT, (**B)** -Δ182-198, 279-292, **(C)** -Δ182-198, **(D)** -Δ279-292 or **(E)** -Δ175-196 displayed gap junction formation at the plasma membrane of two adjoining cells as indicated by the arrows. An increase in intracellular deposits was observed with rCx36 Δ175-196. Scale bar 5µm. **(F)** Gap junction plaque area (µm²) was averaged across pEYFP-rCx36 wild-type and mutant variant transfected cells. N2a cells expressing rCx36 Δ182-198, 279-292, -Δ182-198 and -Δ279-292 were indistinguishable from the wild-type. A significant reduction in GJP area was observed for rC36-Δ175-196 expressing cells.

To ensure that the reduction in CTF_{GJP} was not a direct reflection of a reduction in whole cell protein production, corrected total cell fluorescence (CTF_{cell}) was measured, and averaged across the population of adjoining cells. In this way, the effect of cell stage or cell age on whole cell protein production could be normalized across the trials in which the measurements were taken. The CTF_{cell} of N2a cells expressing rCx36 mutant variants was determined to be indistinguishable in comparison to the wild-type **(Table 11)**. Therefore, it was concluded that the reduction in CTF_{GJP} of rCx36 mutant variants was not directly correlated to the total cell protein production and likely representing a reduction in hemichannel accumulation. As such, we speculated that amino acid residues spanning from 175-196 and 279-297 is involved in rCx36 trafficking, and insertion/removal of rCx36 at the gap junction plaque was compromised in its absence.

In addition to rCx36 Δ279-297, the mutant variant specific to tubulin, rCx36 Δ175-196 was of particular interest since this mutant displayed a significant reduction in observable puncta, GJP size and CTF_{GJP} in addition to increased intracellular deposits. We speculated that this region might be involved in a compensatory trafficking mechanism that afforded rCx36 Δ182-198, 279-292, -Δ182-198 and -Δ279-292 mutant variants gap junction plaque areas comparable to the wild-type.

Table 11: Corrected total fluorescence in GJP-coupled N2a cells.*

	WT	Δ182-198, 279-292	Δ 182-198	Δ175-196	Δ 279-297
CTF_{GJP}	58335.13±8949.49	**434.28±42.37**	**263.30±59.86**	**384.73±52.52**	**239.77±40.71**
p-value	-	**1.41^{-3}**	**4.00^{-4}**	**7.31^{-6}**	**6.76^{-5}**
CTF_{cell}	9376.16±2019.27	3362.71±418.57	9297.53±2915.06	3944.72±1286.13	4283.12±1731.38
p-value	-	1.19^{-1}	9.82^{-1}	6.38^{-2}	9.56^{-2}

*values determined to be significant from the wild-type are bolded.

5.2.3 Identification of a Potential Actin Binding Region

Since localization studies revealed atypical distribution in cells expressing the rCx36 Δ175-196 mutant variant, we suspected that this region may be critical for the stabilization and/or trafficking of rCx36. As such, a Eukaryotic Linear Motif (ELM) was performed to investigate short linear motifs of the rCx36 protein in all cell compartments with the motif probability cut-off set to 100. Output generated identified a potential actin binding domain (DCLEVKELAPHPSGLRTA) spanning amino acid residues Asp167-Ala184 **(*See Appendix E*)**. Since this region was largely deleted in the rCx36 Δ175-196 mutant, we hypothesized that actin may be an interacting partner of rCx36, and partial deletion of the binding motif modulating transport and/or stabilization of the protein post-insertion. Additionally, we speculated that amino acid residues between Ala175-Ala184 may be most critical in mediating the interaction since the deletion of aa: 175-196 alone was sufficient in altering the distribution and characteristics of the GJP.

Next, a sequence alignment was performed across species using the hypothesized rCx36 (*rattus norvegicus)* actin binding domain generated from ELM; in the case of zebrafish, the ortholog zfCx35 was used **(Figure 20A)**. Protein sequences were obtained from the NCBI Protein database and the alignment was achieved using ClustalW2 for the multiple sequence alignment tool. The selected species, human (*homo sapien*), chicken (*gallus gallus*) and zebrafish (*danio rerio*), all displayed a high degree of amino acid conservation of the hypothesized actin binding region inferring structural preservation and biological significance despite speciation. Similarly, sequence alignment of the hypothesized rCx36 actin binding domain was compared to full length rCx43 (382 amino acids) and full length rCx30 (261 amino acids) **(Figure 20B)**. Since it has been previously shown that actin interaction with rCx43 occurs indirectly, we hypothesized that the proposed actin binding domain of rCx36 would be minimally conserved. Additionally, alignment with rCx30, which has been shown to interact with actin directly, would expose the uniqueness of the hypothesized actin binding domain to rCx36. Results generated from ClustalW2 revealed minimal conservation of a potential actin binding domain when comparing neuronal rCx36 to rCx30 and rCx43 expressed in astrocytes, suggesting that this potential actin binding domain is restricted to rCx36 and respective orthologs.

A

```
Actin          ---------------DCLEVKELAPHPSGLRTA----------------
Rat        152 GVLQNTETTSKETEPDCLEVKELAPHPSGLRTAARSKLRRQEGISRFY- 199
Human      152 GVLQNTENTSKETEPDCLEVKELTPHPSGLRTASKSKLRRQEGISRFY- 199
Chicken    138 GVLQNTENSTKEAEPDCLEVKEIP--NPAIRTT-KSKMRRQEGISRFYI 183
Zebrafish  138 GVLQNTENSTKESEPDCLEVKEIP--NSAMRTT-KSKMRRQEGISRFYI 183
                              *******:.   ..:**:
```

B

```
Actin          ----------D-C-LEVKELAPHPSG--------LRTA--------
rCx43      180 SLSAVYTCKRDPCPHQVDCFLSRPTEKTIFIIFMLVVSLVSLALNI 225
rCx30      162 HLPWVLKCGIDPCPNLVDCFISRPTEKTVFTVFMISASVICMLLNV 207
                       * *   *. : .:*:         : .:
```

Figure 20| Cross-species sequence alignment of the actin binding domain identified in rCx36.
(A) Sequence alignment of the potential actin binding domain identified in rCx36 (*rattus norvegicus*) was performed against the human (*homo sapiens*), chicken (*gallus gallus*), and zebrafish (*danio rerio*) species. Sequence alignment identified the potential actin binding region as being highly conservation across species. **(B)** Sequence alignment of the proposed rCx36 actin binding domain showed minimal conservation across rCx43 and rCx30 proteins.

5.2.4 The rCx36 Connexons are Dynamically Transported to the Laterals of the GJP and Removed from the Center

It was previously reported that Cx43 hemichannels are delivered singly or in small groups to the lateral ends of the gap junction plaque and removal of older channels occurs from the center of the GJP (Lauf et al., 2002b). Additionally, a similar report has supported this trafficking mechanism for Cx35, the fish ortholog of Cx36, at mixed synapses of the goldfish Mauthner cells (Flores et al., 2012). Therefore, time lapsed imaging of rCx36-EGFP was performed to confirm if rCx36 hemichannels behaved similarly to these reports. N2a cells were transfected with wild-type pEGFP-rCx36 and analyzed 48h post-transfection. A time series experiment was achieved using LSM 700 confocal microscope system under Zeiss 63X oil immersion lens. The selected gap junction plaque was briefly observed to confirm activity prior to recording, and subsequently monitored over a period of 26 minutes; images were generated in 20 second intervals.

Delivery of wild-type rCx36-EYFP hemichannels to the gap junction plaque were successfully identified to occur at the lateral ends of the plaque. Initiation of hemichannel contact with the 'plaque lateral' ends was observed at t=20s **(Figure 20A)** and t=420s **(Figure 20B)** of the timed series experiment.

Additionally, removal of rCx36 hemichannels was also successfully documented over a time span of approximately 280 seconds, with the initiation of removal beginning at t=1020s. Interestingly, prior to hemichannel removal, the rCx36 GJP was observed to invaginate at the center of the plaque (t=1040s). Invagination of the GJP lead to total plaque separation (t=1080s), thus allowing for the removal of hemichannels at the center of the plaque (t=1100s and t=1200s). Upon completion, the separated GJP rejoined as a functional unit (t=1280s) **(Figure 21)**. Taken together, dynamics of the rCx36 GJP, with respect to lateral replenishment and center removal, was found to be consistent to the reports of Lauf et al. (2002) on Cx43 and Flores et al. (2012) on Cx35. This result was novel, as trafficking dynamics of Cx36 in N2a cells has not been previously studied.

A

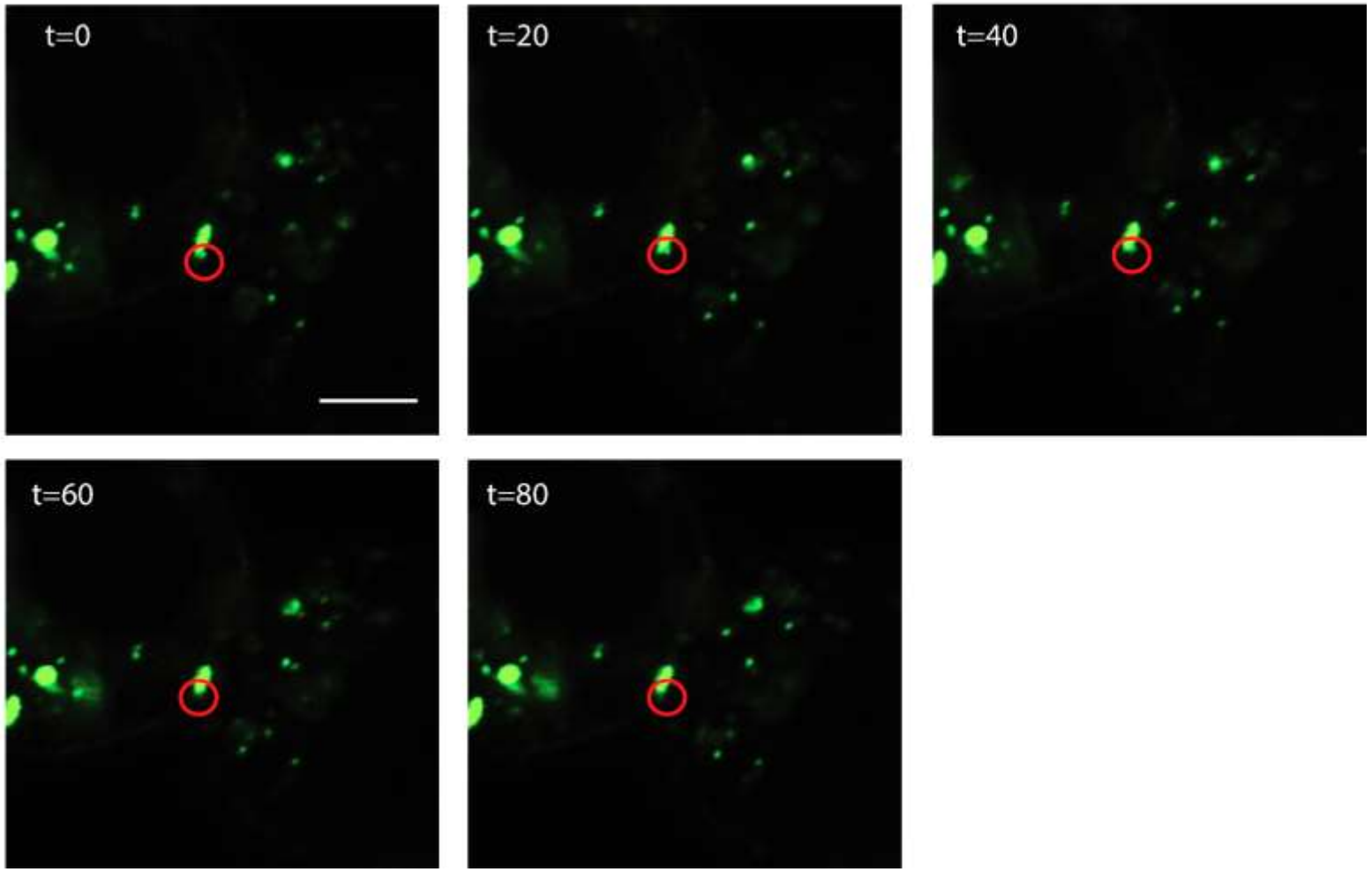

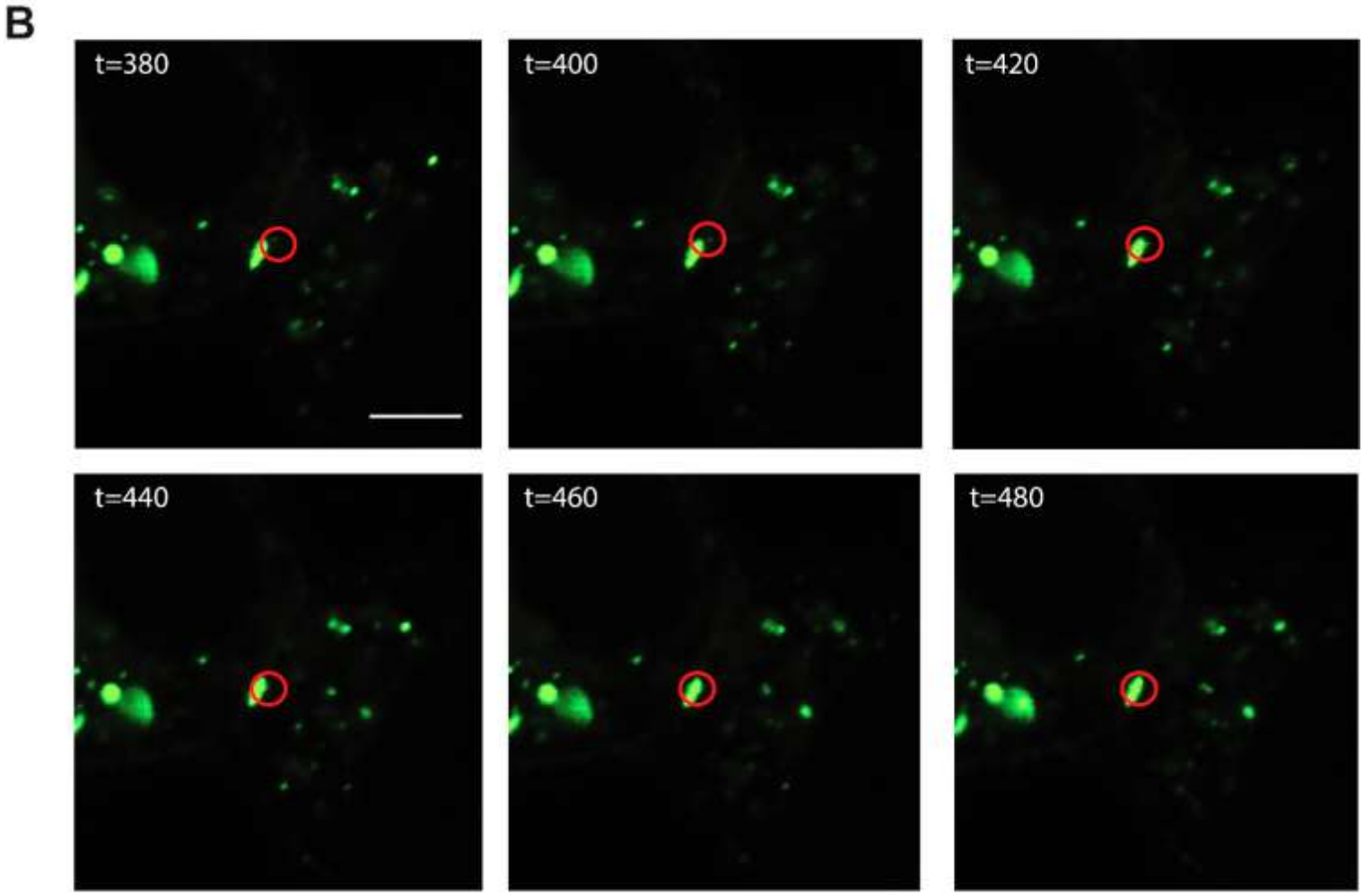

Figure 21| Delivery of wild-type rCx36-EGFP hemichannels to the gap junction plaque lateral ends.
N2a cells were transfected with wild-type pEGFP-rCx36 and observed for delivery and removal dynamics 48h post-transfection. **(A)** First recorded occurrence of rCx36-EGFP hemichannel delivery to the lateral end of the gap junction plaque. Connexons are seen in close proximity to the gap junction plaque at t=0s-20s and merges at t=20s-60s as indicated by the circle. **(B)** Second recorded occurrence of rCx36-EGFP hemichannel delivery to the lateral end of the gap junction plaque. Connexons are seen in close proximity to the GJP at t=380s-400s and merges at t=420s-440s, as indicated by the circles. Scale bar = 5µm

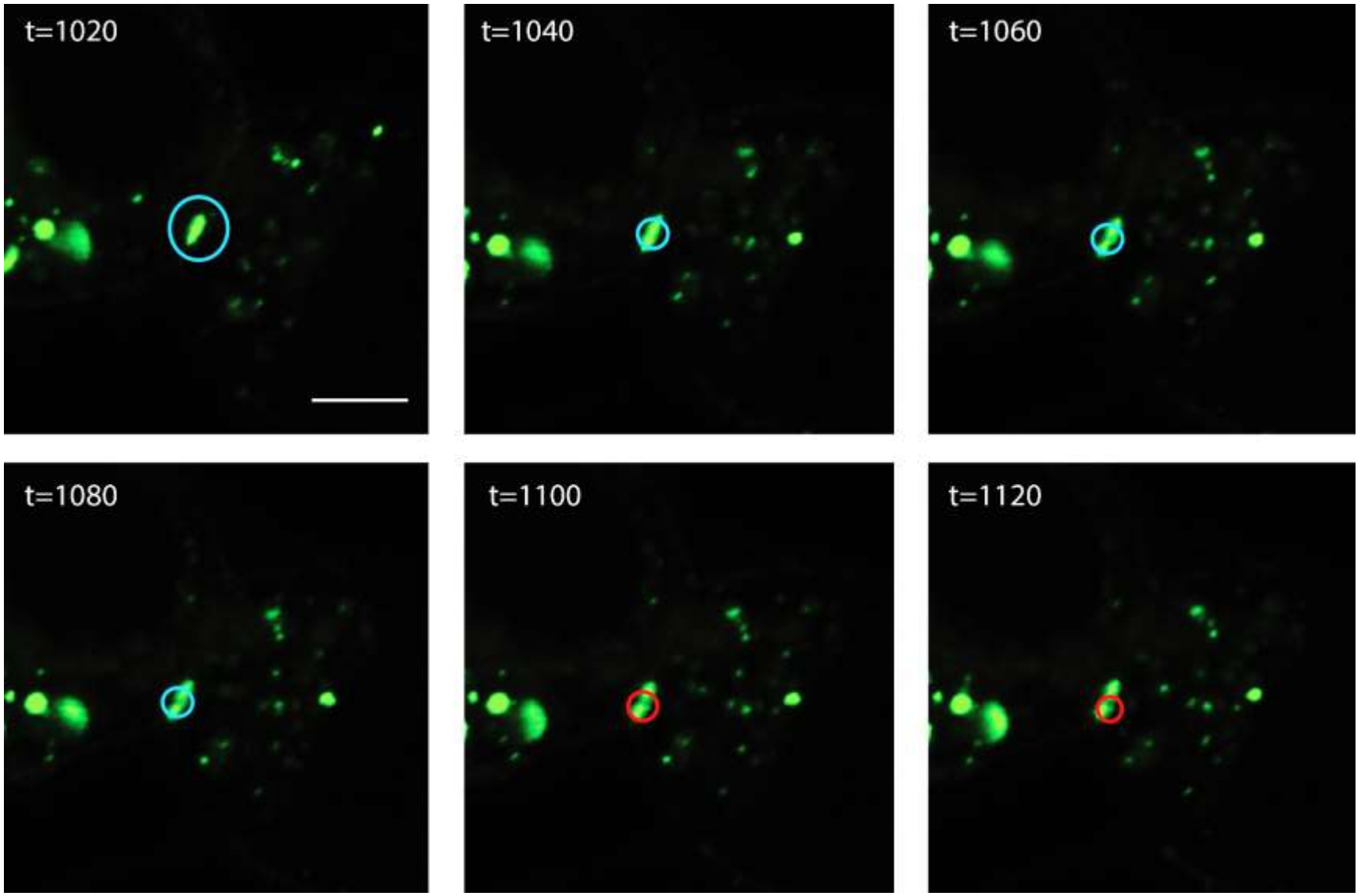
t=1020
t=1040
t=1060
t=1080
t=1100
t=1120

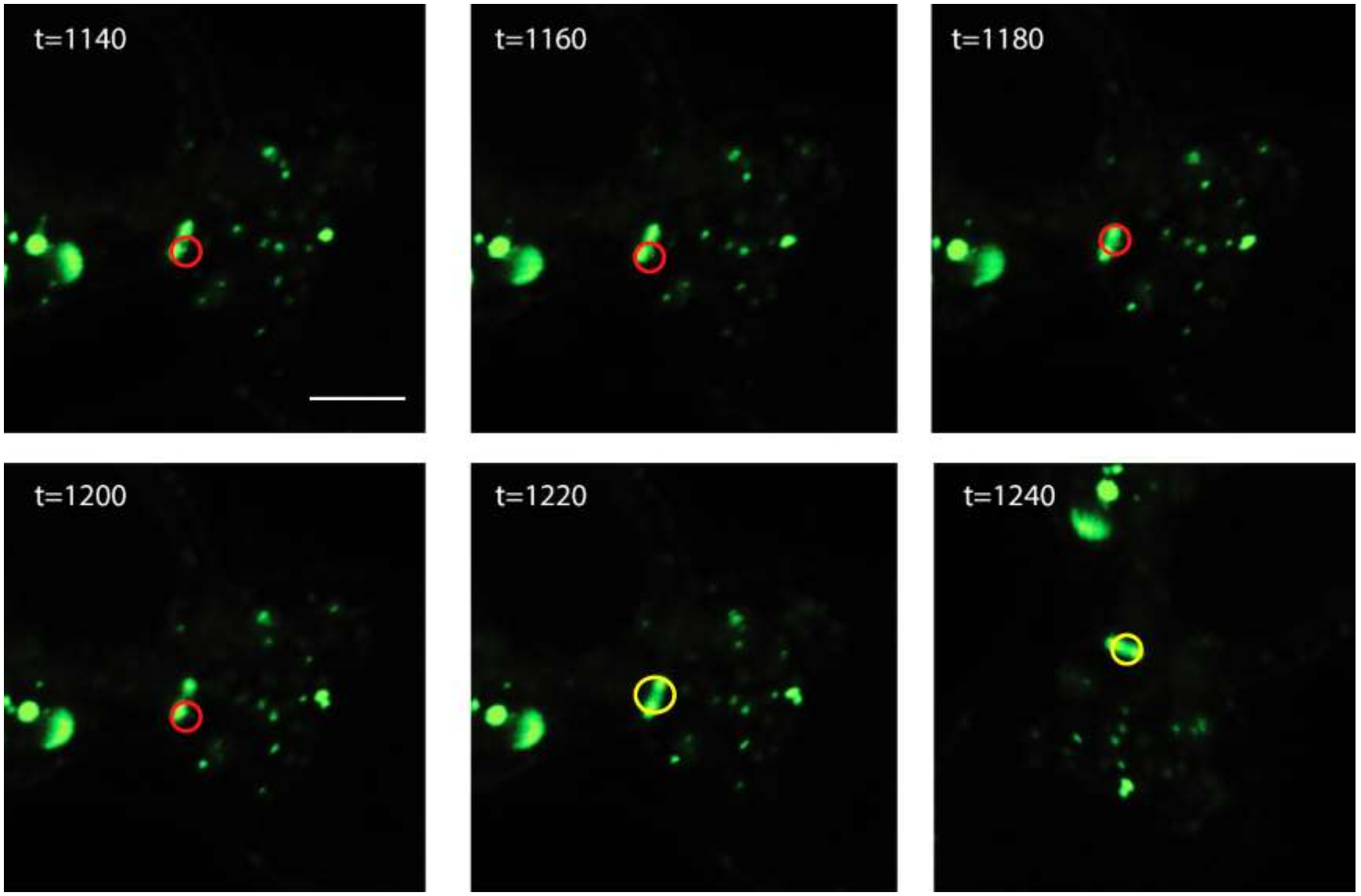
t=1140
t=1160
t=1180
t=1200
t=1220
t=1240

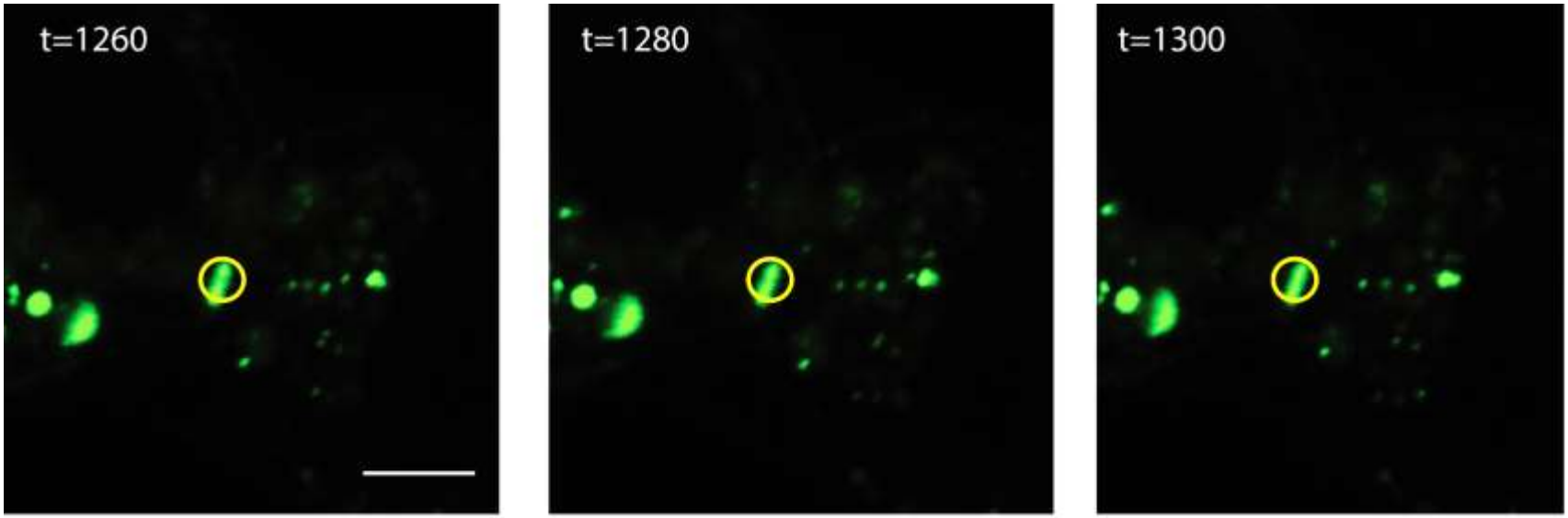

Figure 22| Removal of wild-type rCx36-EGFP hemichannels from the center of the gap junction plaque.
Recorded occurrence of wild-type rCx36-EGFP hemichannel removal from the center of the gap junction plaque. N2a cells were transfected with wild-type pEGFP-rCx36 and observed for removal dynamics 48h post-transfection. An invagination event was initiated at t=1040s and complete separation was achieved at t=1080s. Removal of wild-type rCx36-EGFP connexons was observed between t=1100s-1200s. Rejoining of the separated gap junction plaque was initiated at t=1220s and completed at t=1280s. Invagination, removal, and rejoining is indicated by the blue, red, and yellow circles respectively. Scale bar = 5µm

5.2.5 Wild-Type rCx36 Gap Junction Plaques are Stable

Since we were interested in determining whether dynamics of connexin hemichannel insertion into the rCx36 gap junction plaque were comparable to existing literature reports about other connexins, a quantitative study using FRAP was performed. The mobile fraction (%) and half-time of recovery ($t_{½}$) in seconds were the chosen parameters for analysis. The following ROIs were selected: (1) intracellular space (2) left lateral end of Cx36 gap junction plaque (3) center of the Cx36 gap junction plaque (4) right lateral end of the Cx36 gap junction plaque (5) plasma membrane and (6) extracellular space for background subtraction. The left/right assignments for the 'plaque lateral' ends were arbitrarily chosen and did not reflect any functional polarity of the gap junction plaque. For this reason, values obtained for both 'plaque lateral' ends were combined and referenced as the 'plaque lateral' end ROI. It was hypothesized that given the relative stability of the GJP, mobility would be reduced in comparison to the intracellular space and plasma membrane. We predicted that the half-time of recovery at the plaque would be quicker in comparison to the intracellular space. However, we expected half-time of recovery of the GJP would be comparable to the plasma membrane since trafficking to this region is a prerequisite to hemichannel insertion. In this way, the intracellular space and the plasma membrane served as comparative references. N2a cells were transfected with wild-type pEYFP-rCx36 and was analyzed 48h post-transfection (see section 4.4.3 for details).

The mobile fraction (%) was plotted as an average across wild-type rCx36-EYFP recovering plaques (n=8) and respective regions of interest **(Figure 23A)**. It was determined that all regions of the rCx36 GJP were significantly less mobile than the plasma membrane (plaque center 10.46±1.32%, p=0.009; 'plaque lateral' 11.01±1.25%, p=0.000418). Similarly, the intracellular space showed a significantly greater mobile fraction in comparison to the GJP lateral end (p=0.001685); no significant difference was found between the intracellular space and the center of the GJP (p=0.022). The mobile fraction of the plasma membrane (33.77± 7.5%) was indistinguishable from the intracellular space (37.02±10.2%; p=0.801). As expected, variation between the gap junction plaque ROIs appeared to be negligible as no statistical significance was found.

Half-time of recovery ($t_{½}$) was graphed as an alternative to recovery time **(Figure 23B)**. Although the plasma membrane (20.33±9.69s) and the intracellular space (11.85±6.01s) appeared to display long recovery times, no statistical significance was found between the ROIs analyzed.

As expected, all regions of the plaque showed little mobility indicating that wild-type rCx36-EYFP GJPs were stable in nature, more so than the intracellular space and plasma membrane. We hypothesized that all regions of the GJP would recovery more quickly than the intracellular space since the protein would be dynamically traffic in/out of the latter region for delivery to the plasma membrane. However, our results have shown that the half-time of recovery time was unaffected across the analyzed regions thus rejecting this hypothesis.

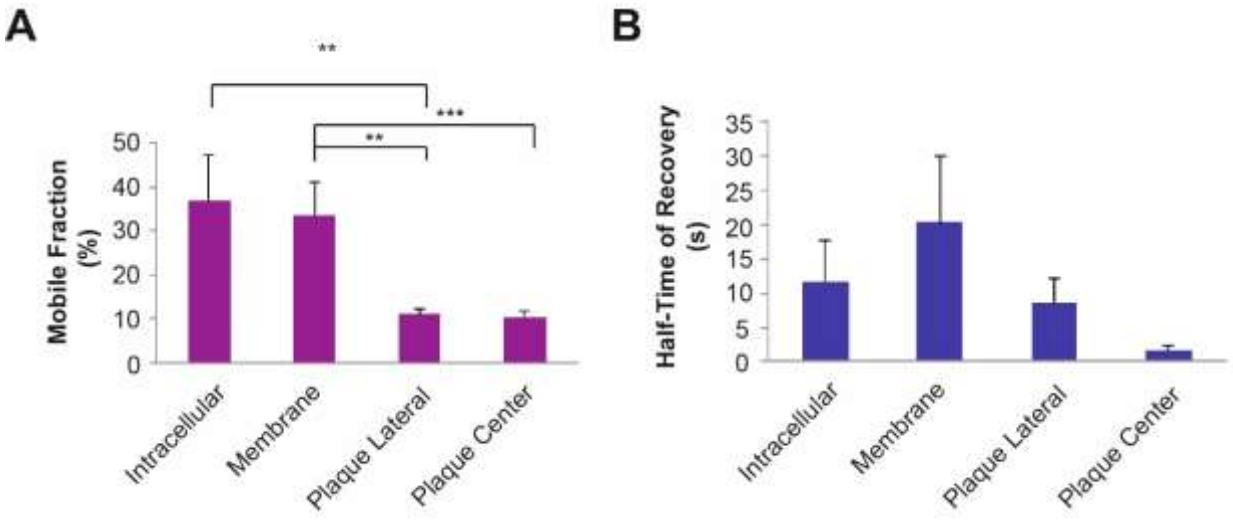

Figure 23| Mobile fraction and half-time of recovery of selected ROIs for wild-type rCx36-EYFP
N2a cells were transfected with wild-type pEYFP-rCx36 to determine the dynamics of the gap junction plaque. ROIs were bleached briefly at 70% laser power and recorded over 200 cycles at 1.0-second intervals. Results were normalized against the extracellular space. **(A)** Mobile fraction (%) was averaged across recovering gap junction plaques and represented as the mean±SEM. No significant difference was found between the regions of the plaque or between the intracellular space and the plasma membrane. All regions of the gap junction plaque showed a significant reduction in the mobile fraction in comparison to the plasma membrane indicating that the gap junction plaque was stable in nature; however, no significant difference between the intracellular space and plaque center was found. **(B)** Half-time of recovery was averaged across recovering gap junction plaques and represented as the mean±SEM. No significant difference was found between the ROIs analyzed.

5.2.6 Alteration of the CL or CT rCx36 Domains Reduces Stability

To assess the functional consequences of the aforementioned rCx36 deletion mutants, N2a cells were transfected with the respective pEFYP-rCx36 DNA (Δ182-198, 279-292, Δ182-198, Δ279-292 and Δ175-196) to be used in FRAP studies. Since literature has reported insertion of connexin hemi-channels at the lateral ends, a phenomenon which was consistent with our previous observations, the lateral ends were taken for comparison against the membrane region across the various mutants. The pre-determined wild-type values for both mobile fraction (%) and half-time of recovery (s) were maintained as a comparative reference.

Analysis of the mobile fraction across ROIs revealed that the membrane region and the respective 'plaque lateral' ends of all rCx36 mutant variants were indistinguishable. This was in contrast to the previous observations with wild-type rCx36 where it was found that the mobile fraction of the 'plaque lateral' ends was significantly lower than that of the plasma membrane (see section 5.2.5). Since stability of the GJP was impaired in cells expressing rCx36 mutant constructs, this further supported the hypothesis that amino acid residues spanning 175-196 and 279-297 are involved in transport and/or stability. To support this, cross comparison of the 'plaque lateral' end ROIs to the wild-type revealed that cells expressing rCx36 Δ182-198 (35.47±4.98%, $p=5.34^{-6}$), rCx36 Δ279-292 (24.80±2.31%, $p=7.40^{-5}$) or rCx36 Δ175-196 (25.68±3.26%, $p=7.50^{-4}$) were all significantly greater in mobility. Interestingly, no significant difference in the mobile fraction was found between the lateral ends of rCx36 Δ-182-198,279-292 (18.42±3.60%) and the WT (11.02±1.25%). When the plasma membrane ROIs of the rCx36 mutants were crossed compared to the wild-type, it was determined that no significant difference existed **(Figure 24A)**. Therefore we concluded that the fluidity of the protein in the membrane region was not affected by the existing mutations. As such it was inferred that the activity of rCx36 at the GJP (or lack thereof) was independent of the plasma membrane dynamics and specific interaction candidates affected by the deletions.

From the half-time of recovery it was determined that no significant difference between the membrane region and the respective 'plaque lateral' ends existed in rCx36 Δ182-198, 279-292, -Δ182-198, -Δ279-292 or -Δ175-196. Each mutant was subsequently cross compared to the wild-type, which revealed no significant difference at the either the plasma membrane ROIs or 'plaque lateral' ends ROIs **(Figure 24B)**.

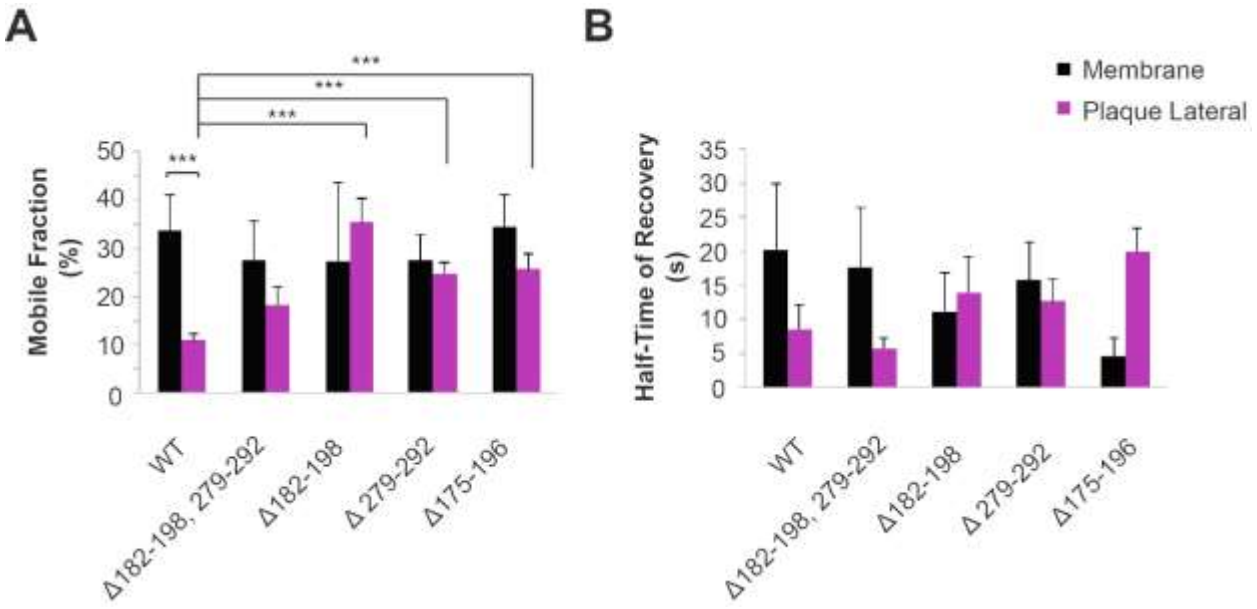

Figure 24| Mobile fraction and half-time of recovery of selected ROIs for EYFP-tagged rCx36 WT and deletion mutant variants.

N2a cells were transfected with pEYFP-Cx36 WT, Δ182-198, 279-292, Δ182-198, Δ279-292 or Δ175-196 to determine functional consequences of region-specific deletions. ROIs were bleached briefly at 70% laser power and recorded over 200 cycles at 1.0-second intervals. Results were normalized against the extracellular space and averaged across each ROI, represented as the mean±SEM. **(A)** Mobile fraction (%) of the 'plaque lateral' end showed no significant difference to the respective membrane region of cells transfected with mutant constructs. Cells expressing rCx36 Δ182-198, -Δ279-292 and -Δ175-196 showed a significant increase in the mobile fraction of the 'plaque lateral' end in comparison to the respective wild-type indicating a reduction in stability. **(B)** No significant difference in the half-time of recovery (s) was found between the ROIs analyzed.

5.3 Chemical Disruption and Alteration of Cytoskeletal Interaction

5.3.1 Competitive Binding of the Tubulin Binding Region with TAT

To determine the functional consequences of competitive binding at the proposed tubulin binding region, peptide blocking was achieved with the TAT peptide. The TAT peptide, utilized for its cell-penetrating ability, is derived from the transactivator of transcription (TAT) of human immunodeficiency virus. Cell penetrating peptides (CPPs) are typically used to overcome the lipophilic barrier of the cellular membranes to deliver molecules inside the cell for their specified biological actions. Here, this property was used to carry the C-terminal binding (CTB) sequence, and respective controls, into N2a cells as a competitor for tubulin binding. The TAT peptide used to target the tubulin binding region was denoted as TAT CT-ON, meaning that it was "on target" to the CT binding domain. Additionally, we made use of a TAT peptide outside of the tubulin binding region referred to as TAT CT-OFF, meaning that was "off target" to the CT binding domain. Instead, TAT CT-OFF targeted the CTP region and served as the first of three controls. Scrambled sequences of both TAT CT-ON/OFF were generated and were denoted as '(scrambled)'; these peptides generated served as the remaining two (positive) controls **(see Table 9)**. We anticipated that blocking of the tubulin binding region could only be achieved with the TAT CT-ON peptide. As such, we expected that treatment with TAT CT-ON would significantly increase the recovery time and mobile fraction, reflecting a reduction in trafficking and stability, in comparison to the untreated wild-type. Additionally, we hypothesized that the control peptides would yield similar results to untreated wild-type, with any observed differences being statistically negligible.

Previously it was determined that the mobile fraction of wild-type rCx36-EYFP expressing cells at the lateral ends of the GJP was significantly reduced in comparison to the respective membrane region. Similar to this observation, the mobile fraction at the ‘plaque lateral’ ends was considerably lower than the respective plasma membrane region in cells treated with TAT CT-OFF ($p=2.00^{-5}$), TAT-CT-OFF (scrambled) ($p=0.002$), and TAT CT-ON (scrambled) ($p=0.0002$). Comparison to the untreated wild-type revealed no significant difference in the mobile fraction at either the plasma membrane ROIs or the ‘plaque lateral’ end ROIs, regardless of treatment with the control TAT

peptides. Our observations confirmed that the treatment of wild-type rCx36 expressing cells with TAT CT-OFF, TAT CT-OFF (scrambled) and TAT CT-ON (scrambled) showed similar behavior to the untreated wild-type. Therefore, we concluded that these peptides were not targeting a region that compromised the stability of the GJP.

In contrast, cells treated with TAT CT-ON showed no significant difference in the mobile fraction between the 'plaque lateral' ends (32.81±3.31%) and the respective membrane region (37.53±5.25). Comparison to the untreated wild-type cells revealed a significant increase in the mobile fraction ($p=4.00^{-6}$) at the 'plaque lateral' ends. However, the plasma membrane ROI of cells treated with TAT CT-ON was indistinguishable from the untreated wild-type expressing cells **(Figure 25A)**. As expected, treatment with TAT CT-ON diminished the stability of the GJP at the lateral ends suggesting that the CTB domain was successfully targeted and is involved in the stabilization of rCx36 at the GJP post-insertion. Therefore, it is inferred that tubulin may be a necessary interaction candidate for stabilization. Furthermore, since the mobility of rCx36 at the plasma membrane was unaffected across treatments, it was successfully confirmed that the addition of the TAT peptides did not affect the integrity of the plasma membrane post-penetration.

We previously reported that the half-time of recovery at the 'plaque lateral' ends of wild-type rCx36-EYFP expressing cells was indistinguishable from the plasma membrane. Similarly, no significant difference was found between the plasma membrane and respective 'plaque lateral' ends of wild-type rCx36 expressing cells treated with either of the control TAT peptides. Comparison of the control TAT peptides to the untreated wild-type expressing cells revealed no significant difference in recovery at either the plasma membrane ROIs or the 'plaque lateral' end ROIs. However, with TAT CT-ON treatment, half-time of recovery significantly increased at the 'plaque lateral' ends (26.17±4.63s) in comparison to the respective membrane region (4.92±1.23s, $p=3.21^{-3}$). Comparison of the TAT CT-ON treatment to the untreated wild-type revealed no significant difference in recovery time at the membrane region. However, a considerable increase in recovery time at the 'plaque lateral' ends was observed **(Figure 25B)**. By this, we were successfully able to achieve inhibition of recovery exclusively at the 'plaque lateral' ends with the use of TAT CT-ON. This result suggested that the CTB domain, and more specifically tubulin, is involved in the delivery of rCx36 to the lateral ends of the GJP.

Interestingly, the gap junction plaque area of wild-type rCx36 expressing cells treated with TAT CT-OFF and TAT CT-OFF (scrambled) was found to be 1.43±0.21μm² and 2.34±0.51μm² respectively. However, only the former of which was significantly reduced in comparison to the untreated wild-type (2.22±0.19μm²). Therefore, it is probable that TAT CT-OFF targets a region of the rCx36 protein implicated in tubulin-independent trafficking and/or stabilization. Wild-type rCx36-expressing cells treated with TAT CT-ON (1.71±0.14μm²) or TAT CT-ON (scrambled) (1.50±0.18μm²), however, were both found to be indistinguishable from the untreated wild-type **(Figure 25C)**. This result further supports the hypothesis of a compensatory trafficking mechanism, likely attributable to actin, which may operate in a temporal and/or spatial manner.

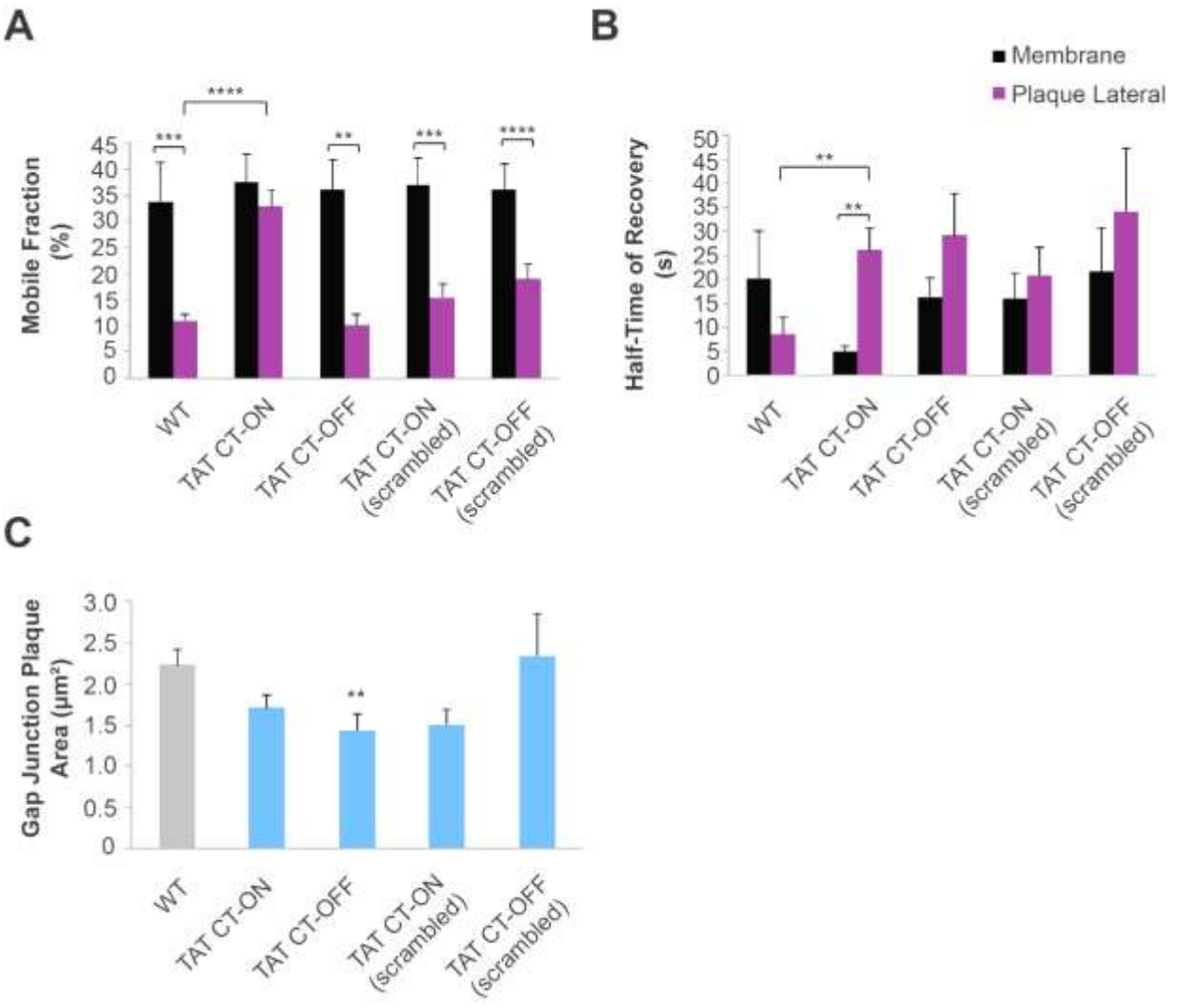

Figure 25| Effects of TAT-driven competitive binding of the rCx36 tubulin binding region in N2a cells.
N2a cells were transfected with wild-type pEYFP-rCx36 and subsequently treated with various TAT peptides to determine the function consequence of inhibiting tubulin interaction. ROIs were bleached briefly at 70% laser power and recorded over 200 cycles at 1.0-second intervals. Results were normalized against the extracellular space and averaged across each ROI, represented as the mean±SEM. **(A)** Mobile fraction (%) of the 'plaque lateral' end of cells treated with TAT CT-ON showed a significant increase to the respective region of untreated wild-type cells suggesting that tubulin interaction was successfully inhibited. Control treatments were indistinguishable from the untreated wild-type. **(B)** A significant increase in half-time of recovery was observed at the 'plaque lateral' ends of wild-type rCx36 expressing cells treated with TAT CT-ON in comparison to the untreated wild-type. This result indicated that inhibition of the tubulin binding region produces trafficking impairments. No significant difference in half-time of recovery was recorded for cells treated with the control TAT peptides. **(C)** GJP area was similar in N2a cells treated with TAT CT-ON, ON (scrambled) and OFF. A significant reduction in gap junction plaque size was observed in cells treated with TAT CT-OFF (scrambled).

5.3.2 Pharmacological Alteration of Tubulin Dynamics

We aimed to further determine the interaction of rCx36 with tubulin, and confirm its role in delivery and stabilization *in vivo*, by analyzing the effects of the tubulin-specific pharmacological agents: colchicine and paclitaxel. Colchicine, responsible for binding to the tubulin heterodimer, prevents microtubule (MT) polymerization, promoting disassembly. Paclitaxel, also known by its common name taxol, displays the opposite effect and stabilizes MTs. Therefore, we hypothesized that colchicine and paclitaxel treatment would display opposite effects on wild-type rCx36 expressing cells. In cells treated with colchicine, an increase in the mobile fraction, indicating a reduction in stability, at the 'plaque lateral' ends was predicted. Additionally, we expected an impairment in lateral end replenishment, thus promoting a prolonged recovery time with colchicine treatment. In contrast, we predicted that treatment with paclitaxel would decrease the mobile fraction at the 'plaque lateral' ends to indicate an increase in stability. Finally, we anticipated that recovery would be promoted with paclitaxel treatment, leading to a reduction in recovery time would be observed. In addition to wild-type rCx36-EYFP, rCx36 Δ279-292-EYFP was also utilized since the predicted tubulin binding domain is largely deleted in this mutant. Because a direct interaction was not expected, it was hypothesized that no significant difference in the mobile fraction or recovery time would exist regardless of treatment applied.

Wild-type rCx36 expressing cells treated with colchicine displayed no significant difference in the mobile fraction at the plasma membrane (30.48±3.93%) in comparison to the 'plaque lateral' ends (23.34±3.76%, p=0.25). Comparison of the 'plaque lateral' end ROIs to the untreated wild-type revealed that colchicine treatment significantly increases mobility ($p=5.71^{-3}$). Overall, this would suggest that the inhibition of tubulin polymerization interferes with the stability of the gap junction plaque. The plasma membrane ROIs were indistinguishable between the untreated and treated wild-type rCx36 expressing cells, indicating that the dynamics of rCx36 at the plasma membrane was maintained regardless of colchicine treatment. As predicted, in cells expressing rCx36 Δ279-292, treatment with colchicine revealed no significant difference in the mobile fraction between the 'plaque lateral' ends (30.10±4.78%) and the plasma membrane (36.25±5.92%, p=0.45). Similarly, comparison to the untreated rCx36 Δ279-292 expressing cells showed that the plasma membrane ROIs (p=0.28) and the 'plaque lateral' end ROIs (p=0.29) were both indistinguishable **(Figure 26A)**.

Upon the analysis of the half-time of recovery, no significant difference was found between the plasma membrane (7.09±4.77s) and respective 'plaque lateral' ends (47.66±20.94s) of wild-type rCx36 expressing cells treated with colchicine. Similarly, comparison to the untreated wild-type revealed that the plasma membrane ROIs and the 'plaque lateral' end ROIs were indistinguishable. As such, it was suggested that colchicine treatment did not significantly impair recovery of the gap junction plaque. The addition of colchicine to rCx36 Δ279-292 expressing cells revealed that the plasma membrane region (11.88±233s) was indistinguishable from the respective 'plaque lateral' ends (28.80±8.96s, p=0.20). Likewise, comparison to the untreated rCx36 Δ279-292 showed no significant difference in the half-time of recovery at either the plasma membrane ROIs or the 'plaque lateral' end ROIs **(Figure 26B)**.

As expected, the GJP area was significantly reduced to 1.37±0.21μm^2 in wild-type expressing cells treated with colchicine in comparison to its untreated counterpart (2.22± 0.19μm^2). In contrast, GJP area was unaffected in rCx36 Δ279-292 expressing cells regardless of colchicine treatment. As such, it was further supported that tubulin inhibition is non-effective in the absence of aa: Lys279-Lys292; this is due to the lack of interaction **(Figure 26C)**.

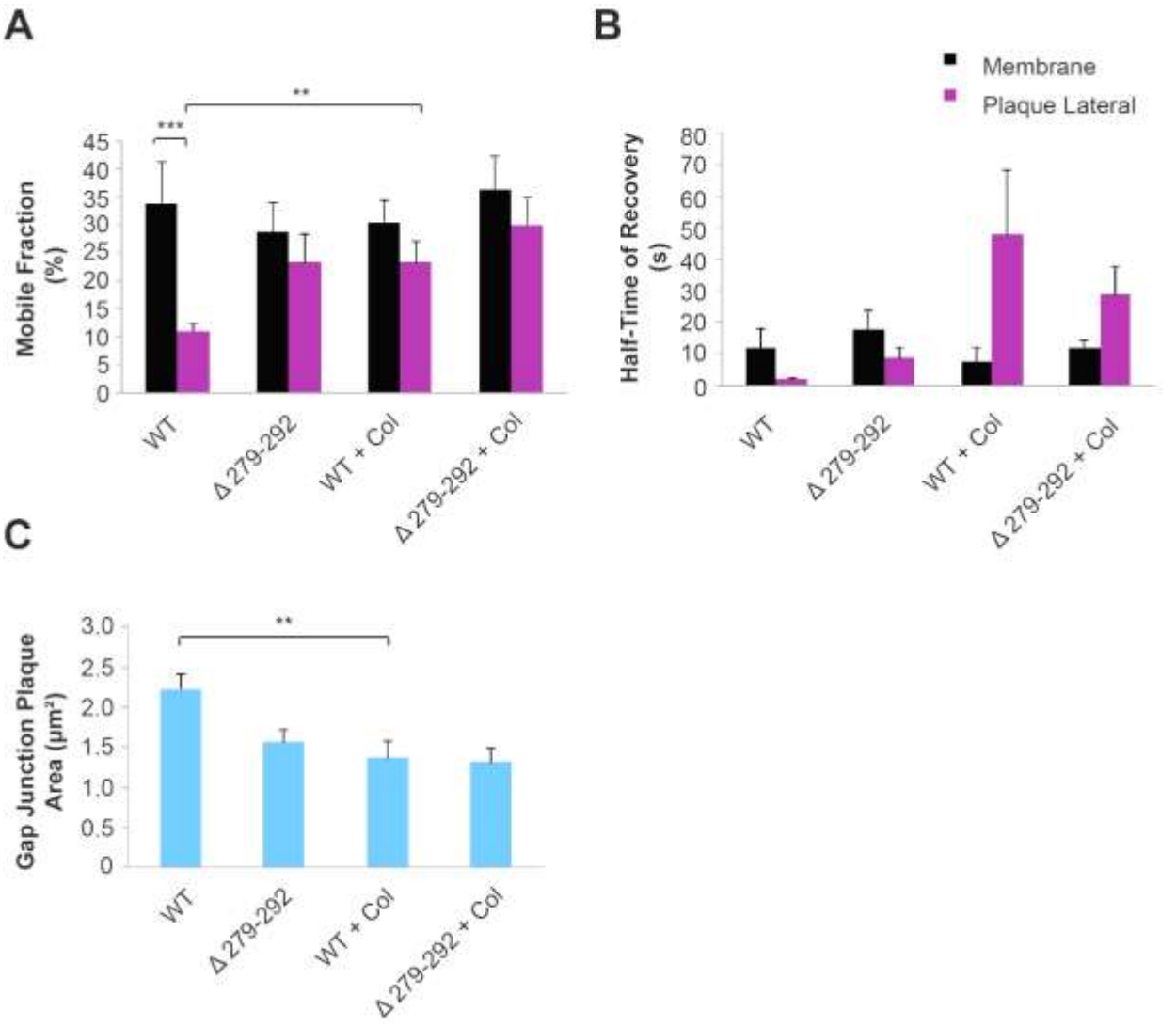

Figure 26| Effect of tubulin polymerization inhibition with colchicine on rCx36 dynamics in N2a cells.
N2a cells were transfected with pEYFP-rCx36 WT or -Δ279-292 and subsequently treated with colchicine to determine the function consequence of inhibition tubulin polymerization. ROIs were bleached briefly at 70% laser power and recorded over 200 cycles at 1.0-second intervals. Results were normalized against the extracellular space and averaged across each ROI, represented as the mean±SEM. **(A)** Mobile fraction (%) at the 'plaque lateral' ends significantly increased in wild-type N2a cells treated with colchicine in comparison to the untreated wild-type. No significant difference was found in rCx36 Δ279-292 treated with colchicine compared to its untreated counterpart. **(B)** Treatment with colchicine had no significant difference on the half-time of recovery at the 'plaque lateral' ends of rCx36 WT or -Δ279-292 expressing cells. **(C)** A reduction in the GJP area occurred in wild-type rCx36 cells treated with colchicine; no significant difference was found on the gap junction plaque size of treated rCx36 Δ279-292 expressing cells.

The mobile fraction of wild-type rCx36 expressing cells treated with paclitaxel showed a significant reduction at the 'plaque lateral' ends (11.46±1.50%) in comparison to the respective plasma membrane region (21.54±.06%, $p=7.22^{-3}$). When treated cells were compared to their untreated counterpart, no significant difference was found at either the plasma membrane ROIs (p=0.13) or the 'plaque lateral' end ROIs (p=0.83). Interestingly, a considerable reduction in the mobile fraction of the 'plaque lateral' ends (17.39±1.74%) in comparison to the respective membrane region (40.54±5.99%) was observed with rCx36 Δ279-292 expressing cells treated with paclitaxel. This result is in contrast to previous observations of the untreated rCx36 Δ279-292 expressing cells that showed no significant difference between the plasma membrane ROI and respective 'plaque lateral' end ROI (see section 5.2.6). However, comparison of rCx36 Δ279-292 treated with paclitaxel to the untreated counterpart showed no significant difference in the mobile fraction at the 'plaque lateral' end ROIs (p=0.012) or plasma membrane ROIs (p=0.63) **(Figure 27A)**. Therefore, it was confirmed that no additional effects on stability could be achieved with the addition of paclitaxel in rCx36 Δ279-292 expressing cells due to the lack of tubulin interaction.

Analysis of the half-time of recovery revealed that the 'plaque lateral' ends (11.86±5.02s) were indistinguishable to the respective membrane region (14.58±5.75s, p=0.74). In comparison to the untreated wild-type, no significant difference in half-time of recovery was found at the plasma membrane ROIs (p=0.59) or the 'plaque lateral' end ROIs (p=0.65). The half-time of recovery for rCx36 Δ279-292 expressing cells treated with paclitaxel was found to be indistinguishable between the 'plaque lateral' ends (25.58±7.45s) and the respective membrane region (12.12±3.14s). Similarly, no significant difference was recorded at the plasma membrane ROIs or the 'plaque lateral' end ROIs upon cross analysis to the non-treated rCx36 Δ279-292 expressing cells **(Figure 27B)**.

As expected, treatment with paclitaxel had no additional effects on the GJP area of rCx36 Δ279-292 expressing cells (1.22±0.08μm^2, p=0.08) further supporting that tubulin interaction was abolished in this mutant. However, a significant reduction was observed in wild-type rCx36 expressing cells (1.44±0.20μm^2) in comparison to the untreated counterpart (2.22± 0.19μm^2) **(Figure 27C).** Therefore, it was suggested that paclitaxel did inhibit trafficking and/or stabilization despite MT stabilizing effects.

In summary, colchicine, which inhibits the polymerization of tubulin, reduced the stability of wild-type rCx36 GJPs at the lateral ends but failed to have an impact on of rCx36 Δ279-292 expressing cells. The absence of additional effects on the CTB mutant, in comparison to the untreated counterpart, was likely observed due to its inability to interact with tubulin. This further supports the role of tubulin in the stabilization of rCx36 GJPs, specifically through interactions between aa: Lys279-Lys292. In contrast, paclitaxel, which stabilizes MTs and inhibits its depolymerization, was shown to have no additional effects on the mobility of rCx36 WT or -Δ279-292 GJPs. The half-time of recovery was not impacted in rCx36 WT or -Δ279-292 expressing cells with either paclitaxel or colchicine in comparison to the untreated counterpart. However, a significant reduction in the GJP area of rCx36 treated with either paclitaxel or colchicine was observed. As such this served as an illustration of impairments in tubulin-specific trafficking, achieved with pharmacological agents.

.

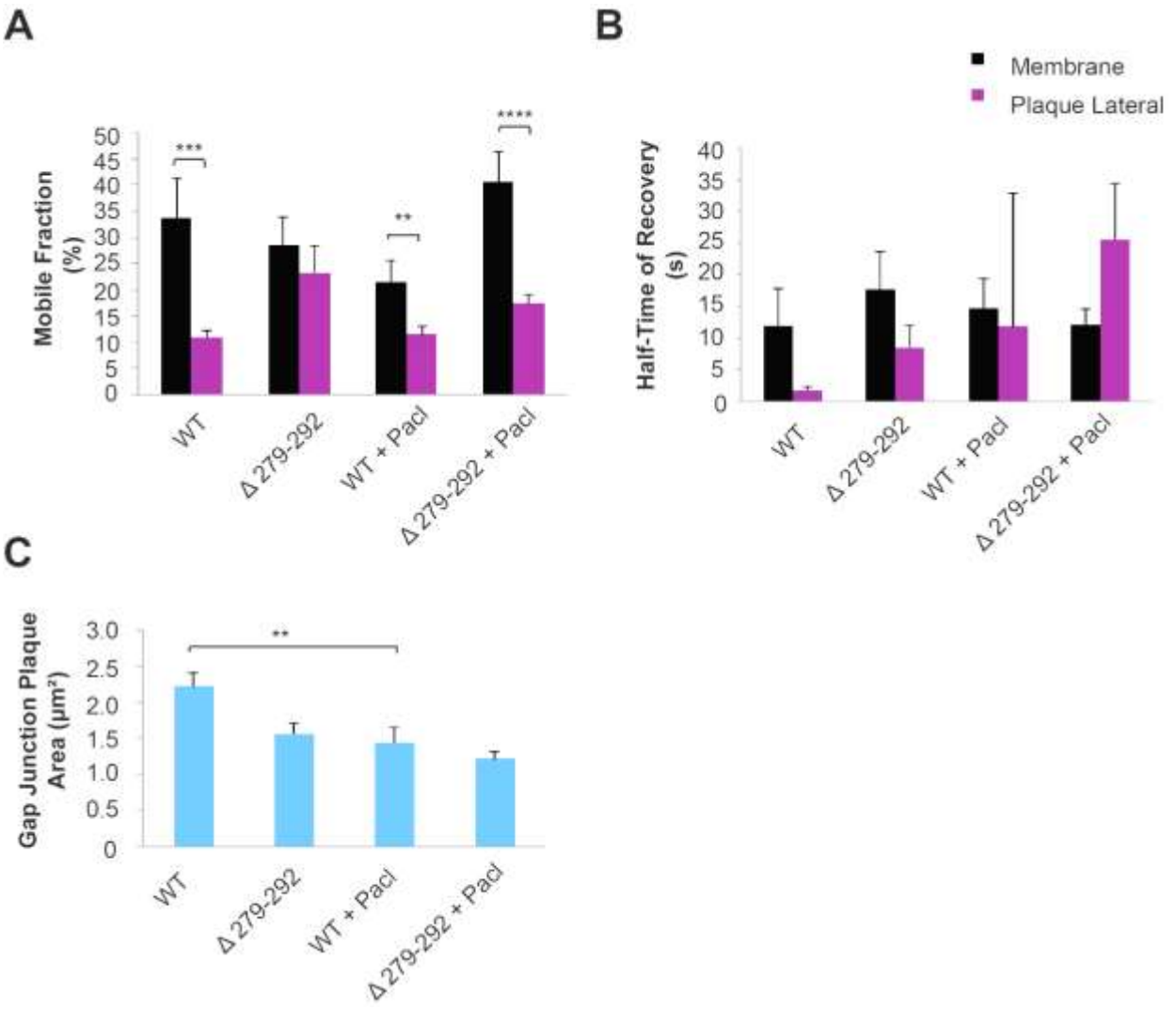

Figure 27| Effects of promoting tubulin stabilization with paclitaxel on the dynamics of wild-type rCx36 in N2a cells.

N2a cells were transfected with pEYFP-rCx36 WT or -Δ279-292 and subsequently treated with paclitaxel to determine the function consequence of tubulin polymerization promotion. ROIs were bleached briefly at 70% laser power and recorded over 200 cycles at 1.0-second intervals. Results were normalized against the extracellular space and averaged across each ROI, represented as the mean±SEM. **(A)** Mobile fraction (%) at the 'plaque lateral' ends showed no significant difference in either rCx36 WT or Δ279-292 expressing cells treated with paclitaxel in comparison to the respective untreated counterpart. **(B)** Treatment with paclitaxel had no significant difference on the half-time of recovery at the 'plaque lateral' ends of rCx36 WT or Δ279-292 expressing cells. **(C)** A reduction in the GJP area occurred in rCx36 WT cells treated with paclitaxel; no significant difference was found in the gap junction plaque size of treated rCx36 Δ279-292 expressing cells in comparison to the respective untreated counterpart.

5.3.3 Pharmacological Blocking of Actin

Next, we further investigated the role of actin interaction with rCx36. For this study, cytochalasin D was chosen to inhibit polymerization of actin microfilaments. Previously, we proposed that actin may be involved with transport and stability of rCx36 at the GJP in addition to tubulin. Therefore, it was hypothesized that inhibition of actin polymerization would result in an increase of mobile fraction and half-time of recovery as well as a reduction in gap junction plaque size.

The mobile fraction of wild-type rCx36 expressing cells treated with cytochalasin D was found to be 27.61±2.61% at the 'plaque lateral' ends; this was indistinguishable from the respective plasma membrane region (34.26±7.05%). Comparison to the untreated wild-type revealed a significant increase in mobile fraction at the 'plaque lateral' ends of wild-type rCx36 expressing cells treated with cytochalasin D. However, no significant difference was found between the membrane regions of the untreated WT and cytochalasin D treatment **(Figure 28A)**. Therefore, this result indicated that cytochalasin D had no effect on the plasma membrane dynamics or the fluidity of rCx36 at the membrane. Half-time of recovery of rCx36 expressing cells treated with cytochalasin D at the plasma membrane ROI (10.83±4.67s) was indistinguishable to the respective 'plaque lateral' end ROI (12.87±3.78s). Similarly, no significant difference was found at the plasma membrane ROIs ($p=0.34$) or the 'plaque lateral' end ROIs ($p=0.44$) when compared to the untreated wild-type **(Figure 28B)**. Additionally, blocking of actin polymerization with cytochalasin D revealed no significant effect on GJP area in wild-type rCx36 expressing cells (2.13±0.41μm^2) in comparison to non-treated cells **(Figure 28C)**. However, a considerable reduction in the CTF_{GJP} was recorded at the gap junction plaque of wild-type expressing cells treated with cytochalasin D. Therefore, we suspect that the accumulation of connexons decreased, potentially as a result of impaired trafficking or stability **(Table 12)**.

These results support actin as a major contributor to rCx36 stabilization post-insertion at the gap junction plaque. Additionally, since the half-time of recovery and gap junction plaque area were minimally impacted. This result would suggest that actin's role in trafficking of rCx36 to the lateral ends of the gap junction plaque is minor in comparison to tubulin.

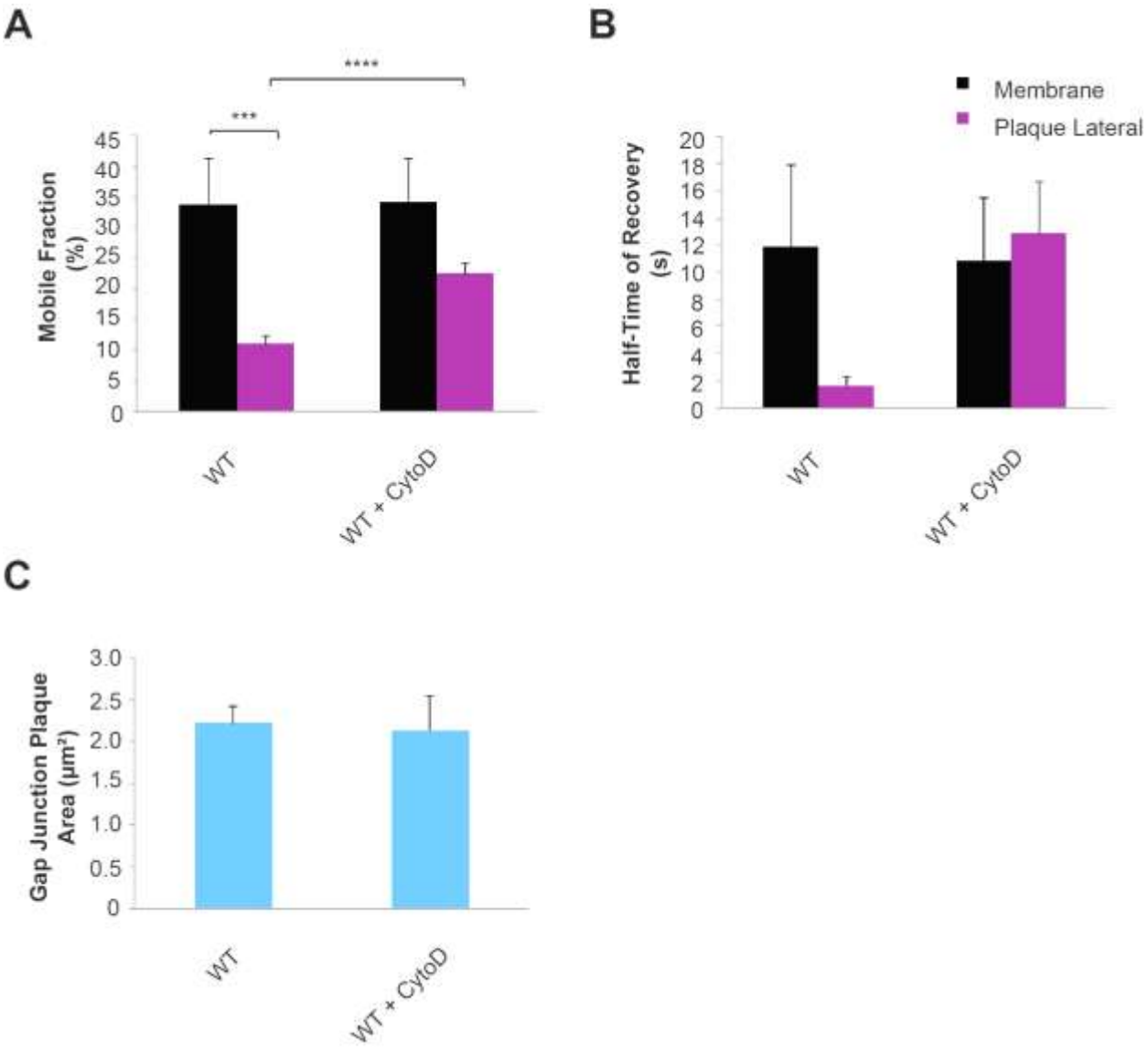

Figure 28| Effect of inhibiting actin polymerization with cytochalasin D on the dynamics of wild-type rCx36 in N2a cells.

N2a cells were transfected with pEYFP-Cx36 WT subsequently treated with cytochalasin D 48h post-transfection to determine the function consequence of the inhibition of actin polymerization. ROIs were bleached briefly at 70% laser power and recorded over 200 cycles at 1.0-second intervals. Results were normalized against the extracellular space and averaged across each ROI, represented as the mean±SEM. **(A)** Mobile fraction (%) of the 'plaque lateral' ends showed a significant increase when treated with cytochalasin D in comparison to the untreated cells. **(B)** Half-time of recovery of the ROIs were indistinguishable regardless of treatment with cytochalasin D. **(C)** No significant difference was found in the gap junction plaque size of treated rCx36 WT expressing cells in comparison to the untreated counterpart.

Table 12: Corrected total fluorescence of wild-type gap junction plaques under cytochalasin D treatment.*

	WT	WT+ CytoD
CTF_{GJP}	58335.13±8949.49	**465.60±104.85**
p-value	-	**7.13^{-5}**

*Significant values are bolded.

5.4 IDENTIFICATION OF CRITICAL RESIDUES IN CX36-TUBULIN INTERACTION WITH SITE-DIRECTED MUTAGENESIS

5.4.1 Generation and Cloning of CTB and CLB Point Mutation Constructs

To determine the amino acid residues critical for cytoskeletal interaction with rCx36, site-directed mutagenesis was performed. We suspected that amino acids large in size might be significant contributors for interaction to occur. As such, our aim was to introduce single residue substitutions in rCx36 at the hypothesized binding region for actin (aa: Asp167-Ala184), and tubulin (aa: Lys279-Ala287). For actin specifically, since we previously predicted that residues spanning 175-184 might be most critical for interaction, amino acids pertaining to this region were targeted; one amino acid outside of this range was arbitrarily chosen for preliminary studies. As such, Val171, His177, Ser179, Leu181 and Arg182 were selected as initial targets to study the rCx36-actin interaction. For the study of the rCx36-tubulin interaction, Lys279, Ile280, Lys281, Leu282, Val284, Arg285 and Gly286 were chosen as targets for site-directed mutagenesis. Alanine, a non-polar amino acid, was chosen for mutation because its small size and inability to interfere with protein function due to the non-reactive methyl group. Primers were designed accordingly to introduce point mutations into the rCx36 gene, using the pEGFP-rCx36 template, so that an alanine residue would be encoded at the designated CLB and CTB regions of rCx36.

Mutant pEGFP-rCx36 plasmids were generated using Q5® Site-Directed Mutagenesis Kit as per manufacturer's protocol and transformed into NEB 5-alpha competent *E. coli* cells. The bacteria were subsequently plated onto LB-AMP plates and single bacterial colonies were isolated and grown in LB-AMP media overnight. DNA was isolated via small-scale plasmid purification, sequenced and aligned with the wild-type rCx36 gene to identify mutants. By this technique, we

were successfully able to introduce alanine point mutations at the targeted residues in the rCx36 CLB domain (V171A, H177A, S179A, L181A and R182A) and the CTB domain (K279A, I280A, K281A, L282A, V284A, R285A and G286A).

5.4.2 Confirmation of Point Mutant Expression and Localization in N2a

Upon confirmation of pEGFP-rCx36 point mutant variants, expression was verified by transfecting N2a cells with the respective DNA. Whole cell protein lysates were fractionated on a 10% SDS/PAGE gel 48h post-transfection, and transferred to a nitrocellulose membrane for western blotting. For the detection and validation of EGFP-tagged protein expression, the anti-GFP primary antibody was applied; β-actin served as a loading control. By this, rCx36-EGFP WT and point mutant variants of the CLB **(Figure 29A)** and CTB **(Figure 29B)** domains were successfully detected. All rCx36 CLB and CTB point mutant variants were capable of expression in the N2a cell line as confirmed by the presence of a band approximately 60kDa. However, expression of the rCx36 CLB and CTB mutant variants was significantly reduced in comparison to the wild-type; particularly with the CLB mutants: H177A, S179A, L181A and R182A and CTB mutants: K279A and I280A.

Localization studies confirmed that rCx36-EGFP CLB **(Figure 30)** and CTB **(Figure 31)** mutant variants were capable of forming GJPs. However, for the remainder of this thesis, only the interaction between rCx36 and tubulin achieved with the CTB point mutants will be addressed.

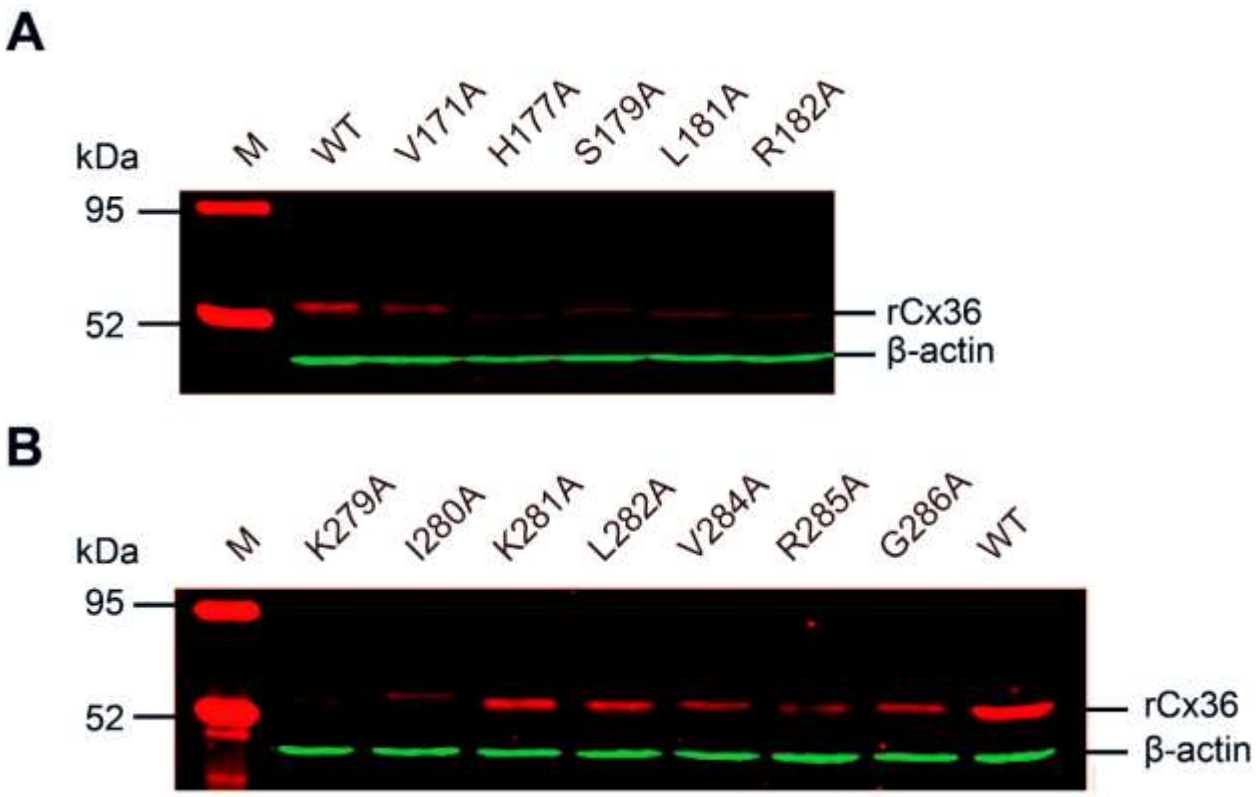

Figure 29| Western blot analysis of rCx36-EGFP WT, CLB and CTB point mutations expression in N2a cells. Western blot of the (A) CLB point mutations and (B) CTB point mutants (denoted in red) generated using the Q5 site-directed mutagenesis protocol. N2a cells transfected with pEGFP-rCx36 WT, CLB and CTB point mutant constructs were lysed 48h post-transfection. Lysates were fractionated on a 10% SDS-PAGE gel and subsequently used for western blot analysis with the anti-GFP and anti-β-actin primary antibodies; anti-rabbit IRDye680 and anti-mouse IRDye800 served as the secondary antibodies respectively. (**A)** Poor expression was observed in both CTB mutants and all CLB mutants with the exception of V171 in comparison to the wild-type. **(B)** Although all the mutants expressed poorly in comparison to the wild-type, K279A and I280A were particularly low in expression. β-actin labeled in green served as a loading control. Expression was confirmed by a band approximately 60 kDa.

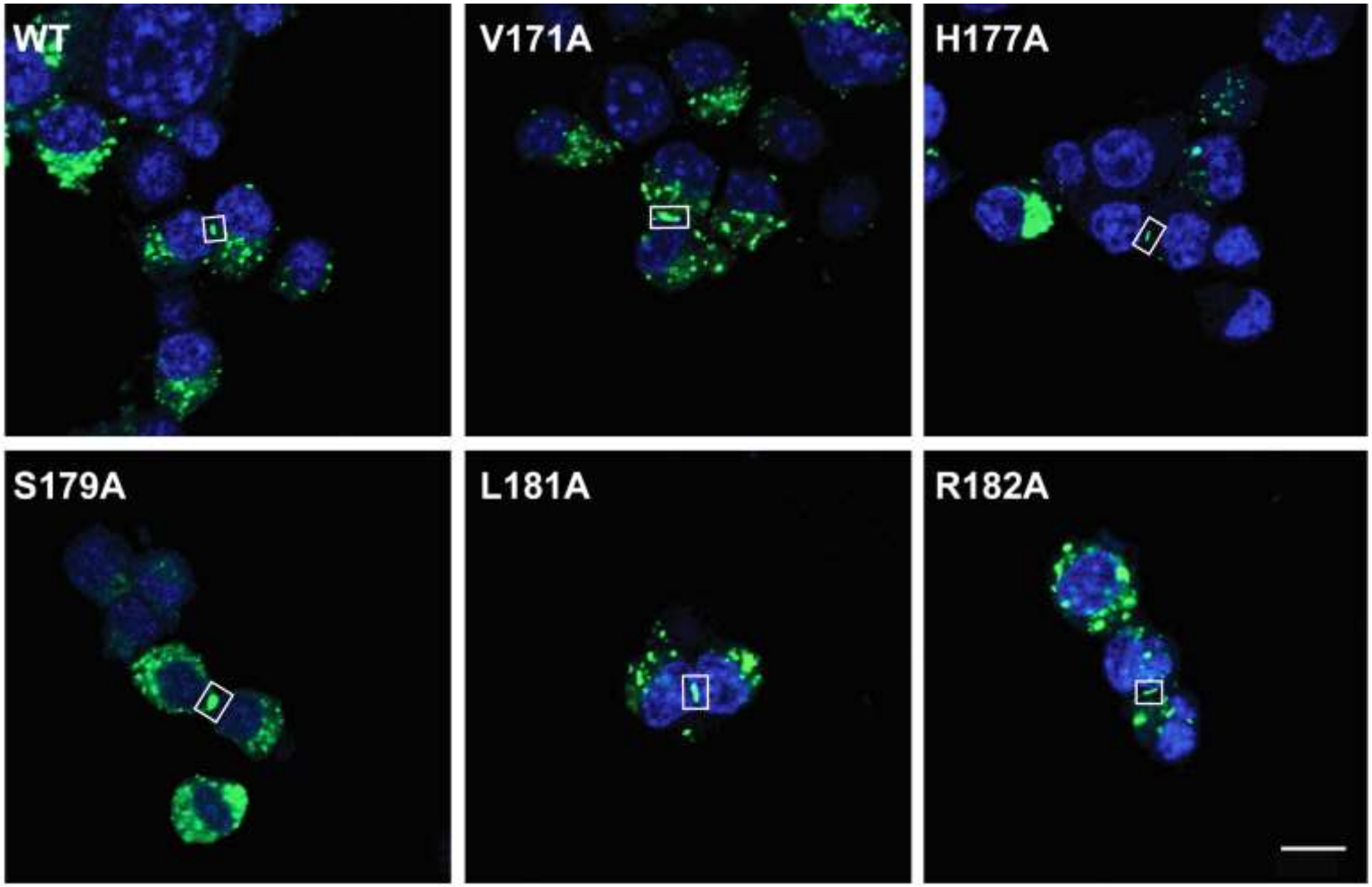

Figure 30| Localization of EGFP-tagged rCx36 wild-type and various CLB point mutant variants.
N2a cells were transfected with pEGFP-rCx36 WT, -V171A, -H177A, S179A, -L181A, or –R182A to determine localization. Confocal images were obtained 48h post-transfection. Localization studies have indicated that rCx36 WT and mutant variants were capable of forming gap junction plaques; GJPs (in green) are indicated with boxes. Staining of the nucleus was achieved with DAPI (blue). Scale bar = 10µm

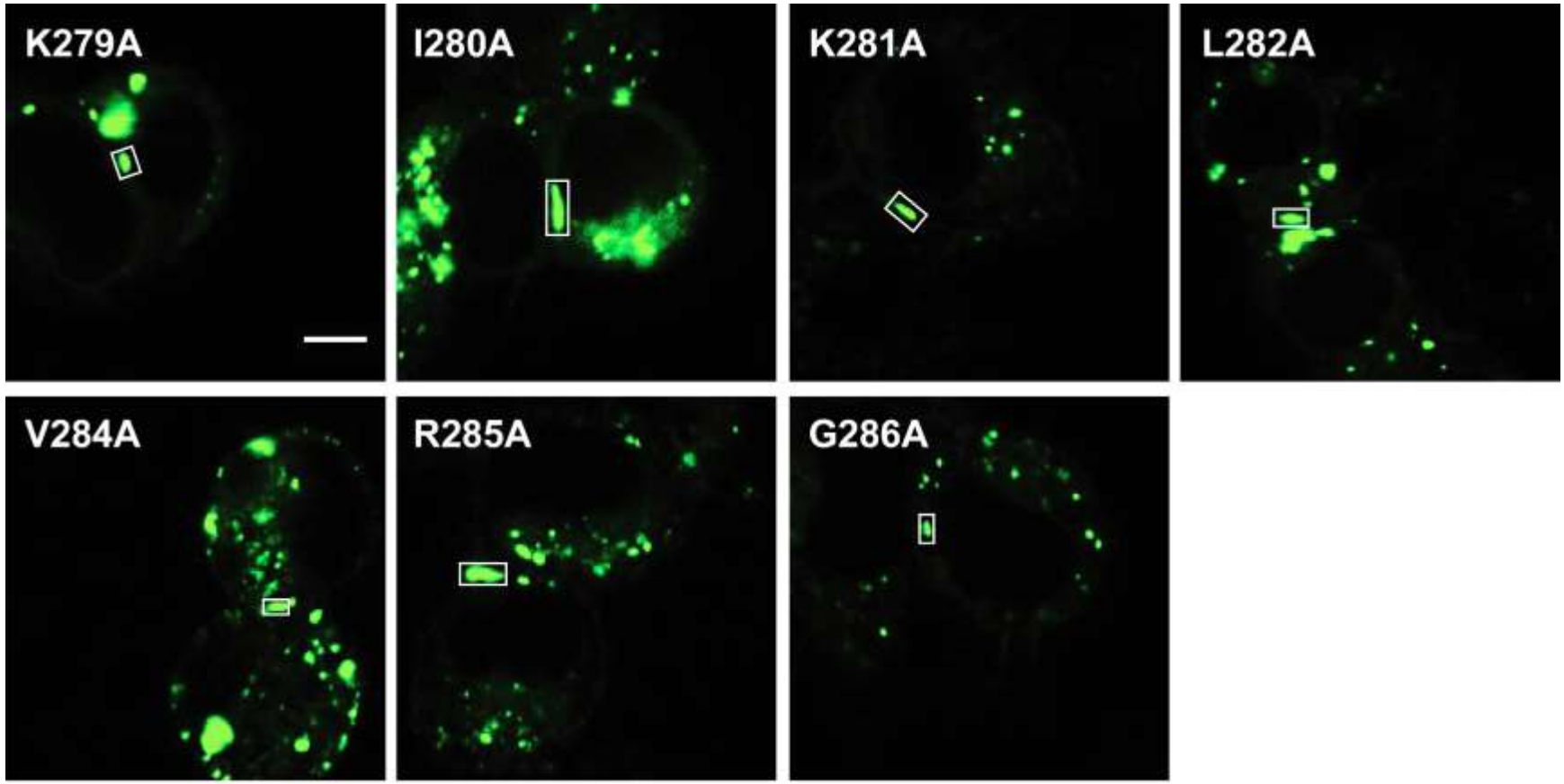

Figure 31| Localization of EGFP-tagged rCx36 CLB point mutant variants.
Localization studies have indicated CTB point mutants were capable of forming GJPs; GJPs (in green) are indicated with boxes. Although rCx36 K279A was able to form GJPs, trafficking was significantly impaired as indicated by the minimal amount of GJPs observed, low fluorescence and the presences of large intracellular deposits. Scale bar = 5µm

5.4.3 Identification of Critical Binding Residues in the rCx36-Tubulin Interaction

Although all CTB point mutant variants generated for rCx36 were capable of forming gap junction plaques **(Figure 31)**, EGFP-tagged rCx36 K279A (0.90±0.18µm²), -K281A (1.06±0.15µm²), -L282A (1.26±0.11µm²) and -G286A (1.13±0.19µm²) displayed a significant reduction in gap junction plaque area in comparison to the wild-type (2.22±0.19µm²). Most notably, rCx36 K279A (0.90±0.18µm^2) was shown to have more than a 50% reduction in GJP size in comparison to wild-type. In addition, qualitative assessment of localization revealed that the number of observable plaques for rCx36 K279A significantly diminished indicating that this residue may be most critical in the trafficking of rCx36 to the plasma membrane. No significant difference was found in the plaque area of cells expressing EGFP-tagged rCx36 I280A, -V284 or -R285A with respect to the wild-type **(Figure 32)**.

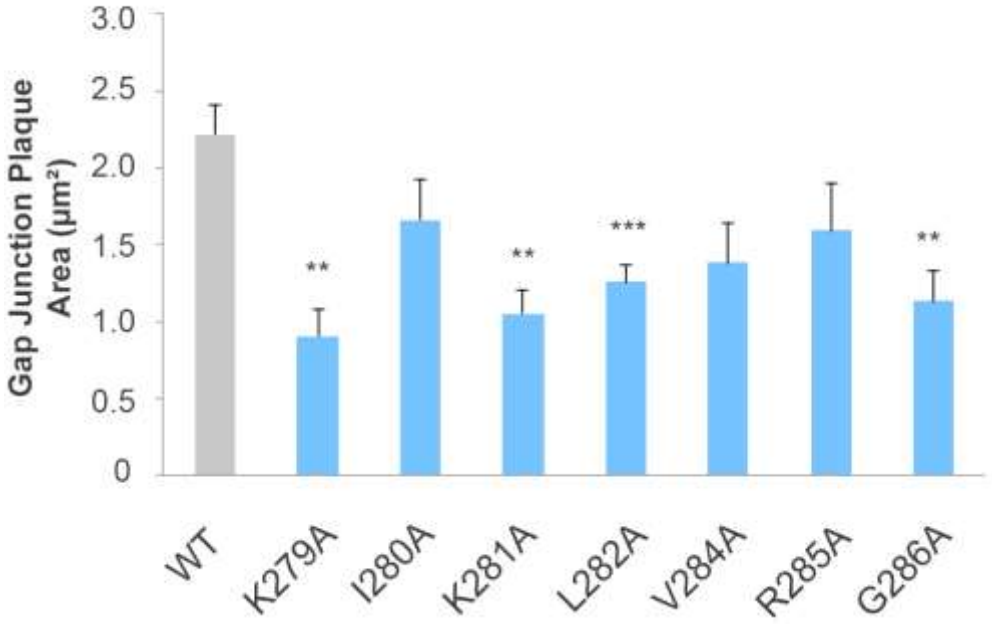

Figure 32| Gap junction plaque area across N2a cells expressing EGFP-tagged rCx36 WT and CTB point mutant variants.

N2a cells were transfected with pEGFP-tagged rCx36 WT and CTB point mutant variants for imaging 48h post transfection. GJPs were optimized along the axis that yielded the largest surface area and subsequently traced with ImageJ. Gap junction plaque area was averaged and presented as mean±SEM. A significant reduction in gap junction plaque was observed for G276A, K279A, K281A, L282A and G286A in comparison to WT rCx36 expressing cells.

Although we previously found that the mobile fraction of wild-type rCx36 expressing cells at the lateral ends of the GJP was significantly reduced in comparison to the respective membrane region, this affect was nearly abolished in the CTB rCx36 point mutant variants. Within the tubulin binding region, the mobile fraction at the plasma membrane of rCx36 K279A (37.84±4.84%), -I280 (32.85±8.07%), -K281 (27.93±7.45%), -V284 (30.64±7.08%), -R285A (23.69±5.42%) and -G286A (23.99±4.98%) were found to be indistinguishable from the respective 'plaque lateral' regions. In comparison to the wild-type, a significant increase in the mobile fraction at the 'plaque lateral' end ROIs of rCx36 K279A ($p=7.0^{-4}$) and -G286A ($p=8.0^{-3}$) was found. This result suggested that these two residues are critical for the stability of the GJP upon insertion. The mobile fraction at the plasma membrane ROIs of rCx36 K279A and -G286A was unaffected in comparison to the wild-type. Similarly, rCx36 I280A, -K281A, -V284A and -R285A were indistinguishable from the wild-type at both the plasma membrane ROIs and the 'plaque lateral' end ROIs suggesting that the reduction in stability was negligible. Interestingly, the rCx36 L282A mutant retained its stability; the mobile fraction of the 'plaque lateral' ends was determine to be 13.74±2.48%, a significant reduction in comparison to the respective membrane region (33.02±6.85%). Comparison to the wild-type revealed no significant difference between either the plasma membrane ROIs or at the 'plaque lateral' end ROIs **(Figure 33A)**.

Half-time of recovery of the 'plaque lateral' ends in comparison to the respective plasma membrane region were indistinguishable across the CTB point mutations with the exception of rCx36 R285A. This mutant showed a significant increase in half-time of recovery to 25.57±4.71s with respect to the plasma membrane region 3.73±1.72s. A modest reduction in the half-time of recovery was also recorded at the 'plaque lateral' ends of rCx36 G286A in comparison to the respective plasma membrane, however, was deemed as insignificant by our statistical measures. Upon cross-analysis to wild-type rCx36, a significant increase in recovery time at the gap junction lateral ends was reported for rCx36 R285A ($p=6.90^{-3}$). In turn, this suggested that the Arg285 residue may be critical in the transport of the rCx36 to the 'plaque lateral' ends of the GJP. Similarly, a modest increase in half-time of recovery was also reported with rCx36 K279A ($p=2.98^{-2}$). Although by our statistical standard this was deemed as insignificant, taken together with the reduction in gap junction plaque size, stability and observable puncta, Lys279 was determined to be the most critical mediator in the rCx36-tubulin interaction. Half-time of recovery

was reported to be indistinguishable between the plasma membrane region of rCx36 K282A expressing cells (4.80±2.10s) and the respective ‘plaque lateral’ ends (19.64±5.77s). In comparison to the wild-type, no significant difference existed between the plasma membrane ROIs or the ‘plaque lateral’ and ROIs **(Figure 33B)**.

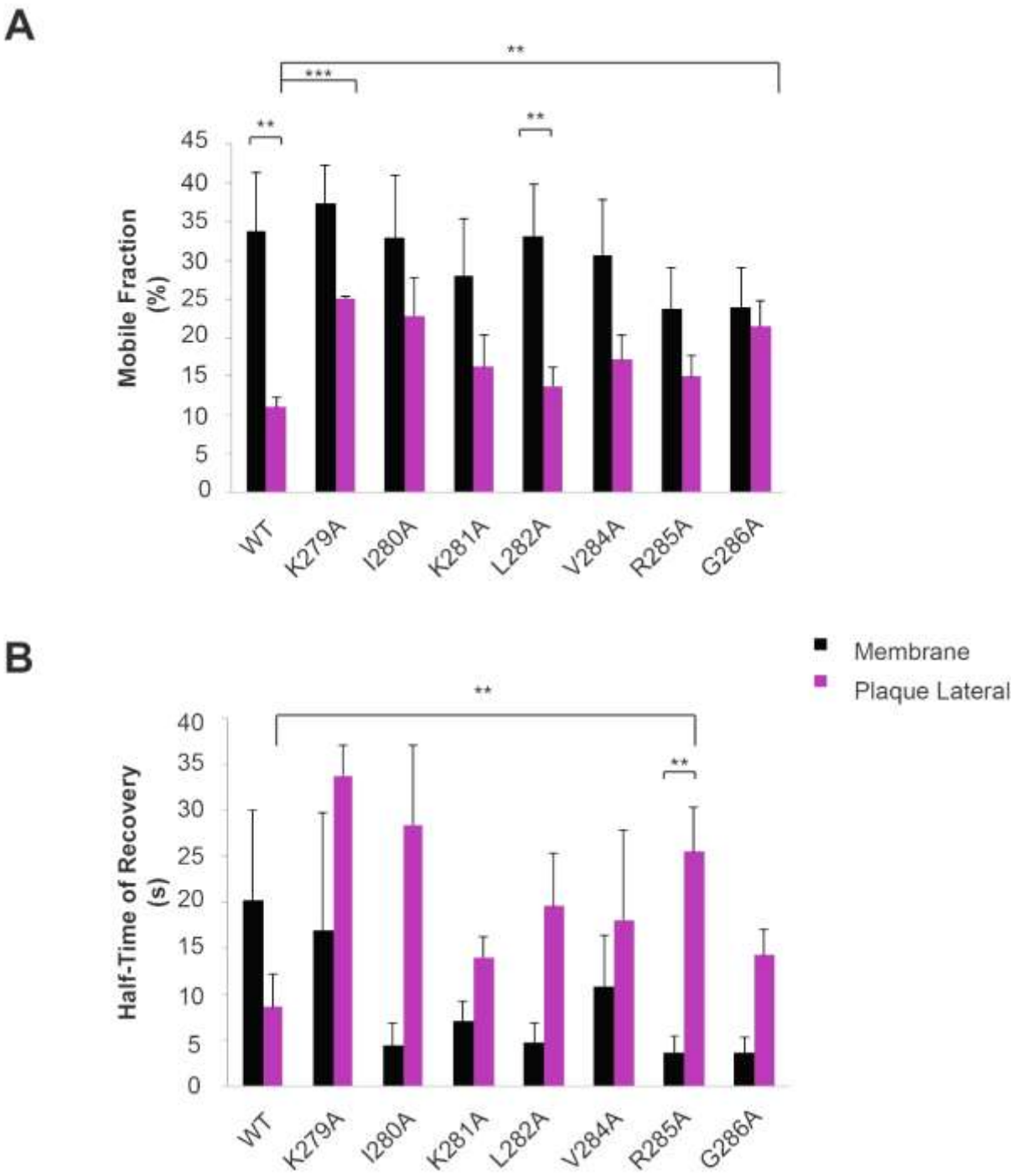

Figure 33| Mobile fraction and half-time of recovery at selected ROIs of wild-type rCx36 and various CTB point mutants.

N2a cells were transfected with various pEGFP constructs to identify the residue(s) critical for interaction with tubulin and to determine the functional consequence of mutation. ROIs were bleached briefly at 70% laser power and recorded over 200 cycles at 1.0-second intervals. Results were normalized against the extracellular space. **(A)** Although modest impairments in the mobile fraction were recorded across the various CTB mutants, rCx36 K279A and G286A expression significantly increase the mobile fraction at the 'plaque lateral' ends in comparison to the WT indicated that these two results may be critical mediators in rCx36 GJP stability. **(B)** Half-time of recovery was significantly impaired at the 'plaque lateral' ends of rCx36 R285A, suggesting that this residue may be critical in transport mediation.

5.5 INVESTIGATING CYTOSKELETAL DEPENDENCY DURING THE CX36 RUN-UP PHENOMENON OF PLASTICITY

Previously, del Corsso *et al*. (2012) have shown that rCx36 is capable of exhibiting LTP-like behavior in a phenomenon known as the run-up. Similar to LTP at chemical synapses, during this phenomenon, gap junction conductance increases 10-fold in a CaMKII-dependent manner (Del Corsso et al., 2012). However, what remains unclear is the means by which the run-up phenomenon is achieved. Two possibilities are that (I) more channels are being recruited into the GJP or (II) the already existing channels in the GJP open to allow for a greater exchange of signaling molecules. A third potential possibility would involve a combination of increased Cx36 hemichannel recruitment and opening of channels at the gap junction plaque. As such, we sought to investigate whether the cytoskeletal-dependent transport was likely involved in the run-up phenomenon by assessing dynamics under conditions similar to the run-up.

5.5.1 Influences of Double Transfection on rCx36 in N2a

Prior to our investigations, the impact of double transfection on rCx36 behavior in N2a cells was assessed to confirm consistency in the chosen cell model. As such, localization, mobile fraction, half-time of recovery and gap junction plaque area was compared between pEGFP-rCx36 single transfected cells and cells double transfected with pDsRed-CaM. For rCx36 behavior to be considered consistent across the transfection conditions, we expected that the parameters, as mentioned above, would be indistinguishable.

As a qualitative measurement, localization studies revealed that double transfected cells were capable of forming gap junction plaques at the plasma membrane of two adjoining cells. Although CaM expression was observed widely throughout N2a cells, CaM was shown to co-localize heavily at regions rCx36 was highly concentrated (i.e. intracellular deposits, gap junction plaques) **(Figure 34A)**. Moreover, no observable differences in gap junction formation (i.e. observable puncta, intracellular deposits) was noted. In support of this, quantitatively it was found that the gap junction plaque area of double transfected cells (1.72±0.20μm²) was indistinguishable from the wild-type (2.22± 0.19μm^2) **(Figure 34B)**.

Upon review of FRAP analyzes, the mobile fraction of the ‘plaque lateral’ end (22.58±4.19%) was determined to be indistinguishable from the respective membrane region (24.86±4.54%). Comparison to the single transfection condition revealed no significant difference at the plasma membrane ROIs ($p=0.31$) or the ‘plaque lateral’ end ROIs ($p=0.02$) **(Figure 34C)**. Therefore, the stability of the GJP was comparable between single and double transfection conditions. Additionally, no significant difference in the half-time of recovery was reported between the ‘plaque lateral’ ends (12.10±2.67s) and the respective membrane region (7.35±2.41s) of double transfection cells. Similarly, half-time of recovery was indistinguishable at the plasma membrane ROIs and ‘plaque lateral’ end ROIs upon cross comparison to the single transfection condition **(Figure 34D)**. This result indicated that double transfected cells behaved similarly to their single transfection counterpart. Therefore, we were successful in confirming that behavior of rCx36 remained consistent across transfection conditions in the N2a cell model.

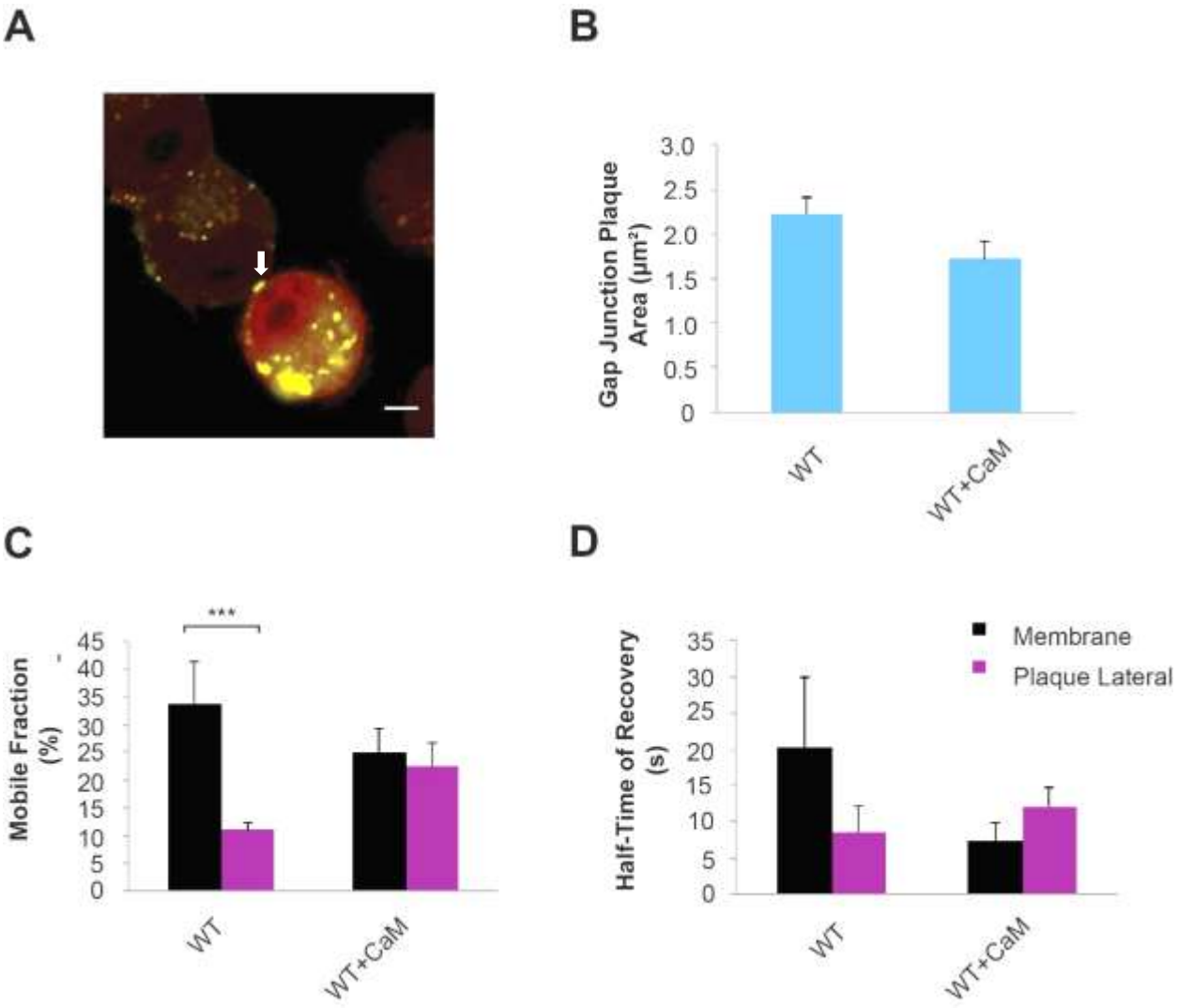

Figure 34| Effects of double transfection with calmodulin on rCx36 dynamics in N2a cells.
Qualitative and quantitative assessments were carried out to determine if double transfection introduced impairments in the ability of rCx36 to function. N2a cells were transfected with either pEGFP-rCx36 WT (as the single transfection condition) or a combination of pEGFP-rCx36 WT and pDsRed-CaM WT (as the double transfection condition) constructs. ROIs were bleached briefly at 70% laser power and recorded over 200 cycles at 1.0-second intervals. Results were normalized against the extracellular space, represented as the mean±SEM. **(A)** Localization studies confirmed that double transfected cells were capable of gap junction plaque formation. CaM was found to co-localize heavily at areas highly concentrated in rCx36. Scale bar = 5µm. **(B)** Although mild impairments in the mobility were observed in double transfected cells, no significant difference was found when compared to the wild-type. **(C)** Half-time of recovery was found to be indistinguishable at the selected ROIs. **(D)** No significant difference was observed in the gap junction plaque area suggesting that double transfected cells were indistinguishable from the single transfected counterpart.

5.5.2 Stability and Transport of rCx36 Under Run-Up-Like Conditions

Finally, to assess whether cytoskeletal-dependent transport was a regulator in the run-up phenomenon, double transfected cells were treated with ionomycin. Calcium-dependent effects on mobility, half-time of recovery and gap junction plaque formation were recorded relative to the untreated counterpart. Ionomycin, a selective calcium ionophore agent, stimulates Ca^{2+} entry across the cell membrane. In doing so, intracellular calcium levels increase and allows for CaM activation; once CaM is activated, this in turn activates CaMKII. In this way, CaMKII was indirectly activated, and cells were primed to maximally simulate run-up-like conditions for assessment. Once active, CaMKII is known to be involved in a number of processes, including the enhancement of tubulin polymerization through MAP2 association upon phosphorylation (Khan & Ludueña, 1996) and activation of rCx36 run-up. Since our group has shown that run-up is inhibited in the presence of colchicine (unpublished), we speculated that cytoskeletal-dependent trafficking of rCx36 to the GJP may be a requirement of the run-up phenomenon. Therefore it was hypothesized that an increase in mobile fraction, relative to the increase in activity at the 'plaque lateral' ends, would be observed with ionomycin treatment. Additionally, we predicted a decrease in recovery time and increase in gap junction plaque area would be observed in parallel to the increase in rCx36 channel recruitment.

In cells treated with ionomycin, a significant reduction in the mobile fraction was recorded at the 'plaque lateral' ends (7.30±1.14%) in comparison to the respective membrane region (39.91±7.94%, $p=6.50^{-6}$). Further, the 'plaque lateral' end ROI of treated cells was significantly reduced compared to its untreated equivalent ($p=1.27^{-3}$) suggesting that the stability of rCx36 gap junction plaques was promoted upon Ca^{2+} stimulation. The mobile fraction of the plasma membrane ROIs was determined to be indistinguishable from the treated and untreated conditions **(Figure 35A)**. No significant difference in the half-time of recovery was found between the plasma membrane region of double transfected cells treated with ionomycin in comparison to the respective 'plaque lateral; end. Similarly, both the plasma membrane ROI and 'plaque lateral' end ROI of wild-type rCx36-EGFP/CaM-dsRed treated with ionomycin were indistinguishable from the untreated double transfected cells **(Figure 35B)**. This result indicated that transport was neither impaired nor promoted. In support of this, the GJP area in cells treated with ionomycin (0.74±0.20µm²) was found to be indistinguishable from its untreated counterpart **(Figure 35C)**.

Additionally, no significant difference in the CTF_{GJP} of stimulated cells (293.77±43.64 RFU) was found in comparison to the unstimulated counterpart (188.87±30.12 RFU) **(Figure 35D)**. Therefore, it is likely that cytoskeletal-dependent trafficking to the existing gap junction plaques does not serve as a prerequisite to the run-up phenomenon.

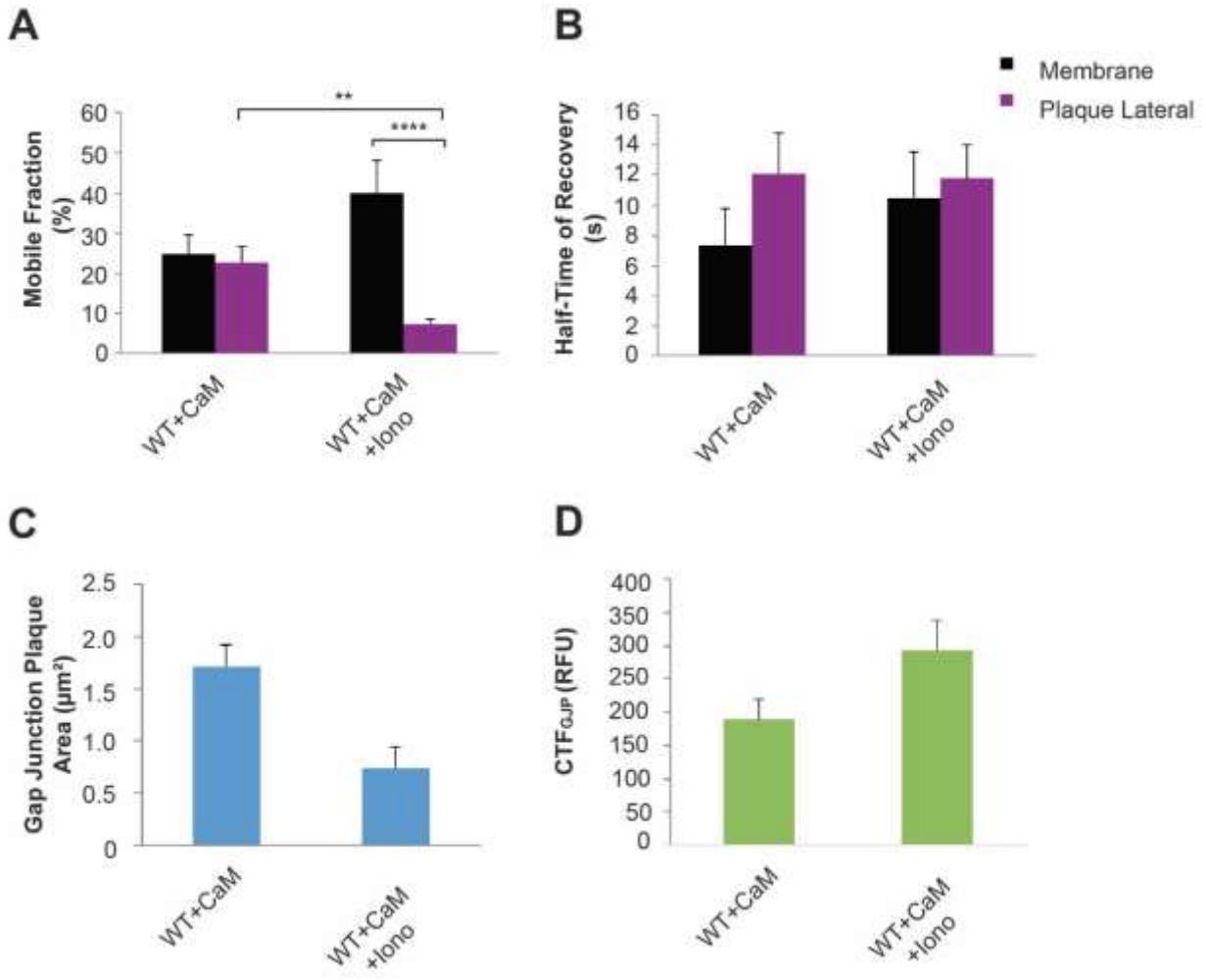

Figure 35| Modulation of rCx36 in the presence of Ca^{2+}/ionomycin in N2a cells double transfected with CaM. Quantitative and qualitative assessments were carried out to determine if cytoskeletal-dependent trafficking was a mediator in the conditions similar to the run-up phenomenon. N2a cells were transfected with a combination of wild-type pEGFP-Cx36 WT and pDsRed-CaM (as the double transfection condition) constructs and treated with ionomycin. ROIs were bleached briefly at 70% laser power and recorded over 200 cycles at 1.0-second intervals. Results were normalized against the extracellular space, represented as the mean±SEM. **(A)** The mobile fraction of the 'plaque lateral' ends in cells treated with ionomycin displayed a significant reduction in comparison to the untreated cells suggesting the stabilization of the GJP is calcium mediated. **(B)** Half-time of recovery was found to be indistinguishable at the selected ROIs despite ionomycin treatment. **(C)** No significant difference was observed in the gap junction plaque area between stimulated and unstimulated double transfected cells. **(D)** CTF_{GJP} was not impacted upon calcium stimulation. Overall these results suggest that tubulin-dependent trafficking to existing gap junction plaques is not a prerequisite for the run-up phenomenon.

6 DISCUSSION

6.1 SUMMARY OF RESULTS

This thesis addressed the interaction between rCx36 and the cytoskeletal proteins tubulin and actin, in N2a cells. It was hypothesized that interaction with the cytoskeleton is critical for the transport of rCx36 hemichannels into the GJP, particularly during the run-up. This thesis demonstrates the following:

I. rCx36 interacts with tubulin-beta 3 *in vivo* as confirmed by BioID.
II. rCx36 hemichannels are delivered to the lateral ends of the GJP and removed from the center.
III. Deletion mutants altering the CLB and CTB domains are less stable than wild-type rCx36.
IV. Disruption of tubulin interaction with rCx36 impairs trafficking and aggregation of hemichannels as determined by TAT peptides, colchicine and paclitaxel interference.
V. Disruption of actin interaction with rCx36 reduces GJ stability and has minor effects on hemichannel transport.
VI. Lys279 was determined to be the most critical residue supporting tubulin interaction with rCx36.
VII. Intracellular calcium elevation stabilizes rCx36 GJPs and hemichannel recruitment ceases.

6.2 BIOID CONFIRMS *IN VIVO* INTERACTION BETWEEN RCX36 AND TUBULIN

6.2.1 Tubulin-Beta III and rCx36 Interact *In Vivo*

The first aim of this thesis was to confirm the interaction between rCx36 and tubulin *in vivo* while simultaneously assessing the efficiency of the newly developed BioID methodology (see section 5.1). A fusion protein with BirA* and rCx36 wild-type and mutant variants (Δ175-196 and Δ279-292) were successfully generated and expressed in the N2a cell model (see section 5.1). Initial pull-down of biotinylated proteins captured with wild-type rCx36-BirA* revealed tubulin as a potential interacting candidate via mass spectrometry **(*See Appendix D*)** and western blotting with the β-tubulin antibody **(Figure 15)**. Specifically the tubulin-beta 3 (βIII-tubulin) isotype was

identified as being unique to rCx36-BirA* with respect to the negative control BirA*. While biotin affinity capture of tubulin was also achieved with BirA* alone, only the βIII-tubulin monomer and isotype could be exclusively identified as an interacting candidate of rCx36. This is in contrast to reports on Cx43 confirming interaction with both α- and β-tubulin monomers (Giepmans, Verlaan, Hengeveld, et al., 2001). Data interpretation needs to be cautious since tubulin is present in the cytoplasm in high concentrations. Therefore, it can't be excluded that interaction between BirA* and tubulin is due to the high abundance of the target protein and the overlapping distribution in the cytoplasm. However, we are the first to describe and confirm βIII-tubulin as an interacting candidate of rCx36. In mammalian cell lines, tubulin isoforms are differentially expressed depending on tissue and stage of development. In the mammalian brain specifically, presence of tubulin isoforms is most prominent; the tubulin-beta 3 isotype is known to be exclusively expressed in neuronal cells and unique in that a Ser444 phosphorylation site is present and used (Ferreira & Caceres, 1992; Khan & Ludueña, 1996; Ludueña, Zimmermann, & Little, 1988). Thus, interaction between rCx36 and βIII-tubulin may be critical in mediation of transport and additional cellular functions in neurons with the potential of the tubulin Ser444 phosphorylation site being of significance for this process.

In our experiments, the amount of biotinylated proteins captured with BirA* was significantly reduced in comparison to the rCx36-BirA* **(Figure 16)**. Although the mechanism for targeting remains unclear in mammals, acetyl-CoA carboxylases such as BirA* are located in the cytosol (Robinson, Oei, Saunders, & Gravel, 1983; Shi & Chang, 2007). As such, protein interaction achieved with BirA* fused to the rCx36 protein should allow a greater range of specific interactions since the fusion protein is bound to membranes; not surprisingly, additional rCx36 interacting proteins were identifiable via mass spectrometry, particularly those associated with the golgi apparatus and mitochondria **(*See Appendix D*)**. However, an increase in biotinylated tubulin captured with BirA* was observed in comparison to wild-type rCx36-BirA* **(Figure 16)**, suggesting that fusion of BirA to rCx36 limits the amount of interaction with cytosolic tubulin. This result is likely caused by spatial restrictions due to the membrane localization of rCx36.

As expected, a reduction in the fluorescence signal detected on the western blot was observed for the CTB mutant (rCx36 Δ279-292) **(Figure 17B, D, F)**, which indicated that the deletion of the

proposed tubulin binding site reduces interaction with βIII-tubulin (and potentially other isoforms common to both rCx36 and BirA*). As such, the remaining signal detected for tubulin is likely attributable to an unspecific interaction with BirA*. Unexpectedly, a reduction in the fluorescence signal in the CLB mutant (rCx36 Δ175-196) was also observed **(Figure 17A, C, E)**, which suggests that an indirect interaction specific to tubulin exists between the CLB and CTB domains. This result may be attributed to additional interacting partner capable of mediating interactions with tubulin through the CLB either directly or indirectly.

6.2.2 Efficiency and Limitation of BioID

The original authors of the BioID methodology used this technique to identify a novel interacting partner of LaA. Limitations addressed in the publication were pertaining to solubility of the bait proteins (where conditions required to solubilize the protein may bias interaction with candidates) and low abundance of interaction proteins (resulting in false-negative results) (Roux et al., 2012b). However, here we propose an additional limitation to the methodology: highly abundant proteins, such as tubulin, may lead to both false-negative results and false-positive results. False-negative results may become evident in the comparison of identified protein candidates between the bait and the BirA* control, where proteins capable of interaction with both may be disregarded as non-specific to the bait. Similarly, false-positive results may arise due to spatial constraints, where proteins are biotinylated due to close proximity rather than true interaction. In such cases, users interested in confirming interaction with highly abundant proteins must design control experiments strategically to eliminate a BirA*-specific bias; we found that the authors failed to address BirA* specific interactions as a control. In this thesis, we demonstrated that BirA* was able to interact with tubulin **(Figure 16)**, but only one isotype; βIII-tubulin showed specific interaction with rCx36. This method wasn't able to clarify whether the α-tubulin monomer is capable of interacting at the CTB in a similar fashion to what has been shown for Cx43 (Giepmans, Verlaan, Hengeveld, et al., 2001). Although the region of interaction could be predicted, we could not determine beyond doubt whether amino acids Lys279-Ala287 are the tubulin binding region under the BioID methodology, thus limiting the effectiveness of studying protein-protein interactions with this technique. However, since interaction between tubulin and rCx36 was successfully identified *in vivo*, we

propose that BioID can serve as an initial screening method to identify potential interacting candidates, in combination with additional *in vivo* studies optimized for specificity.

6.3 DYNAMICS OF THE CX36 GAP JUNCTION PLAQUE

6.3.1 Transport of rCx36 is Consistent with Literature

Previous studies have indicated that Cx43 hemichannels are delivered to the lateral ends of the gap junction plaque whereas the removal of hemichannels occurs from the center (Lauf et al., 2002a). This mechanism for transport is supported for Cx35, the fish ortholog of Cx36, at the mixed synapses of the goldfish Mauthner cells (Flores et al., 2012). Here we report that the dynamic delivery of rCx36 to the gap junction plaque coincides with the reports of Lauf et al. (2002) and Flores et al. (2012). Through time lapsed imaging observations, rCx36 connexons were reported to be delivered in small groups, in multiple instances; no observation of single channel delivery was recorded. We also have reported removal of rCx36 at the center of the nexus. As a precursor to removal, we recorded an invagination event and subsequent division of the gap junction plaque. Early literature reports that internalization of connexons is preceded by the invagination, restriction, and pinching off of both junction membranes into one of the adjoining cells (Larsen, Tung, Murray, & Swenson, 1979). As such, both the delivery and removal of rCx36 from the nexus was successfully recorded and shown to be consistent with previous reports on Cx43 and Cx35.

6.3.2 Characteristics of the rCx36 Gap Junction Nexus

Relative to the plasma membrane and intracellular space, wild-type rCx36 at the lateral ends of the gap junction plaque was determined to be stable in nature as indicated by the measurement of the mobile fraction. At the center of the gap junction plaque, mobility was more stable in comparison to the plasma membrane, yet dynamics were comparable to the intracellular space. Most likely this reflects an equilibrium between dynamic insertion and removal of Cx36 from the plaque **(Figure 23A)**. Although integration and removal of connexons is a continual and dynamic process, gap junctions are known to typically be stable in nature for hours while embedded in the plasma membrane for the duration of its lifetime. Gap junctions can be stabilized by direct and

indirect interactions with proteins such as actin and ZO-1, and may potentially serve as anchoring junctions for microtubules as suggested for Cx43 (Giepmans, Verlaan, & Moolenaar, 2001; Giepmans, Verlaan, Hengeveld, et al., 2001; Li, Olson, Lu, Kamasawa, et al., 2004). Lauf et al. (2002) has found that upon reaching the plasma membrane, Cx43 hemichannels can move freely, where the mobile fraction was determined to be approximately 70% (Lauf et al., 2002a). This in turn correlated to the rapid repopulation of the gap junction plaque upon bleaching (Shaw et al., 2007). The mobile fraction of rCx36 was found to be much less motile at the plasma membrane relative to Cx43, suggesting that rCx36 dynamics are uniquely controlled and regulated. This novel finding may be indicative of rCx36 modulation through cytoskeletal interactions, and differences thereof, in terms of regulatory proteins.

We expected to see a reduction in the half-time of recovery at the gap junction plaque, particularly at the lateral ends, relative to the intracellular space. We also predicted that the recovery of the GJP would comparable to the recovery at the plasma membrane as an indication of trafficking dynamics. However, this was not the case as all ROIs analyzed were indistinguishable from each other **(Figure 23B)**. Two plausible, and potentially related, explanations could account for this result. Firstly, since recordings were taken noninvasively *in vivo*, lack of observable difference could be a true reflection of the dynamic trafficking of rCx36 throughout the cell. In this case, the required transition through cytosolic and membrane stages prior to docking at the gap junction plaque would be accounted for. As connexons are continuously transported throughout these regions, indistinguishable recovery times seems plausible as it not an indication of single protein velocity. Secondly, this also may indicate a lack in sensitivity in the method dependent upon ROI selection. Since FRAP is a live cell imaging technique, it is sensitive to fluctuations in cellular movements, which are more prominent at the plasma membrane and intracellular space ROIs. Consequently, the shuffling of rCx36 in and out of these ROIs produces a large degree of variability, which in turn makes it more difficult to detect minor changes in half-time of recovery.

To date, few reports have addressed gap junction area as a characteristic of connexin isoforms. Here we reported the mean gap junction plaque area of EYFP-tagged rCx36 to be 2.22± 0.19μm^2 **(Figure 19F)**. More precisely, since we didn't aim at 3D reconstructions of the entire plaque area, this value represents a tangential cut through the widest section of this plaque, thus reflecting its extension in the plasma membrane. Further, it is important to take into consideration that measurements were obtained based on fluorescence, which radiates outward of the GJP, decaying with distance from its origin, and creating an image that is larger than the actual plaque size. Comparative to the reported value mean gap junction plaque area of Cx43 (0.26 μm^2, SD ± 0.145) (Jones et al., 1993), the rCx36 gap junction plaque therefore appears relatively large. Although this would still fall between typical values reported for gap junction plaques, which ranges from 0.3 μm² to ≥ 5 μm² depending on isoform expressed and tissue type, further confirmation via electron microscopy would be required. However, it is interesting to note that typically, gap junctions with larger surface areas display a reduction gap junctional conductance per μm² (Jongsma & Wilders, 2000). Therefore, a relatively large GJP area for rCx36 would complement earlier reports of low single channel conductance for Cx36 (Srinivas et al., 1999), although the number of open/closed channels might equally well explain this observation.

6.4 THE CYTOSKELETON IS CRITICAL FOR CX36 INTEGRATION AT THE GJP

6.4.1 Interactions with the Actin Cytoskeleton

6.4.1.1 Mutant variant rCx36-Δ175-196 reveals potential actin binding domain

In this thesis, we have proposed that an actin binding site is present within the cytoplasmic loop of the rCx36 protein. As predicted by ELM we investigated a region encompassing amino acid residues Asp167-Ala184 as potential actin binding site **(*See Appendix E*)**. Although Cx36 has been shown to interact directly with Zonula occludens (ZO) proteins, known interactors of actin (Li, Olson, Lu, & Nagy, 2004; Li, Olson, Lu, Kamasawa, et al., 2004), it has yet to be shown that a direct relationship between actin and Cx36 exists. Therefore, we are the first to propose actin and an interacting partner of Cx36. The hypothesized actin binding domain was found to be highly conserved across species yet less conserved across connexin isoforms **(Figure 20)**. Sequence

alignment against the glial connexins rCx43 and rCx30 revealed the presence of spacer sequences between conserved residues not present in rCx36 or respective orthologs. As such, we speculate that the Cx36 actin binding region may be unique to this neuronal isoform. Although the functional significance of these spacer residues is currently unknown, one can speculate that in similar notion to that of actin cross-linking proteins, these spacer sequences may act to provide variability in actin bundling and/or actin-specific plasma membrane association (Matsudaira, 1991) directly or indirectly. The proposed actin binding domain of rCx36 is rich in non-polar (hydrophobic) amino acids, particularly leucine, alanine and proline. The presence of hydrophobic amino acids is characteristic of most actin binding domains such as the WASP homolog 2 (WH2) domain, gelsolin and the thymosin-β domain, which have been shown to associate with the cleft of hydrophobic amino acids in actin (Chereau et al., 2005; Hertzog et al., 2004; Irobi et al., 2004; Quinlan, Heuser, Kerkhoff, & Mullins, 2005; Schutt, Myslik, Rozycki, Goonesekere, & Lindberg, 1993; Yarmola, Parikh, & Bubb, 2001). Additionally, a number of electrically charged amino acids, particularly glutamic acid, were present in the proposed rCx36 actin binding domain. It is worth mentioning that of the electrically charged amino acids, 50% were basic residues which have been shown to facilitate actin binding in the cytoskeletal binding protein coronin (Gatfield, Albrecht, Zanolari, Steinmetz, & Pieters, 2005). Taken together, this provides strong evidence that actin interaction with rCx36 and orthologs may be direct rather than indirect, however, this still remains to be proven experimentally.

At the cellular level, actin is known to maintain and regulate vesicular pools by acting as a scaffold to restrict mobility thus creating a barrier preventing fusion or by serving as a transport pathway, guiding vesicles for docking. In this scenario, the functional role of actin is dependent on synaptic type, state and organism. Additionally, actin has been shown to anchor receptors through the interaction with scaffolding proteins (Kuriu, Inoue, Bito, Sobue, & Okabe, 2006). Thus, we hypothesized that interference of actin-dependent interaction with rCx36 may influence both vesicular and docked connexons at the gap junction plaque, particularly at the lateral ends. As such, our analyses were focused at this region. We aimed to characterize the functional significance of actin interaction with a two-step approach of (1) understanding interaction at the level of gap junction plaque and (2) understanding the interaction with respect to the whole cell. Initially,

localization studies revealed that expression of the CLB mutant rCx36 Δ175-196 resulted in a reduction in observable puncta and gap junction plaque area, in comparison to the wild-type **(Figure 19)**, without impairments to total cell protein production **(Table 11)** (see section 5.2.2). As a result, an increase in intracellular vesicles of rCx36 Δ175-196 was observable suggesting that the lack of actin interaction impairs trafficking and/or promotes removal of connexons from the gap junction plaque. In this way, actin may be functionally linked to transport and/or anchoring of the rCx36 connexons respectively. Quantitatively, the mobile fraction of rCx36 Δ175-196 gap junction plaques was significantly higher than the wild-type at the lateral ends, yet indistinguishable from the respective plasma membrane region **(Figure 24A)**. Here, we suggest that an increase in mobility is a direct reflection of the reduction in anchoring ability rather than enhanced transport as determined by the reduction in gap junction plaque area. Since no significant difference in half-time of recovery was observed **(Figure 24B)**, it is likely that actin-dependent trafficking of rCx36 connexons is minor and an additional mechanism for transport is involved. We find that our proposal is in agreement with the proposal of Qu, Gardner, & Schrijver (2009) suggesting the implication of actin in connexon anchoring and short distance transport.

6.4.1.2 Actin interference with Cytochalasin D reduces stability

To determine the effects of actin inhibition on rCx36, pharmacological blocking of actin was achieved with cytochalasin D. In this way, the effects of actin impairment on the whole cell level was assessed. Previously, it was demonstrated that cytochalasin B treatment of Cx26-YFP and Cx43-GFP inhibited connexon recruitment and assembly at the GJP (Thomas et al., 2005). Upon treatment of wild-type rCx36 expressing cells with cytochalasin D, mobility at the gap junction 'plaque lateral' ends significantly increased, in comparison to the untreated counterpart, such that mobility was indistinguishable from the respective plasma membrane region (see section 5.3.3). This observed increase in mobility could be attributed to more movement at the lateral ends, as a result of anchoring impairment of docked connexons, or an increase in activity specific to an increase in vesicular recruitment. For the latter to hold true, this would imply that an actin meshwork near the GJP could act as a barrier to limit the amount of vesicular fusion of hemichannels under basal conditions. In this case, cytochalasin D treatment would disrupt the actin barrier, allowing for an increase in vesicular fusion and hemichannel insertion. However, this

theory would require further investigation. Within the scope of this thesis, since gap junction plaque area with cytochalasin D treatment was indistinguishable from the untreated counterpart, we cannot confidently conclude that actin possesses barrier capabilities at the rCx36 nexus in the N2a cell model. Since we found a reduction in CTF_{GJP} in cells treated with cytochalasin D suggesting a reduction in connexons at the GJP, our findings are parallel to the reports of Thomas et al. (2005) on Cx26 and Cx43. However, our results suggest that the primary role of actin interaction is the anchoring of rCx36 hemichannels, particularly at the lateral ends; we deemed actin's role in trafficking as secondary. Again, this supports the work of Qu, Gardner and Schrijver (2009) providing evidence to suggest that actin anchors and supports Cx30 GJPs at the plasma membrane, with minor roles in short distance trafficking (Qu et al., 2009). Since we are the first to describe such relationship with rCx36, one can speculate then that such interaction improves efficiency of connexon integration upon docking at the gap junction plaque.

6.4.2 Interactions with the Tubulin Cytoskeleton

6.4.2.1 Deletion of the tubulin binding domain reduces trafficking and aggregation

Previous studies have shown that connexon delivery, in some instances, is tubulin-dependent and relative dependency is determined by connexon isoform. Therefore, it has been speculated that tubulin enhances transport (Laird, 2010). We hypothesized that interference of tubulin interaction would negatively impact rCx36 transport such that gap junction plaque size and recovery time would be impaired if trafficking was indeed tubulin-dependent. Our research initiative was again designed in a two-step approach of understanding effects of tubulin interference at the (1) gap junction plaque (2) whole cell levels. Although localization studies confirmed the presence of rCx36 Δ279-292 gap junction plaques, unexpectedly, the gap junction plaque size **(Figure 19)**, and half-time of recovery **(Figure 24B)** was found to be indistinguishable from the wild-type. As such we propose that a tubulin-independent transport mechanism is involved in the delivery of rCx36 hemichannels, with actin as a potential candidate. However, we found that the gap junction fluorescence of rCx36 Δ279-292 expressing cells was significantly reduced in comparison to the wild-type **(Table 11)**. In combination with the maintained gap junction plaque size, this would suggest that less rCx36 Δ279-292 connexons are participating at the gap junction plaque and thus are likely less densely packed. Therefore, it is probable that in the absence of amino acid residues

spanning from Lys279-Lys292, trafficking was impaired. By this we suggest that tubulin aids in mediation of trafficking in addition to the aggregation and tight clustering of hemichannels at the gap junction plaque. In support of the latter, the mobile fraction at the 'plaque lateral' ends was found to increase considerably in comparison to wild-type **(Figure 24)**. Overall, this indicated a greater exchange in bleached connexons for the unbleached, which we attribute to the loss in aggregation ability. Therefore, this resulted in more mobility and exchange of connexons at the GJP.

6.4.2.2 Tubulin interference reduces trafficking and stability of the rCx36 GJP

Several pharmacological targets of tubulin were used in this study to confirm the role of tubulin-rCx36 interaction. Firstly, competitive blocking of the tubulin binding domain was achieved with the cell penetrating TAT peptide. In this way, tubulin interference was specific to the gap junction plaque. Wild-type rCx36 expressing cells treated with TAT CT-ON showed a significant increase in the half-time of recovery at the 'plaque lateral' ends, in comparison to the untreated wild-type, indicating that there was an impairment in trafficking at the 'plaque lateral' ends **(Figure 25B)**. We attribute this impairment to the inhibition of tubulin interaction at the cytoplasmic binding domain of rCx36. Similar to the expression of the rCx36 Δ279-292 mutant variant, gap junction plaque size was maintained upon tubulin interference at the gap junction plaque **(Figure 25C)**. Therefore, some functionality with respect to transport is maintained when alteration occurs at the level of the gap junction. It is important to note that TAT, within the boundaries of this thesis, served as competitive blocker and therefore not all functionality is completely abolished with treatment. Nevertheless, this does suggest that a tubulin-independent mechanism for transport exists and can be used as an alternative. However, it is likely less efficient at doing so as indicated by the increase in half-time of recovery. We speculate that this transport mechanism involves actin, and may be dependent temporally and spatially on connexon reserves near the plaque. Further, wild-type rCx36 cells treated with TAT CT-ON showed a significant increase in the mobile fraction in comparison to the untreated wild-type **(Figure 25A)**, rendering mobility indistinguishable from the respective plasma membrane region. This result may be a reflection of the inability of tubulin to aggregate connexons, thus allowing for more mobility and exchange of hemichannels within the gap junction plaque. To date, there are no reports outlining the effects of

TAT-peptide blocking of the tubulin binding region specific to connexins as a reference. As such, our results are the first of its kind to be described, specifically at the Cx36 nexus.

Interestingly, treatment of wild-type rCx36 expressing cells with TAT CT-OFF revealed a significant reduction in gap junction plaque size **(Figure 25C)**. Therefore, it was suggested that another interacting partner important in trafficking and/or anchoring of connexons at the GJP is housed within the CLP. Outside of the scope of this project, a number of C-terminal interacting partners have been identified as connexin stabilizers. In particular, ZO-1 has been shown to interact with the C-terminal domain of Cx36 and is speculated to be involved in formation, distribution, turnover and the indirect regulation of communication (J.-C. Hervé, Derangeon, Sarrouilhe, Giepmans, & Bourmeyster, 2012). These interactions are likely impaired with CT TAT-OFF treatment, promoting removal and recycling of rCx36 connexons and thus resulting in a reduction in gap junction plaque size without impairments in mobile fraction at the 'plaque lateral' ends.

6.4.2.3 Total cell tubulin interference causes trafficking impairments

On the whole cell level, the effects of tubulin alteration on rCx36 *in vivo* was characterized pharmacologically with the tubulin polymerization inhibitor, colchicine, and promoter, paclitaxel. In Novikoff hepatoma cells, inhibition of MTs with 100 µM colchicine showed no impairments on the initiation of gap junction assembly or hemichannel aggregation under basal conditions (Johnson et al., 2002). Unlike Cx43, Colchicine treatment of wild-type rCx36 expressing cells resulted in a decrease in gap junction plaque area in comparison to the untreated cells, yet no change in the half time of recovery **(Figure 26B-C)**. As such, a reduction in the gap junction plaque size could be attributed to either an increase in pre-mature removal and/or decrease in trafficking. However, since half-time of recovery was not largely impacted, in combination with our building evidence, it is likely that the decrease in gap junction plaque size is a reflection of a trafficking impairment. In such case, a compensatory mechanism allows for recovery to be relatively maintained. We find that these results further support the potential of actin-dependent trafficking as a compensatory mechanism, most likely over a short distance. Additionally, a significant increase in the mobile fraction is likely attributable to a reduction in clustering ability as previously detailed **(Figure 26A)**. Therefore, these results are not in conjunction with the reports of Cx43 by Johnson et al. (2002) and are seemingly unique to rCx36.

Previous studies have demonstrated that paclitaxel treatment was sufficient to impair recovery of Cx43 hemichannels at the GJP, thus disrupting the fast repopulation, post-bleach (Shaw et al., 2007). Paclitaxel treatments on wild-type rCx36 expressing cells had no adverse effects on the mobile fraction or half-time of recovery, but did reveal an impairment in gap junction plaque area **(Figure 26)**. Although paclitaxel is known to promote the polymerization of microtubules, it has also been shown to promote MT bundling which negatively affects anterograde transport (i.e. forward trafficking) (Theiss & Meller, 2000). Therefore, we suspect that the reduction in gap junction plaque size is a reflection of the adverse effects of paclitaxel on trafficking. In comparison to Cx43, no change in half-time of recovery under paclitaxel treatment demonstrates that fast-repopulation is not a characteristic of Cx36. Instead, this suggests that trafficking of Cx36 to the GJP is distinguishable from Cx43, likely due to difference in interaction candidates.

Neither colchicine nor paclitaxel treatment had additional effects on rCx36 Δ279-286 expressing cells **(Figure 26-27)**. Therefore, it was reaffirmed that rCx36 interacts with tubulin *in vivo* and the binding domain is located within this region. Interestingly, paclitaxel did seem to have some stabilizing effects on the rCx36 Δ279-286 mutant, however this was found to be insignificant in comparison to the untreated counterpart **(Figure 27)**.

6.4.2.4 Point Mutations Disrupt rCx36-tubulin interaction

The tubulin binding region of rCx43 was previously determined to be conserved at the cytoplasmic terminal of rCx36 **(Figure 6)**. The participating residues spanning from Lys279-Ala287 are a combination of non-polar and electrically charged (basic) amino acids, typical of microtubule binding regions. In the third aim of this thesis, the critical binding residues involved in tubulin-specific interaction was determined via site-directed mutagenesis (see section 5.4). Of the mutated amino acids, replacement of alanine at Ile280 and Val284 was minimally impacted and thus were not deemed as critical residues in the tubulin-rCx36 interaction. However, Lys279, Lys281, Leu282, Arg285, Gly286 were confirmed as residues of importance **(Figure 32-33)**. In particular, we are the first to report Lys279 as the most critical residue in the interaction between rCx36 and

tubulin. The rCx36 K279A mutation resulted in a significant reduction in observable puncta, gap junction plaque area well as an increase in mobile fraction and moderate impairments in the half-time of recovery **(Figure 31-33)**. Although it is unclear why the effects of rCx36 K279A mutation was more pronounced than that of rCx36 Δ279-292, one can only speculate that the size of the replacement amino acid at this position may be of functional significance. In such case, large amino acids may enhance the ability to access tubulin-rCx36 interaction. For our purpose, a polar serine residue replaced lysine at position 279 with the rCx36 Δ279-292 mutant variant. Earlier reports on Cx43 have identified a short region in the CT juxtamembrane (Glu227-Val231) as critical for facilitating tubulin interaction. In contrast to Lys279, these residues (ELFYV) are mainly non-polar. As such, our reports supporting Lys279 as critical for tubulin interaction is unique to rCx36.

6.4.3 Additional Cytoskeletal Interactions at the rCx36 Nexus

Throughout this thesis, several lines of evidence let us conclude that rCx36 is modulated at the nexus by proteins that may work in conjunction with cytoskeletal proteins. The biotin pull-down achieved with rCx36 Δ175-196 revealed a reduction in biotinylated tubulin **(Figure 17)**. As such, we inferred that a non-direct interaction specific to tubulin exists between the CLB and CTB domains. Therefore it is undoubtedly possible that through a mediating candidate and/or post-translational modification providing structurally favorable conditions, interaction between tubulin and rCx36 can be facilitated. In support of this, it was found that β-tubulin is capable of binding to the CL domain of Cx43. However, the affinity of this interaction was reduced by 80% (Kang et al., 2009). Therefore it is plausible that a third interaction candidate is involved. An already known interaction partner known to be involved in dual domain interaction of Cx36 is CaMKII (Alev et al., 2008). Although it is not yet conclusive, we speculate that CaMKII might be involved in the mediation of tubulin and actin interaction at the Cx36 nexus to influence synaptic strength. It is worth mentioning that in support of this, half-time of recovery was impaired when cells were treated with TAT-CT ON, which also reduces CaMKII interaction at rCx36. Therefore, it is likely that an interplay between rCx36 and CaMKII, along with additional protein candidates at the nexus, may be intricately related. In turn, we suspect that the delay in tubulin-specific trafficking may be in partner with CaMKII.

The expression of rCx36 Δ182-198 revealed an increase in the mobile fraction, yet reduction in connexons participating at the gap junction plaque **(Figure 24, Table 11)**. Therefore, this implied that transport and/or stabilization (through aggregation ability) of connexons could still be modulated outside of direct tubulin- and actin-dependency. This would be of significance in neurons where tubulin is restricted by the dendritic spine. Interestingly, rCx36 Δ182-198, 279-292 behaved similarly to rCx36 Δ279-292 with respect to fluorescence, half-time of recovery and gap junction plaque size **(Table 11, Figure 19F, and 24B)**. However, no significant difference in the mobile fraction was found between the wild-type and rCx36 Δ182-198, 279-292 **(Figure 24)**. Although it is unclear why these gap junction plaques appeared to be as stable as the wild-type, alteration of protein structure and/or net charge may be of influence.

It should not go unsaid, however, that half-time of recovery was seldom affected throughout this thesis, particularly in comparison to the plasma membrane ROIs. Therefore, we propose that rCx36 can be transported to the plasma membrane in tubulin- and/or actin-dependent manners. However, upon reaching the plasma membrane, lateral movement towards the gap junction plaque may occur independently of actin and tubulin interactions. Our findings thus coincides with reports of Lauf et al. (2002) stating that Cx43 is able to move freely in the plasma membrane (Lauf et al., 2002a). Connexons near to- or already docked at the GJP may participate in cytoskeletal interactions where we suggest that actin facilitates anchoring and tubulin subsequently facilitates aggregation in the N2a cell model. Our findings are the first to describe the influence of cytoskeletal interactions on Cx36. Since the potential of gap junction plaques serving as tubulin anchors still exists, tubulin may potentially regulate the degree of third party interactions. In such case, this would be achieved by regulating the degree of clustering (i.e. amount of channels participating at the gap junction plaque); however, this may be dependent on the cell model. Since it was previously shown that inhibition of tubulin was sufficient to abolish the run-up phenomenon (unpublished), in which gap junctional conductance increases 10-fold, this stands as a strong possibility.

6.5 ASSESSMENT OF CYTOSKELETAL INVOLVEMENT IN THE RUN-UP

6.5.1 Double Transfected Cells Behave Similar to Single Transfected Cells

The LTP-like "run-up" phenomenon has been exclusively described at the Cx36 nexus and was found to be CaMKII dependent (Alev et al., 2008; Del Corsso et al., 2012). This phenomenon resembles the phosphorylation of NMDARs by CaMKII to further evoke an influx of Ca^{2+}, a critical mediating step in LTP-based plasticity at chemical synapses. In our efforts to design a model to maximally simulate conditions similar to run-up, we double transfected N2a cells with wild-type rCx36 and calmodulin (CaM). CaM, a precursor to CaMKII activation, is a key component in the run-up phenomenon and acts in a calcium-dependent manner. Prior to our analysis of cytoskeletal involvement in the run-up phenomenon, we confirmed that double transfected cells were indistinguishable from single transfected cells in the recovery, mobility and size of rCx36 gap junction plaques **(Figure 34)**. To our knowledge, such comparison has not been addressed in previous literature reports, yet is crucial to ensure validity and reliability of results.

6.5.2 Studying Cytoskeletal Involvement in the Run-Up Phenomenon

As previously mentioned, this research project was based on results confirming rCx36-tubulin interaction *in vitro* and determining that tubulin interference was sufficient to abolish the run-up phenomenon. As such, we predicted that tubulin might be a critical mediator in the run-up phenomenon, primarily by recruiting more channels to the gap junction plaque. Unexpectedly, double transfected cells stimulated with ionomycin had a significantly reduced mobile fraction at the ‘plaque lateral’ ends in comparison to the untreated counterpart, yet half-time of recovery and gap junction area were unaffected. Furthermore, CTF_{GJP} was indistinguishable between the stimulated and unstimulated conditions **(Figure 35)**. Overall, this suggested that upon the indirect activation of CaMKII via calcium stimulation of CaM, the gap junction plaque stabilizes and further recruitment to the existing GJP ceases.

Our initial hypothesis proposed that cytoskeletal-dependent trafficking of rCx36 to the GJP may be a requirement of the run-up phenomenon and would be reflected by an increase in hemichannel

activity during calcium stimulation. Although our results rejected this hypothesis, we have gained new insight into the dynamics of rCx36 under stimulated conditions. This in turn will help us to understand, in full, the involvement of cytoskeletal proteins in mediating run-up. In part, our understanding of such interaction would need to be in conjunction with understanding the relationship between CaMKII and the cytoskeleton. Firstly, activated CaMKII is known to bind and bundle F-actin (Okamoto, Narayanan, Lee, Murata, & Hayashi, 2007). Alternatively, CaMKII also phosphorylates actin, through a β-PIX mediated pathway, thus increasing polymerization (Meng et al., 2002; Park et al., 2003; Xie et al., 2007) which may serve as an inhibitory barrier to vesicular fusion at existing gap junction plaques. However, this too would require further investigation. In contrast, effects of CaMKII phosphorylation on tubulin is dependent on its state; in the case of unpolymerized tubulin, it has been shown that phosphorylation inhibits subsequent polymerization (Wandosell, Serrano, Hernandez, & Avila, 1986) whereas phosphorylation of polymerized tubulin promotes MT polymerization through association with MAPs, particularly MAP2. Specifically, CaMKII mediated phosphorylation of the βIII-tubuin Ser444 residue is crucial for MAP2 mediated polymerization (Khan & Ludueña, 1996). Interestingly, Bricki-Nigassa et al. (2012) showed that Cx43-tubulin interaction can be inhibited by phosphorylation of a residue down-stream of the tubulin binding domain (Saidi Brikci-Nigassa et al., 2012). Although this interaction however was not CaMKII-mediated, it reflects the significance in the mediation of connexin-tubulin interaction via phosphorylation. As such, defining and refining the exact mechanism for cytoskeletal contribution to the run-up will be a new and upcoming challenge ahead.

6.6 CONCLUSION AND OUTLOOK

In conclusion, we have successfully confirmed the interaction between rCx36 and tubulin *in vivo* through both BioID and FRAP methodologies in combination with mutant variant expression and pharmacological blockers. We propose that rCx36 interacts primarily with the βIII-tubulin isotype to regulate the trafficking of connexons to the plasma membrane and connexon aggregation at the gap junction plaque. Furthermore, we report that Lys279 is most critical in the tubulin-specific interaction with rCx36. Our studies have also lead to the identification of a potential actin binding site within the CLB domain of rCx36, which appears to be unique to this isoform. Partial deletion of this site in combination with pharmacological blocking suggest that actin is an interacting

partner of rCx36, and mediates stabilization of the gap junction plaque with minor roles in trafficking. However, whether rCx36-actin interaction is direct or indirect has yet to be shown. We propose that trafficking of rCx36 connexons requires a tubulin/actin-dependent stage prior to delivery at the plasma membrane. At the plasma membrane, the lateral movements of rCx36 occur independently of actin or tubulin. Subsequent docking at the gap junction plaque requires both actin and tubulin interaction for anchoring and aggregation respectively. Although the exact contribution of the cytoskeleton to the run-up is still inconclusive, we reject the proposal of enhanced trafficking to existing gap junction plaques.

To further characterize cytoskeletal involvement at the Cx36 nexus, additional studies directed at actin involvement would be required. Confirmation of actin interaction would strongly be supported with complementary *in vitro* studies, such as GST-pull down or co-immunoprecipitation, in addition to *in vivo* studies such as FRET or bi-molecular fluorescence complementation assays. We are currently in the stages of pursuing these. In such ways, whether actin interaction is direct or indirect can be deciphered. Additionally, critical binding residues involved in actin interaction needs to be identified; this process has already been initiated using site-directed mutagenesis as outlined in this thesis.

On a structural level, exact binding mechanics of cytoskeletal interactions with Cx36 are, as of yet, undefined but may aid in our understanding of association ability. In efforts to define such mechanics, we have generated potential models of the rCx36 protein **(*See Appendix F*)**. Previously, Bricki-Nigassa et al. (2012) found that upon the binding of tubulin, the tubulin binding region and subset of down-stream residues take on a helical structure (Saidi Brikci-Nigassa et al., 2012). It is interesting to note that in these proposed models, the tubulin binding domain takes a helical structure, which coincides with the reports of Bricki-Nigassa et al. (2012). Using the generated models of Cx43-tubulin interaction as a comparative reference will be of great advantage in the future to determine Cx36-specific interactions with tubulin, and additional target proteins once the Cx36 structure is solved.

There seems to be an intricate relationship between Cx36, CaMKII and the cytoskeleton which likely influences properties of the run-up phenomenon. Our future focus aims at defining this relationship. Since binding of the βIII-tubulin isotype was identified as being unique to rCx36, exploring whether the Ser444 phosphorylation site is critical for interaction is of interest. Since this residue is a target of CaMKII, such studies may solidify evidence supporting an interaction between rCx36, tubulin and CaMKII. As a start, whether Cx36 interaction with tubulin is a CaMKII-mediated process will be assessed with the use of the CaMKII blocker KN-93 in addition to site-directed mutagenesis of the Ser444 residue of βIII-tubulin.

Finally, we aim to continue identifying additional candidates of rCx36 as contributors of synaptic plasticity at the nexus. In doing so, we anticipate that results from this continuing research project will contribute to our understanding electrical synapse-specific plasticity as a mediator to learning, memory, vision and behavior in conjunction with chemical synapse-mediated pathways. Our hope is that from this understanding, new insight into neurological disorders affecting learning and memory can be gained.

7 REFERENCES

Abascal, F., & Zardoya, R. (2012). Evolutionary analyses of gap junction protein families. *Biochimica et Biophysica Acta (BBA) - Biomembranes*, *1828*(1), 4–14. http://doi.org/10.1016/j.bbamem.2012.02.007

Ahmad, S., Diez, J. A., George, C. H., & Evans, W. H. (1999). Synthesis and assembly of connexins in vitro into homomeric and heteromeric functional gap junction hemichannels. *The Biochemical Journal*, *339 (Pt 2*, 247–253. http://doi.org/10.1042/0264-6021:3390247

Alev, C., Urschel, S., Sonntag, S., Zoidl, G., Fort, A. G., Höher, T., … Dermietzel, R. (2008). The neuronal connexin36 interacts with and is phosphorylated by CaMKII in a way similar to CaMKII interaction with glutamate receptors. *Proceedings of the National Academy of Sciences of the United States of America*, *105*(52), 20964–9. http://doi.org/10.1073/pnas.0805408105

Allen, K., Fuchs, E. C., Jaschonek, H., Bannerman, D. M., & Monyer, H. (2011). Gap junctions between interneurons are required for normal spatial coding in the hippocampus and short-term spatial memory. *The Journal of Neuroscience : The Official Journal of the Society for Neuroscience*, *31*(17), 6542–52. http://doi.org/10.1523/JNEUROSCI.6512-10.2011

Anumonwo, J. M., Taffet, S. M., Gu, H., Chanson, M., Moreno, A. P., & Delmar, M. (2001). The carboxyl terminal domain regulates the unitary conductance and voltage dependence of connexin40 gap junction channels. *Circulation Research*, *88*(7), 666–673. http://doi.org/10.1161/hh0701.088833

Baranova, A., Ivanov, D., Petrash, N., Pestova, A., Skoblov, M., Kelmanson, I., … Panchin, Y. (2004). The mammalian pannexin family is homologous to the invertebrate innexin gap junction proteins. *Genomics*, *83*(4), 706–716. http://doi.org/10.1016/j.ygeno.2003.09.025

Bauer, R., Löer, B., Ostrowski, K., Martini, J., Weimbs, A., Lechner, H., & Hoch, M. (2005). Intercellular communication: The Drosophila innexin multiprotein family of gap junction proteins. *Chemistry and Biology*. http://doi.org/10.1016/j.chembiol.2005.02.013

Baux, G., Simonneau, M., Tauc, L., & Segundo, J. P. (1978). Uncoupling of electrotonic synapses by calcium. *Proceedings of the National Academy of Sciences of the United States of America*, *75*(9), 4577–4581. http://doi.org/10.1073/pnas.75.9.4577

Belousov, A. B., & Fontes, J. D. (2013). Neuronal gap junctions: making and breaking connections during development and injury. *Trends in Neurosciences*, *36*(4), 227–36. http://doi.org/10.1016/j.tins.2012.11.001

Bennett, M. (1977). Electrical transmission:a functional analysis and comparison with chemical transmission. In *Cellular Biology of Neurons, Handbook of Physiology, The Nervous System 1* (pp. 357–416).

Bennett, M. V. L., & Zukin, R. S. (2004). Electrical Coupling and Neuronal Synchronization in the Mammalian Brain. *Neuron*, *41*(4), 495–511. http://doi.org/10.1016/S0896-6273(04)00043-1

Beyer, E. C., Lipkind, G. M., Kyle, J. W., & Berthoud, V. M. (2012). Structural organization of intercellular channels II. Amino terminal domain of the connexins: Sequence, functional roles, and structure. *Biochimica et Biophysica Acta - Biomembranes*. http://doi.org/10.1016/j.bbamem.2011.10.011

Bhalla-Gehi, R., Penuela, S., Churko, J. ., Shao, Q., & Laird, D. W. (2010). Pannexin1 and pannexin3 delivery, cell surface dynamics, and cytoskeletal interactions. *J. Biol. Chem*, *285*, 9147–9160.

Bi, A. ., Wang, Y., Li, B. ., Wang, Q. ., Ma, L., Yu, H., … Chen, Z. . (2010). Region-specific involvement of actin rearrangement-related synaptic structure alterations in conditioned taste aversion memory. *Learn. Mem.*, *17*, 420–27.

Boassa, D., Ambrosi, C., Qiu, F., Dahl, G., Gaietta, G., & Sosinsky, G. (2007). Pannexin1 channels contain a glycosylation site that targets the hexamer to the plasma membrane. *Journal of Biological Chemistry*, *282*(43), 31733–31743. http://doi.org/10.1074/jbc.M702422200

Boassa, D., Qiu, F., Dahl, G., & Sosinsky, G. (2008). Trafficking dynamics of glycosylated pannexin 1 proteins. *Cell Communication & Adhesion*, *15*(1), 119–132. http://doi.org/10.1080/15419060802013885

Bruzzone, R., White, T. W., & Paul, D. L. (1996). Connections with connexins: the molecular basis of direct intercellular signaling. *European Journal of Biochemistry / FEBS*, *238*(1), 1–27. http://doi.org/10.1007/978-3-642-60659-5

Bukauskas, F. F., Jordan, K., Bukauskiene, A., Bennett, M. V, Lampe, P. D., Laird, D. W., & Verselis, V. K. (2000). Clustering of connexin 43-enhanced green fluorescent protein gap junction channels and functional coupling in living cells. *Proceedings of the National Academy of Sciences of the United States of America*, *97*(6), 2556–61. http://doi.org/10.1073/pnas.050588497

Butkevich, E., Hulsmann, S., Wenzel, D., Shirao, T., Duden, R., & Majoul, I. (2004). Drebrin is a novel connexin-43 binding partner that links gap junctions to the submembrane cytoskeleton. *Curr. Biol.*, *14*, 650–658.

Buzsaki, G., Horvath, Z., Urioste, R., Hetke, J., & Wise, K. (1992). High-frequency network oscillation in the hippocampus. *Science*, *256*, 1025–1027.

Cao, F., Eckert, R., Elfgang, C., Nitsche, J. M., Snyder, S. A., H-ulser, D. F., … Nicholson, B. J. (1998). A quantitative analysis of connexin-specific permeability differences of gap

junctions expressed in HeLa transfectants and Xenopus oocytes. *Journal of Cell Science*, *111 (Pt 1*, 31–43.

Cape, E. ., Manns, I. ., Alonso, A., Beaudet, A., & Jones, B. . (2000). Neurotensin-induced bursting of cholinergic basal forebrain tions induced in the rat CA3 region by carbachol in vitro. Eur. J. neurons promotes gamma and theta cortical activity together with Neurosci. 12, 4093–4106. waking and paradoxical sleep. *Journal of Neuroscience*, *20*, 8452–8461.

Carisey, A., Stroud, M., Tsang, R., & Ballestrem, C. (2011). Cell Migration: Developmental Methods and Protocols. *Methods in Molecular Biology*, *769*(2), 387–402. http://doi.org/10.1007/978-1-61779-207-6

Chereau, D., Kerff, F., Graceffa, P., Grabarek, Z., Langsetmo, K., & Dominguez, R. (2005). Actin-bound structures of Wiskott-Aldrich syndrome protein (WASP)-homology domain 2 and the implications for filament assembly. *Proceedings of the National Academy of Sciences of the United States of America*, *102*(46), 16644–16649. http://doi.org/10.1073/pnas.0507021102

Collingridge, G., Isaac, J., & Wang, Y. (2004). Receptor trafficking and synaptic plasticity. *Nature Reviews. Neuroscience*, *5*, 952–962.

Condorelli, D. F., Parenti, R., Spinella, F., Trovato Salinaro, A., Belluardo, N., Cardile, V., & Cicirata, F. (1998). Cloning of a new gap junction gene (Cx36) highly expressed in mammalian brain neurons. *Journal of Neuroscience*, *10*(3), 1202–1208.

Csicsvari, J., Hirase, H., Czurko, A., Mamiya, A., & Buzsaki, G. (1999). Fast network oscillations in the hippocampal CA1 region of Buhl, E.H. (2001). Differential expression of synaptic and nonsynapthe behaving rat. *Journal of Neuroscience*, *19*, RC20.

Deans, M. R., Gibson, J. R., Sellitto, C., Connors, B. W., & Paul, D. L. (2001). Synchronous Activity of Inhibitory Networks in Neocortex Requires Electrical Synapses Containing Connexin36. *Neuron*, *31*, 477–485.

Deans, M. R., Volgyi, B., Goodenough, D. A., Bloomfield, S. A., & Paul, D. L. (2002). Connexin36 Is Essential for Transmission of Rod-Mediated Visual Signals in the Mammalian Retina, *36*(4), 703–712.

Del Corsso, C., Iglesias, R., Zoidl, G., Dermietzel, R., & Spray, D. C. (2012). Calmodulin dependent protein kinase increases conductance at gap junctions formed by the neuronal gap junction protein connexin36. *Brain Research*, *1487*, 69–77. http://doi.org/10.1016/j.brainres.2012.06.058

Derkach, V., Oh, M., Guire, E., & Soderling, T. (2007). Regulatory mechanisms of AMPA receptors in synaptic plasticity. *Nature Reviews. Neuroscience*, *8*, 101–113.

Dermietzel, R., & Spray, D. C. (1993). Gap junctions in the brain: where, what type, how many and why? *Trends in Neurosciences*, *16*(5), 186–192. http://doi.org/10.1016/0166-2236(93)90151-B

Diez, J. A., Ahmad, S., & Evans, W. H. (1999). Assembly of heteromeric connexons in guinea-pig liver en route to the Golgi apparatus, plasma membrane and gap junctions. *European Journal of Biochemistry*, *262*(1), 142–148. http://doi.org/10.1046/j.1432-1327.1999.00343.x

Dillon, C., & Goda, Y. (2005). The actin cytoskeleton: integrating form and function at the synapse. *Annual Review of Neuroscience*, *28*, 25–55. http://doi.org/10.1146/annurev.neuro.28.061604.135757

Eastman, S. D., Chen, T. H.-P., Falk, M. M., Mendelson, T. C., & Iovine, M. K. (2006). Phylogenetic analysis of three complete gap junction gene families reveals lineage-specific duplications and highly supported gene classes. *Genomics*, *87*(2), 265–74. http://doi.org/10.1016/j.ygeno.2005.10.005

Essenfelder, G. M., Bruzzone, R., Lamartine, J., Charollais, A., Blanchet-Bardon, C., Barbe, M. T., … Waksman, G. (2004). Connexin30 mutations responsible for hidrotic ectodermal dysplasia cause abnormal hemichannel activity. *Human Molecular Genetics*, *13*(16), 1703–1714. http://doi.org/10.1093/hmg/ddh191

Falk, M. M., Buehler, L. K., Kumar, N. M., & Gilula, N. B. (1997). Cell-free synthesis and assembly of connexins into functional gap junction membrane channels. *EMBO Journal*, *16*(10), 2703–2716. http://doi.org/10.1093/emboj/16.10.2703

Feigenspan, A., Janssen-Bienhold, U., Hormuzdi, S., Monyer, H., Degen, J., Söhl, G., … Weiler, R. (2004). Expression of connexin36 in cone pedicles and OFF-cone bipolar cells of the mouse retina. *The Journal of Neuroscience : The Official Journal of the Society for Neuroscience*, *24*(13), 3325–34. http://doi.org/10.1523/JNEUROSCI.5598-03.2004

Ferreira, A., & Caceres, A. (1992). Expression of the class III beta-tubulin isotype in developing neurons in culture. *Journal of Neuroscience Research*, *32*(4), 516–529. http://doi.org/10.1002/jnr.490320407

Fischer, A., Sananbenesi, F., Schrick, C., Spiess, J., & Radulovic, J. (2004). Distinct roles of hippocampal de novo protein synthesis and actin rearrangement in extinction of contextual fear. *Journal of Neuroscience*, *24*, 1962–1966.

Fletcher, D. A., & Mullins, R. D. (2010). Cell mechanics and the cytoskeleton. *NIH*, *463*(7280), 485–492. http://doi.org/10.1038/nature08908.Cell

Flores, C. E., Nannapaneni, S., Davidson, K. G. V., Yasumura, T., Bennett, M. V. L., Rash, J. E., & Pereda, A. E. (2012). Trafficking of gap junction channels at a vertebrate electrical synapse in vivo. *Proceedings of the National Academy of Sciences*. http://doi.org/10.1073/pnas.1121557109

Frisch, C., De Souza-Silva, M. a, Söhl, G., Güldenagel, M., Willecke, K., Huston, J. P., & Dere, E. (2005). Stimulus complexity dependent memory impairment and changes in motor performance after deletion of the neuronal gap junction protein connexin36 in mice. *Behavioural Brain Research*, *157*(1), 177–85. http://doi.org/10.1016/j.bbr.2004.06.023

Fukunaga, K., Stoppini, L., Miyamoto, E., & Muller, D. (1993). Long-term potentiation is associated with an increased activity of Ca2+/calmodulin-dependent protein kinase. *Biol Chem*, *268*, 7863–7867.

Gatfield, J., Albrecht, I., Zanolari, B., Steinmetz, M. O., & Pieters, J. (2005). Association of the leukocyte plasma membrane with the actin cytoskeleton through coiled coil-mediated trimeric coronin 1 molecules. *Molecular Biology of the Cell*, *16*(6), 2786–2798. http://doi.org/10.1091/mbc.E05-01-0042

Giepmans, B. N., Verlaan, I., Hengeveld, T., Janssen, H., Calafat, J., Falk, M. M., & Moolenaar, W. H. (2001). Gap junction protein connexin-43 interacts directly with microtubules. *Current Biology : CB*, *11*(17), 1364–8. Retrieved from http://www.ncbi.nlm.nih.gov/pubmed/11553331

Giepmans, B. N., Verlaan, I., & Moolenaar, W. H. (2001). Connexin-43 interactions with ZO-1 and alpha- and beta-tubulin. *Cell Communication & Adhesion*, *8*, 219–223.

González, D., Gómez-Hernández, J. M., & Barrio, L. C. (2007). Molecular basis of voltage dependence of connexin channels: An integrative appraisal. *Progress in Biophysics and Molecular Biology*. http://doi.org/10.1016/j.pbiomolbio.2007.03.007

González-Nieto, D., Gómez-Hernández, J. M., Larrosa, B., Gutiérrez, C., Muñoz, M. D., Fasciani, I., … Barrio, L. C. (2008). Regulation of neuronal connexin-36 channels by pH. *Proceedings of the National Academy of Sciences of the United States of America*, *105*(44), 17169–17174. http://doi.org/10.1073/pnas.0804189105

Goodenough, D. a. (1974). Bulk isolation of mouse hepatocyte gap junctions. Characterization of the principal protein, connexin. *Journal of Cell Biology*, *61*(2), 557–563. http://doi.org/10.1083/jcb.61.2.557

Gu, J., Firestein, B. L., & Zheng, J. Q. (2008). Microtubules in dendritic spine development. *The Journal of Neuroscience*, *28*(46), 12120–4. http://doi.org/10.1523/JNEUROSCI.2509-08.2008

Güldenagel, M., Ammermüller, J., Feigenspan, a, Teubner, B., Degen, J., Söhl, G., … Weiler, R. (2001). Visual transmission deficits in mice with targeted disruption of the gap junction gene connexin36. *The Journal of Neuroscience : The Official Journal of the Society for Neuroscience*, *21*(16), 6036–44. Retrieved from http://www.ncbi.nlm.nih.gov/pubmed/11487627

Hamzei-sichani, F., Kamasawa, N., Janssen, W. G. M., Yasumura, T., Davidson, K. G. V, Hof, P. R., … Traub, R. D. (2007). Gap junctions on hippocampal mossy fiber axons demonstrated by thin-section electron microscopy and freeze – fracture replica immunogold labeling. *PNAS*, *104*(30), 12548–12553.

Hertzog, M., Van Heijenoort, C., Didry, D., Gaudier, M., Coutant, J., Gigant, B., … Carlier, M. F. (2004). The β-thymosin/WH2 domain: Structural basis for the switch from inhibition to promotion of actin assembly. *Cell*, *117*(5), 611–623. http://doi.org/10.1016/S0092-8674(04)00403-9

Hervé, J. C., Derangeon, M., Bahbouhi, B., Mesnil, M., & Sarrouilhe, D. (2007). The connexin turnover, an important modulating factor of the level of cell-to-cell junctional communication: Comparison with other integral membrane proteins. In *Journal of Membrane Biology* (Vol. 217, pp. 21–33). http://doi.org/10.1007/s00232-007-9054-8

Hervé, J.-C., Derangeon, M., Sarrouilhe, D., Giepmans, B. N. G., & Bourmeyster, N. (2012). Gap junctional channels are parts of multiprotein complexes. *Biochimica et Biophysica Acta*, *1818*(8), 1844–65. http://doi.org/10.1016/j.bbamem.2011.12.009

Holland, N. D. (2005). Chordates. *Current Biology : CB*, *15*(22), R911–R914. http://doi.org/10.1016/j.cub.2005.11.008

Hormuzdi, S. G., Filippov, M. a, Mitropoulou, G., Monyer, H., & Bruzzone, R. (2004). Electrical synapses: a dynamic signaling system that shapes the activity of neuronal networks. *Biochimica et Biophysica Acta*, *1662*(1-2), 113–37. http://doi.org/10.1016/j.bbamem.2003.10.023

Hormuzdi, S. G., Pais, I., Lebeau, F. E. N., Towers, S. K., Rozov, A., Buhl, E. H., … Monyer, H. (2001). Impaired Electrical Signaling Disrupts Gamma Frequency Oscillations in Connexin 36-Deficient Mice, *31*, 487–495.

Hotulainen, P., & Hoogenraad, C. C. (2010). Actin in dendritic spines: connecting dynamics to function. *Journal of Cellular Biology*, *189*, 619–629.

Hou, Y. ., Lu, B., Li, M., Liu, Y., Chen, J., Chi, Z. ., & Liu, J. . (2009). Involvement of actin rearrangements within the amygdala and the dorsal hippocampus in aversive memories of drug withdrawal in acute morphine-dependent rats. *Journal of Neuroscience*, *29*, 12244–12254.

Irobi, E., Aguda, A. H., Larsson, M., Guerin, C., Yin, H. L., Burtnick, L. D., … Robinson, R. C. (2004). Structural basis of actin sequestration by thymosin-beta4: implications for WH2 proteins. *The EMBO Journal*, *23*(18), 3599–3608. http://doi.org/10.1038/sj.emboj.7600372

Jabeen, S., & Thirumalai, V. (2013). Distribution of the gap junction protein connexin 35 in the central nervous system of developing zebrafish larvae. *Frontiers in Neural Circuits*, *7*(May), 91. http://doi.org/10.3389/fncir.2013.00091

Johnson, R. G., Meyer, R. a, Li, X.-R., Preus, D. M., Tan, L., Grunenwald, H., … Sheridan, J. D. (2002). Gap junctions assemble in the presence of cytoskeletal inhibitors, but enhanced assembly requires microtubules. *Experimental Cell Research*, *275*(1), 67–80. http://doi.org/10.1006/excr.2002.5480

Jones, S. J., Gray, C., Sakamaki, H., Arora, M., Boyde, A., Gourdie, R., & Green, C. (1993). The incidence and size of gap junctions between the bone cells in rat calvaria. *Anatomy and Embryology*, *187*(4), 343–352. http://doi.org/10.1007/BF00185892

Jongen, W. M. F., Fitzgerald, D. J., Asamoto, M., Piccoli, C., Slaga, T. J., Gros, D., … Yamasaki, H. (1991). Regulation of connexin 43-mediated gap junctional intercellular communication by CA2+ in mouse epidermal cells is controlled by E-cadherin. *Journal of Cell Biology*, *114*(3), 545–555.

Jongsma, H. J., & Wilders, R. (2000). Gap junctions in cardiovascular disease. *Circulation Research*, *86*(12), 1193–1197. http://doi.org/10.1161/01.RES.86.12.1193

Kamermans, M., Fahrenfort, I., Schultz, K., Janssen-Bienhold, U., Sjoerdsma, T., & Weiler, R. (2001). Hemichannel-mediated inhibition in the outer retina. *Science (New York, N.Y.)*, *292*(5519), 1178–1180. http://doi.org/10.1126/science.1060101

Kang, E. Y., Ponzio, M., Gupta, P. P., Liu, F., Butensky, A., & Gutstein, D. E. (2009). Identification of binding partners for the cytoplasmic loop of connexin43: a novel interaction with β-tubulin. *Cell Communication & Adhesion*, *15*(5-6), 397–406. http://doi.org/10.1080/15419060902783833

Khan, I. A., & Ludueña, R. F. (1996). Phosphorylation of beta III-tubulin. *Biochemistry*, *35*(12), 3704–3711. http://doi.org/10.1021/bi951247p

Klebe, R., & Ruddle, F. (1969). Neuroblastoma: Cell culture analysis of a differentiating stem cell system. *Journal of Cell Biology*, *43*, 69A.

Kumar, N. M., & Gilula, N. B. (1996). The gap junction communication channel. *Cell*, *84*, 381–388.

Kuriu, T., Inoue, A., Bito, H., Sobue, K., & Okabe, S. (2006). Differential control of postsynaptic density scaffolds via actin-dependent and -independent mechanisms. *The Journal of Neuroscience : The Official Journal of the Society for Neuroscience*, *26*(29), 7693–7706. http://doi.org/10.1523/JNEUROSCI.0522-06.2006

Laird, D. W. (2010). The gap junction proteome and its relationship to disease. *Trends in Cell Biology*, *20*(2), 92–101. http://doi.org/10.1016/j.tcb.2009.11.001

Larsen, W. J., Tung, H., Murray, S. A., & Swenson, C. A. (1979). Evidence for the participation of actin microfilaments and bristle coats in the internalization of gap junction membrane. *Journal of Cell Biology*, *83*(3), 576–587. http://doi.org/10.1083/jcb.83.3.576

Lauf, U., Giepmans, B. N. G., Lopez, P., Braconnot, S., Chen, S.-C., & Falk, M. M. (2002a). Dynamic trafficking and delivery of connexons to the plasma membrane and accretion to gap junctions in living cells. *Proceedings of the National Academy of Sciences of the United States of America*, *99*(16), 10446–51. http://doi.org/10.1073/pnas.162055899

Lauf, U., Giepmans, B. N. G., Lopez, P., Braconnot, S., Chen, S.-C., & Falk, M. M. (2002b). Dynamic trafficking and delivery of connexons to the plasma membrane and accretion to gap junctions in living cells. *Proceedings of the National Academy of Sciences of the United States of America*, *99*(16), 10446–10451. http://doi.org/10.1073/pnas.162055899

Li, X., Olson, C., Lu, S., Kamasawa, N., Yasumura, T., Rash, J. E., & Nagy, J. I. (2004). Neuronal connexin36 association with zonula occludens-1 protein (ZO-1) in mouse brain and interaction with the first PDZ domain of ZO-1. *European Journal of Neuroscience*, *19*(8), 2132–2146. http://doi.org/10.1111/j.0953-816X.2004.03283.x

Li, X., Olson, C., Lu, S., & Nagy, J. I. (2004). Association of connexin36 with zonula occludens-1 in HeLa cells, βtC-3 cells, pancreas, and adrenal gland. *Histochemistry and Cell Biology*, *122*(5), 485–498. http://doi.org/10.1007/s00418-004-0718-5

Long, M. a, Jutras, M. J., Connors, B. W., & Burwell, R. D. (2005). Electrical synapses coordinate activity in the suprachiasmatic nucleus. *Nature Neuroscience*, *8*(1), 61–6. http://doi.org/10.1038/nn1361

Ludueña, R. F., Zimmermann, H. P., & Little, M. (1988). Identification of the phosphorylated beta-tubulin isotype in differentiated neuroblastoma cells. *FEBS Letters*, *230*(1-2), 142–146. http://doi.org/10.1016/0014-5793(88)80658-6

Matsudaira, P. (1991). Modular organization of actin crosslinking proteins. *Trends Biochem Sci*, *16*(3), 87–92.

Meng, Y., Zhang, Y., Tregoubov, V., Janus, C., Cruz, L., Jackson, M., … Jia, Z. (2002). Abnormal spine morphology and enhanced LTP in LIMK-1 knockout mice. *Neuron*, *35*(1), 121–133. http://doi.org/10.1016/S0896-6273(02)00758-4

Meyer, R. A., Laird, D. W., Revel, J. P., & Johnson, R. G. (1992). Inhibition of gap junction and adherens junction assembly by connexin and A-CAM antibodies. *Journal of Cell Biology*, *119*(1), 179–189. http://doi.org/10.1083/jcb.119.1.179

Moreno, A. P., Chanson, M., Anumonwo, J., Scerri, I., Gu, H., Taffet, S. M., & Delmar, M. (2002). Role of the carboxyl terminal of connexin43 in transjunctional fast voltage gating. *Circulation Research*, *90*(4), 450–457. http://doi.org/10.1161/hh0402.105667

Mostowy, S., & Cossart, P. (2012). Septins: the fourth component of the cytoskeleton. *Nature Reviews. Molecular Cell Biology*, *13*, 183–194.

Musil, L. S., & Goodenough, D. A. (1993). Multisubunit assembly of an integral plasma membrane channel protein, gap junction connexin43, occurs after exit from the ER. *Cell*, *74*(6), 1065–1077. http://doi.org/10.1016/0092-8674(93)90728-9

Nelson, B. ., Witty, C. ., Williamson, E. ., & Daniel, J. . (2012). A role for hippocampal actin rearrangement in object placement memory in female rats. *Neurobiol. Learn. Mem.*, *98*, 284–290.

O'Brien, J., Al-Ubaidi, M. R., & Ripps, H. (1996). Connexin 35: Cloning of a cap junctional protein expressed preferentially in the skate retina. *Investigative Ophthalmology and Visual Science*, *37*(3).

Okamoto, K.-I., Narayanan, R., Lee, S. H., Murata, K., & Hayashi, Y. (2007). The role of CaMKII as an F-actin-bundling protein crucial for maintenance of dendritic spine structure. *Proceedings of the National Academy of Sciences of the United States of America*, *104*(15), 6418–6423. http://doi.org/10.1073/pnas.0701656104

Palacios-Prado, N., Hoge, G., Marandykina, A., Rimkute, L., Chapuis, S., Paulauskas, N., … Bukauskas, F. F. (2012). Intracellular Magnesium-Dependent Modulation of Gap Junction Channels Formed by Neuronal Connexin36. *Journal of Neuroscience*, *33*(11), 4741–4753. http://doi.org/10.1523/JNEUROSCI.2825-12

Panchina, Y., Kelmanson, I., Matz, M., Lukyanov, K., Usman, N., & Lukyanov, S. (2000). A ubiquitous family of putative gap junction molecules [2]. *Current Biology*. http://doi.org/10.1016/S0960-9822(00)00576-5

Park, E., Na, M., Choi, J., Kim, S., Lee, J. R., Yoon, J., … Kim, E. (2003). The Shank family of postsynaptic density proteins interacts with and promotes synaptic accumulation of the βPIX guanine nucleotide exchange factor for Rac1 and Cdc42. *Journal of Biological Chemistry*, *278*(21), 19220–19229. http://doi.org/10.1074/jbc.M301052200

Paul, D. L. (1995). New functions for gap junctions. *Current Opinion in Cell Biology*. http://doi.org/10.1016/0955-0674(95)80108-1

Paul, D. L., Ebihara, L., Takemoto, L. J., Swenson, K. I., & Goodenough, D. A. (1991). Connexin46, a novel lens gap junction protein, induces voltage-gated currents in nonjunctional plasma membrane of Xenopus oocytes. *Journal of Cell Biology*, *115*(4), 1077–1089. http://doi.org/10.1083/jcb.115.4.1077

Penuela, S., Bhalla, R., Gong, X.-Q., Cowan, K. N., Celetti, S. J., Cowan, B. J., … Laird, D. W. (2007). Pannexin 1 and pannexin 3 are glycoproteins that exhibit many distinct characteristics from the connexin family of gap junction proteins. *Journal of Cell Science*, *120*(Pt 21), 3772–3783. http://doi.org/10.1242/jcs.009514

Penuela, S., Bhalla, R., Nag, K., & Laird, D. W. (2009). Glycosylation regulates pannexin intermixing and cellular localization. *Molecular Biology of the Cell*, *20*(20), 4313–4323. http://doi.org/10.1091/mbc.E09-01-0067

Pereda, A. E. (2014). Electrical synapses and their functional interactions with chemical synapses. *Nature Reviews. Neuroscience*, *15*(4), 250–63. http://doi.org/10.1038/nrn3708

Pereda, A. E., Curti, S., Hoge, G., Cachope, R., Flores, C. E., & Rash, J. E. (2013). Gap junction-mediated electrical transmission: Regulatory mechanisms and plasticity. *Biochimica et Biophysica Acta - Biomembranes*. http://doi.org/10.1016/j.bbamem.2012.05.026

Phelan, P., Bacon, J. P., Davies, J. A., Stebbings, L. A., & Todman, M. G. (1998). Innexins: A family of invertebrate gap-junction proteins. *Trends in Genetics*. http://doi.org/10.1016/S0168-9525(98)01547-9

Phelan, P., Stebbings, L. a, Baines, R. a, Bacon, J. P., Davies, J. a, & Ford, C. (1998). Drosophila Shaking-B protein forms gap junctions in paired Xenopus oocytes. *Nature*, *391*(6663), 181–184. http://doi.org/10.1038/34426

Postma, F., Liu, C., Dietsche, C., Khan, M., Lee, H., & Paul, D. (2011). Electrical synapses formed by connexin36 regulate inhibition- and experience-dependent plasticity. http://doi.org/10.1073/pnas.1100166108/-/DCSupplemental.www.pnas.org/cgi/doi/10.1073/pnas.1100166108

Qu, C., Gardner, P., & Schrijver, I. (2009). The role of the cytoskeleton in the formation of gap junctions by Connexin 30. *Exp. Cell Res.*, *215*, 1683–1692.

Quinlan, M. E., Heuser, J. E., Kerkhoff, E., & Mullins, R. D. (2005). Drosophila Spire is an actin nucleation factor. *Nature*, *433*(7024), 382–388. http://doi.org/10.1038/nature03241

Rao, G., Barnes, C. A., & McNaughton, B. L. (1987). Occlusion of hippocampal electrical junctions by intracellular calcium injection. *Brain Research*, *408*(1-2), 267–270. http://doi.org/10.1016/0006-8993(87)90385-4

Revel, J. P., & Karnovsky, M. J. (1967). Hexagonal array of subunits in intercellular junctions of the mouse heart and liver. *Journal of Cell Biology*, *33*(3). http://doi.org/10.1083/jcb.33.3.C7

Robinson, B. H., Oei, J., Saunders, M., & Gravel, R. (1983). [3H]biotin-labeled proteins in cultured human skin fibroblasts from patients with pyruvate carboxylase deficiency. *The Journal of Biological Chemistry*, *258*(10), 6660–6664.

Roux, K. J., Kim, D. I., Raida, M., & Burke, B. (2012a). A promiscuous biotin ligase fusion protein identifies proximal and interacting proteins in mammalian cells. *Journal of Cell Biology*, *196*(6), 801–810. http://doi.org/10.1083/jcb.201112098

Roux, K. J., Kim, D. I., Raida, M., & Burke, B. (2012b). A promiscuous biotin ligase fusion protein identifies proximal and interacting proteins in mammalian cells. *The Journal of Cell Biology*, *196*(6), 801–10. http://doi.org/10.1083/jcb.201112098

Roy, A., Kucukural, A., & Zhang, Y. (2010). I-TASSER: a unified platform for automated protein structure and function prediction. *Nature Protocols*, *5*(4), 725–738. http://doi.org/10.1038/nprot.2010.5

Sahu, G., Sukumaran, S., & Bera, A. K. (2014). Pannexins form gap junctions with electrophysiological and pharmacological properties distinct from connexins. *Scientific Reports*, *4*, 4955. http://doi.org/10.1038/srep04955

Saidi Brikci-Nigassa, A., Clement, M. J., Ha-Duong, T., Adjadj, E., Ziani, L., Pastre, D., … Savarin, P. (2012). Phosphorylation controls the interaction of the connexin43 C-terminal domain with tubulin and microtubules. *Biochemistry*, *51*(21), 4331–4342. http://doi.org/10.1021/bi201806j

Saillour, Y., Broix, L., Bruel-Jungerman, E., Lebrun, N., Muraca, G., Rucci, J., … Chelly, J. (2014). Beta tubulin isoforms are not interchangeable for rescuing impaired radial migration due to Tubb3 knockdown. *Human Molecular Genetics*, *23*(6), 1516–1526. http://doi.org/10.1093/hmg/ddt538

Sanhueza, M., Fernandez-Villalobos, G., Stein, I., Kasumova, G., Zhang, P., Bayer, K., & Al., E. (2011). Role of the CaMKII/NMDA receptor complex in the maintenance of synaptic strength. *Journal of Neuroscience*, *31*(9170-8).

Sarma, J. Das, Wang, F., & Koval, M. (2002). Targeted gap junction protein constructs reveal connexin-specific differences in oligomerization. *Journal of Biological Chemistry*, *277*(23), 20911–20918. http://doi.org/10.1074/jbc.M111498200

Scemes, E., Spray, D. C., & Meda, P. (2009). Connexins, pannexins, innexins: Novel roles of "hemi-channels." *Pflugers Archiv European Journal of Physiology*. http://doi.org/10.1007/s00424-008-0591-5

Schutt, C. E., Myslik, J. C., Rozycki, M. D., Goonesekere, N. C., & Lindberg, U. (1993). The structure of crystalline profilin-beta-actin. *Nature*, *365*(6449), 810–816. http://doi.org/10.1038/365810a0

Shaw, R. M., Fay, A. J., Puthenveedu, M. a, von Zastrow, M., Jan, Y.-N., & Jan, L. Y. (2007). Microtubule plus-end-tracking proteins target gap junctions directly from the cell interior to adherens junctions. *Cell*, *128*(3), 547–60. http://doi.org/10.1016/j.cell.2006.12.037

Sheng, M., & Hoogenraad, C. C. (2007). The postsynaptic architecture of excitatory synapses: a more quantitative view. *Annu. Rev. Biochem.*, *76*, 823–847.

Sheng, M., Sabatini, B. ., & Sudhof, T. . (2012). The Synapse. *Cold Spring Harbor Laboratory*.

Shi, C., & Chang, J. M. (2007). Multiple carboxylase deficiency. *Journal of Clinical Dermatology*, *36*(11), 737–738. http://doi.org/10.1016/0020-711X(88)90202-9

Shimizu, K., & Stopfer, M. (2013). Gap junctions. *Current Biology*, *23*(23). http://doi.org/10.1016/j.cub.2013.10.067

Simon, A. M., & Goodenough, D. A. (1998). Diverse functions of vertebrate gap junctions. *Trends in Cell Biology*. http://doi.org/10.1016/S0962-8924(98)01372-5

Söhl, G., Degen, J., Teubner, B., & Willecke, K. (1998). The murine gap junction gene connexin36 is highly expressed in mouse retina and regulated during brain development. *FEBS Letters*, *428*(1-2), 27–31. http://doi.org/10.1016/S0014-5793(98)00479-7

Söhl, G., Maxeiner, S., & Willecke, K. (2005). Expression and functions of neuronal gap junctions. *Nature Reviews. Neuroscience*, *6*(3), 191–200. http://doi.org/10.1038/nrn1627

Söhl, G., Odermatt, B., Maxeiner, S., Degen, J., & Willecke, K. (2004). New insights into the expression and function of neural connexins with transgenic mouse mutants. In *Brain Research Reviews* (Vol. 47, pp. 245–259). http://doi.org/10.1016/j.brainresrev.2004.05.006

Söhl, G., & Willecke, K. (2003). An update on connexin genes and their nomenclature in mouse and man. *Cell Communication & Adhesion*, *10*(4-6), 173–180. http://doi.org/10.1080/15419060390262877

Sosinsky, G. E., Boassa, D., Dermietzel, R., Duffy, H. S., Laird, D. W., MacVicar, B., … Dahl, G. (2011). Pannexin channels are not gap junction hemichannels. *Channels (Austin, Tex.)*, *5*(3), 193–197. http://doi.org/10.4161/chan.5.3.15765

Srinivas, M., Rozental, R., Kojima, T., Dermietzel, R., Mehler, M., Condorelli, D. F., … Spray, D. C. (1999). Functional properties of channels formed by the neuronal gap junction protein connexin36. *The Journal of Neuroscience : The Official Journal of the Society for Neuroscience*, *19*(22), 9848–9855.

Theiss, C., & Meller, K. (2000). Taxol impairs anterograde axonal transport of microinjected horseradish peroxidase in dorsal root ganglia neurons in vitro. *Cell and Tissue Research*, *299*(2), 213–224. http://doi.org/10.1007/s004410050019

Thomas, T., Jordan, K., Simek, J., Shao, Q., Jedeszko, C., Walton, P., & Laird, D. W. (2005). Mechanisms of Cx43 and Cx26 transport to the plasma membrane and gap junction regeneration. *Journal of Cell Science*, *118*(Pt 19), 4451–4462. http://doi.org/10.1242/jcs.02569

Traynelis, S., Wollmuth, L., McBain, C., Menniti, F., Vance, K., Ogden, K., & Al., E. (2010). Glutamate receptor ion channels: structure, regulation, and function. *Pharmacol Rev*, *62*, 405–496.

Verselis, V. K., Ginter, C. S., & Bargiello, T. A. (1994). Opposite voltage gating polarities of two closely related connexins. *Nature*, *368*(6469), 348–351. http://doi.org/10.1038/368348a0

Wade, R. H. (2009). On and around microtubules: an overview. *Molecular Biotechnology*, *43*(2), 177–91. http://doi.org/10.1007/s12033-009-9193-5

Wandosell, F., Serrano, L., Hernandez, M. a., & Avila, J. (1986). Phosphorylation of tubulin by a calmodulin-dependent protein kinase. *Journal of Biological Chemistry*, *261*(22), 10332–10339.

Wang, Y., & Belousov, A. B. (2011). Deletion of neuronal gap junction protein connexin 36 impairs hippocampal LTP. *Neurosci Lett*, *502*(1), 30–32. http://doi.org/10.1016/j.neulet.2011.07.018.Deletion

Watanabe, H., Washioka, H., & Tonosaki, a. (1988). Gap junction and its cytoskeletal undercoats as involved in invagination-endocytosis. *The Tohoku Journal of Experimental Medicine*, *156*(2), 175–190. http://doi.org/10.1620/tjem.156.175

Weber, P. A., Chang, H.-C., Spaeth, K. E., Nitsche, J. M., & Nicholson, B. J. (2004). The permeability of gap junction channels to probes of different size is dependent on connexin composition and permeant-pore affinities. *Biophysical Journal*, *87*(2), 958–973. http://doi.org/10.1529/biophysj.103.036350

Wei, C. J., Francis, R., Xu, X., & Lo, C. W. (2005). Connexin43 associated with an N-cadherin-containing multiprotein complex is required for gap junction formation in NIH3T3 cells. *Journal of Biological Chemistry*, *280*(20), 19925–19936. http://doi.org/10.1074/jbc.M412921200

Weidmann, S. (1952). The electrical constants of Purkinje fibres. *The Journal of Physiology*, *118*(3), 348–360.

Xie, Z., Srivastava, D. P., Photowala, H., Kai, L., Cahill, M. E., Woolfrey, K. M., … Penzes, P. (2007). Kalirin-7 Controls Activity-Dependent Structural and Functional Plasticity of Dendritic Spines. *Neuron*, *56*(4), 640–656. http://doi.org/10.1016/j.neuron.2007.10.005

Yang, J., Yan, R., Roy, A., Xu, D., Poisson, J., & Zhang, Y. (2014). The I-TASSER Suite: protein structure and function prediction. *Nature Methods*, *12*(1), 7–8. http://doi.org/10.1038/nmeth.3213

Yarmola, E. G., Parikh, S., & Bubb, M. R. (2001). Formation and Implications of a Ternary Complex of Profilin, Thymosin ??4, and Actin. *Journal of Biological Chemistry*, *276*(49), 45555–45563. http://doi.org/10.1074/jbc.M105723200

Young, E. ., Aceti, M., Griggs, E. ., Fuchs, R. ., Zigmond, Z., Rumbaugh, G., & Miller, C. . (2014). Selective, retrieval-independent disruption of methamphetamine- associated memory by actin depolymerization. *Biol. Psychiatry*, *75*, 96–104.

Zhang, Y. (2008). I-TASSER server for protein 3D structure prediction. *BMC Bioinformatics*, *9*, 40. http://doi.org/10.1186/1471-2105-9-40

Zhou, Y., Takahashi, E., Li, W., Halt, A., Wiltgen, B., Ehniger, D., & Al., E. (2007). Interactions between the NR2B receptor and CaMKII modulate synaptic plasticity and spatial learning. *Journal of Neuroscience*, *27*, 13843–53.

Zlomuzica, a, Viggiano, D., Degen, J., Binder, S., Ruocco, L. a, Sadile, a G., … Dere, E. (2012). Behavioral alterations and changes in Ca/calmodulin kinase II levels in the striatum of connexin36 deficient mice. *Behavioural Brain Research*, *226*(1), 293–300. http://doi.org/10.1016/j.bbr.2011.08.028

Zoidl, G., Meier, C., Petrasch-Parwez, E., Zoidl, C., Habbes, H. W., Kremer, M., … Dermietzel, R. (2002). Evidence for a role of the N-terminal domain in subcellular localization of the neuronal connexin36 (Cx36). *Journal of Neuroscience Research*, *69*(4), 448–465. http://doi.org/10.1002/jnr.10284

8 APPENDIX

APPENDIX A: EUKARYOTIC EXPRESSION VECTORS

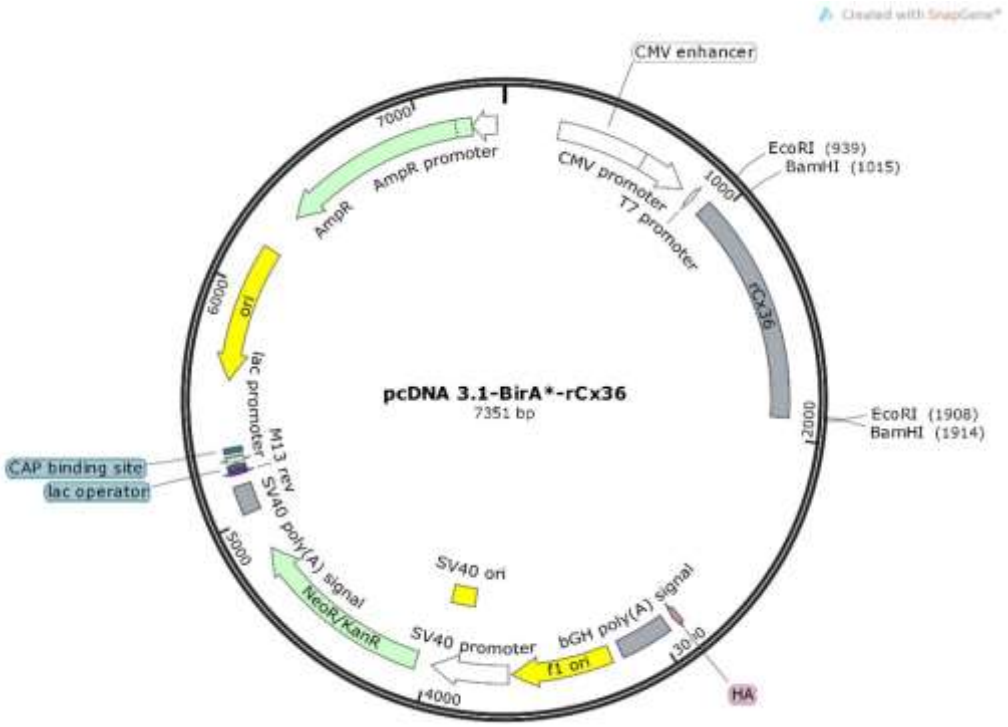

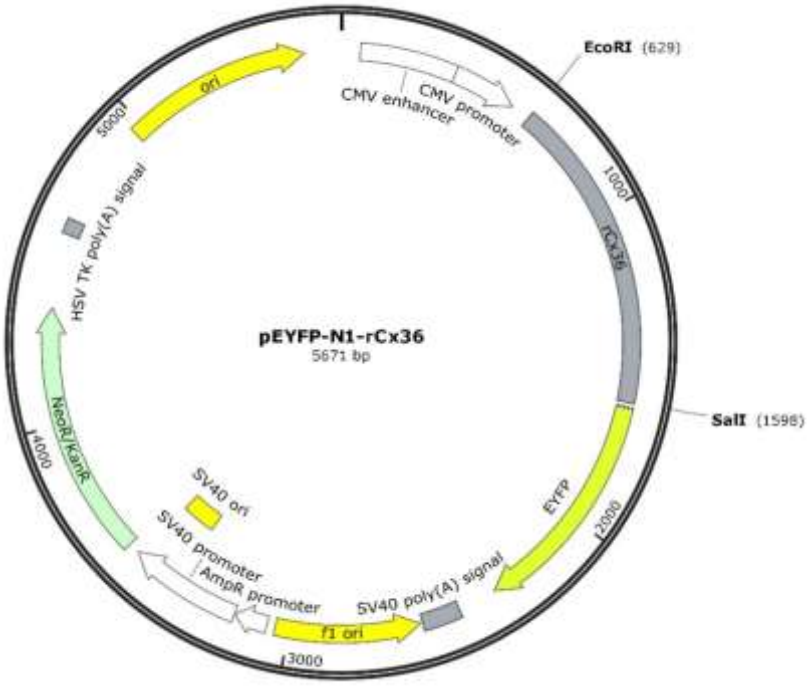

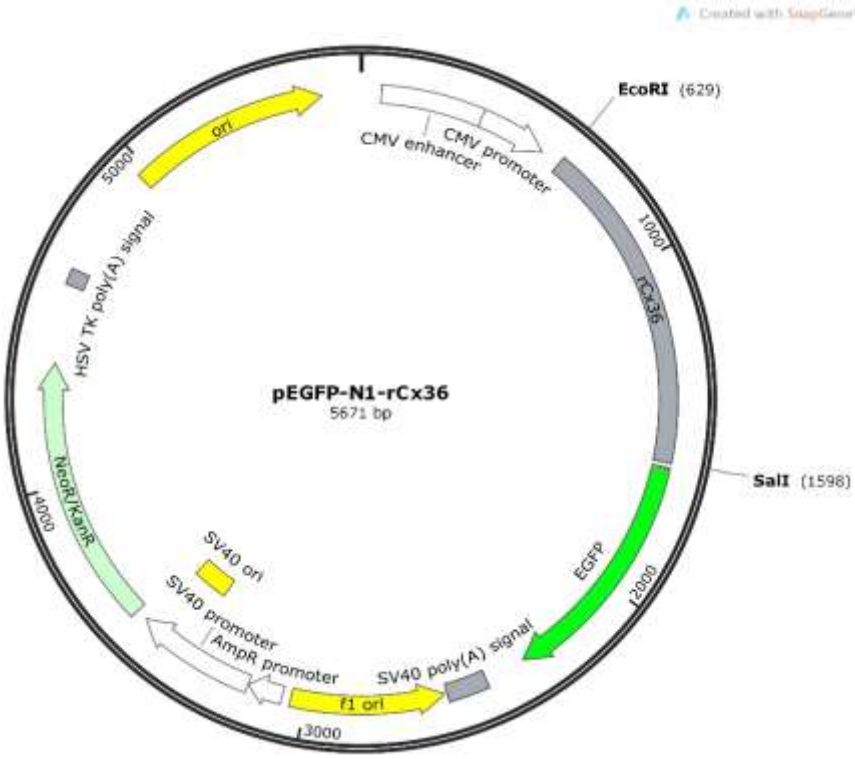
Created with SnapGene®
EcoRI (629)
ori
CMV enhancer
CMV promoter
5000
1000
rCx36
HSV TK poly(A) signal
pEGFP-N1-rCx36
5671 bp
SalI (1598)
NeoR/KanR
4000
SV40 ori
EGFP
SV40 promoter
AmpR promoter
SV40 poly(A) signal
2000
f1 ori
3000

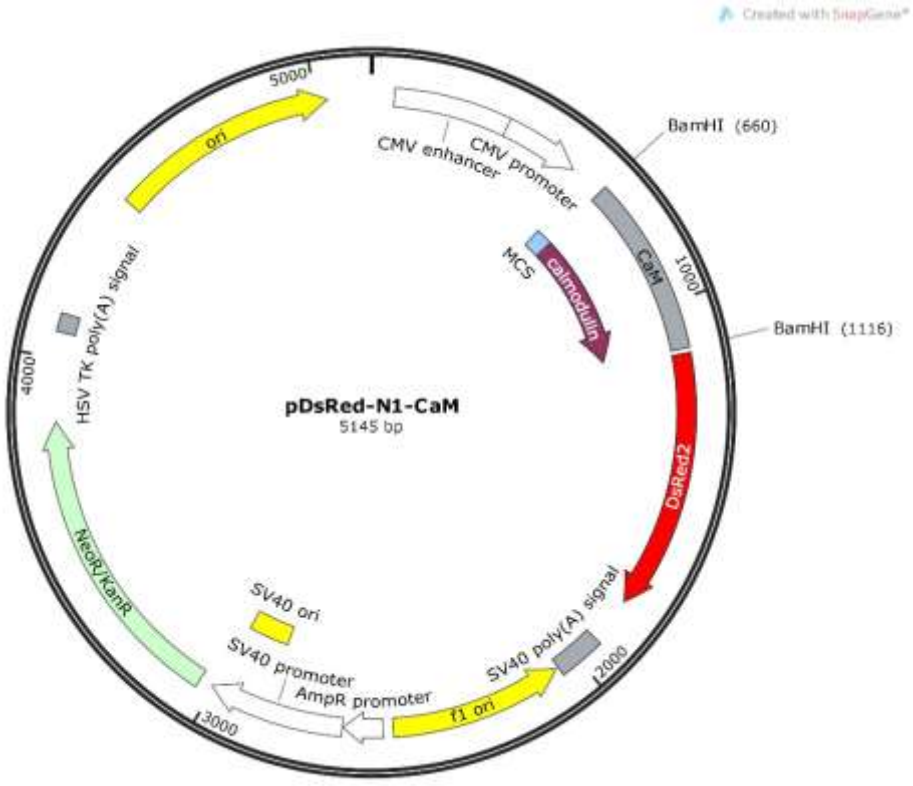
Created with SnapGene®
5000
ori
BamHI (660)
CMV enhancer
CMV promoter
MCS
calmodulin
CaM
1000
BamHI (1116)
HSV TK poly(A) signal
4000
pDsRed-N1-CaM
5145 bp
DsRed2
NeoR/KanR
SV40 ori
SV40 promoter
AmpR promoter
SV40 poly(A) signal
2000
f1 ori
3000

APPENDIX B: DRUGS

Colchicine

Product Description
Molecular Formula: $C_{22}H_{25}NO_6$
Molecular Weight: 399.4
Melting Point: 142-150ºC, 155-157ºC
Solubility: Water; Chloroform; Benzene

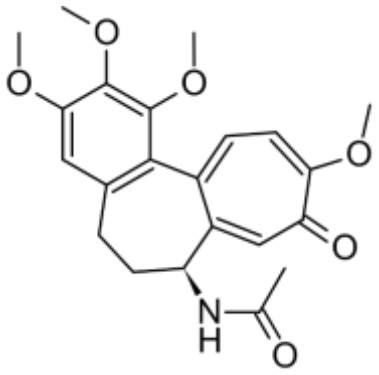

Cytochalasin D

Product Description
Molecular Formula: $C_{30}H_{37}NO_6$
Molecular Weight: 507.62
Melting Point: 268-271ºC
Solubility: Chloroform; DMSO

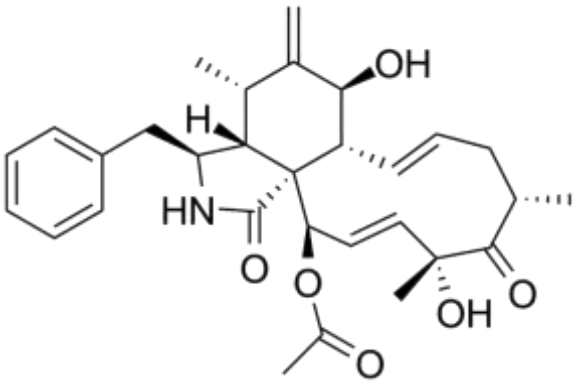

Paclitaxel

Product Description
Molecular Formula: $C_{47}H_{51}NO_{14}$
Molecular Weight: 853.91
Melting Point: 213ºC
Solubility: Methanol; DMSO; Ethanol; Acetonitrile

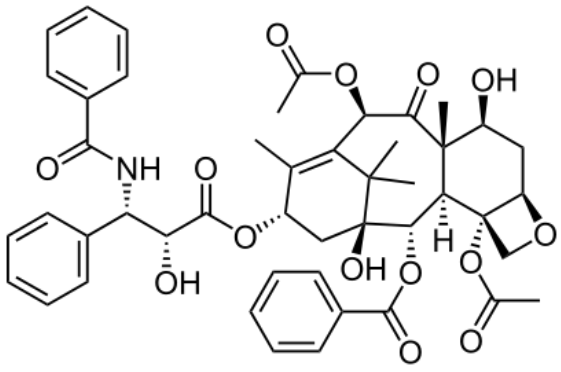

APPENDIX C: MEAN, SEM AND SAMPLE SIZE OF FRAP AND GJP STUDIES

Table A1.1: The mobile fraction (%) and half-time of recovery (s) at the selected ROIs of wild-type rCx36 expressing N2a cells (n=8) represented as the mean ± SEM.

	Mobile Fraction (%)	Half-Time of Recovery (s)
Intracellular	37.02±10.20	11.85±6.00
Membrane	33.77±7.50	20.33±9.69
Plaque Lateral	11.02±1.25	8.67±3.52
Plaque Center	10.46±1.32	1.68±0.58

Table A1.2: The p-values corresponding to the mobile fraction and half time of recovery analyses of wild-type rCx36 expressing N2a cells (n=8).

	Mobile Fraction	Significance	Half-Time of Recovery	Significance
Plaque Center to Membrane	0.008	**	0.075	ns
Plaque Center to Intracellular	0.022	*	0.114	ns
Membrane to Intracellular	0.801	ns	0.469	ns
Plaque Lateral to Membrane	0.000	***	0.178	ns
Plaque Lateral to Intracellular	0.002	**	0.631	ns
Plaque Lateral to Plaque Center	0.783	ns	0.181	ns

Table A2.1: The mobile fraction (%) and half-time of recovery (s) at the selected ROIs of wild-type and (deletion) mutant rCx36 expressing N2a cells represented as the mean ± SEM.

		Mobile Fraction (%)		Half-Time of Recovery (s)	
	n	Membrane	Plaque Lateral	Membrane	Plaque Lateral
WT	8	33.77±7.50	11.02±1.25	11.85±6.00	1.68±0.58
Δ182-198, 279-292	6	27.72±7.89	18.41±3.60	17.68±8.79	5.82±1.56
Δ182-198	5	27.33±16.37	35.47±4.98	11.11±5.77	13.97±5.21
Δ279-292	13	28.61±5.23	23.27±5.08	17.65±5.89	8.51±3.49
Δ175-196	11	34.48±6.71	25.68±3.26	4.66±2.53	20.02±3.33

Table A2.2: The p-values corresponding to the mobile fraction and half time of recovery analyses of (deletion) mutant rCx36 expressing N2a cells.

		Mobile Fraction	Significance	Half-Time of Recovery	Significance
Δ182-198, 279-292	Plaque Lateral to Membrane	0.231434	ns	0.083352	ns
	Membrane	0.593804	ns	0.848208	ns
	Plaque Lateral	0.039772	ns	0.514054	ns

	Plaque Lateral to Membrane	0.54965	ns	0.740678	ns
	Membrane	0.692689	ns	0.500021	ns
Δ182-198	Plaque Lateral	5.34E-06	****	0.390009	ns
	Plaque Lateral to Membrane	0.582355	ns	0.607338	ns
	Membrane	0.490012	ns	0.660993	ns
Δ279-292	Plaque Lateral	7.43E-05	****	0.417485	ns
	Plaque Lateral to Membrane	0.190702	ns	0.004911	**
	Membrane	0.94482	ns	0.089288	ns
Δ175-196	Plaque Lateral	0.000745	****	0.027354	ns

*Shaded areas represent the cross comparisons to the WT rCx36 ROIs (*refer to* ***Table A1.1***).

Table A2.3: Gap junction plaque area represented as the mean ± SEM, and corresponding p-values, of wild-type and (deletion) mutant rCx36 expressing N2a cells.

	GJP area (μm²)	n	p-value	Significance
WT	2.22±0.19	28		
Δ182-198, 279-292	2.33±0.37	24	0.020	ns
Δ182-198	1.38±0.23	19	0.000	***
Δ279-292	1.75±0.19	26	0.009	**
Δ175-196	1.25±0.21	24	0.000	****

*p-value is based on comparisons to WT rCx36.

Table A3.1: The mobile fraction (%) and half-time of recovery (s) at the selected ROIs of wild-type rCx36 expressing N2a cells treated with various TAT-peptides represented as the mean ± SEM.

		Mobile Fraction (%)		Half-Time of Recovery (s)	
	n	Membrane	Plaque Lateral	Membrane	Plaque Lateral
WT	8	33.77±7.50	11.02±1.25	11.85±6.00	1.68±0.58
WT + TAT CT-ON	11	37.53±5.25	32.81±3.31	4.92±1.23	8.67±4.63
WT + TAT CT-OFF	15	36.23±55.5	10.32±1.84	16.32±3.94	26.17±8.85
WT + TAT CT ON (Scrambled)	11	37.12±5.07	15.44±2.53	15.91±5.52	20.91±5.84
WT + TAT CT-OFF (Scrambled)	9	36.22±4.89	18.86±2.82	21.78±8.83	34.31±12.97

Table A3.2: The p-values corresponding to the mobile fraction and half time of recovery analyses of WT rCx36 expressing N2a cells treated with various TAT-peptides.

		Mobile Fraction	Significance	Half-Time of Recovery	Significance
TAT CT-ON	Plaque Lateral to Membrane	0.434544	ns	0.003212	**
	Membrane	0.676485	ns	0.080721	ns
	Plaque Lateral	4.4E-06	****	0.007818	**
TAT CT-OFF	Plaque Lateral to Membrane	0.001983	**	0.522863	ns
	Membrane	0.779183	ns	0.919091	ns
	Plaque Lateral	0.055176	ns	0.16222	ns
TAT CT-ON (Scrambled)	Plaque Lateral to Membrane	0.00016	***	0.5897	ns
	Membrane	0.705413	ns	0.677491	ns
	Plaque Lateral	0.170784	ns	0.111406	ns
TAT CT-OFF (Scrambled)	Plaque Lateral to Membrane	2.46E-05	****	0.24901	ns
	Membrane	0.79184	ns	0.648514	ns
	Plaque Lateral	0.76415	ns	0.047373	ns

*Shaded areas represent the cross comparisons to the WT rCx36 ROIs (*refer to* ***Table A3.1***).

Table A3.3: Gap junction plaque area represented as the mean ± SEM, and corresponding p-values, of wild-type rCx36 expressing N2a cells treated with various TAT-peptides.

	GJP area (μm²)	n	p-value	significance
TAT CT-ON	1.71±0.14	17	0.058637	ns
TAT CT-OFF	1.43±0.21	26	0.006483	**
TAT CT-ON (Scrambled)	1.50±0.18	13	0.022841	ns
TAT CT-OFF (Scrambled)	2.34±0.51	14	0.792181	ns

*p-value is based on comparisons to WT rCx36 (*refer to* ***Table A2.3***).

Table A4.1: The mobile fraction (%) and half-time of recovery (s) at the selected ROIs of wild-type (and Δ279-292 where specified) rCx36 expressing N2a cells treated with colchicine, paclitaxel, or cytochalasin D, represented as the mean ± SEM.

		Mobile Fraction (%)		Half-Time of Recovery (s)	
	n	Membrane	Plaque Lateral	Membrane	Plaque Lateral
WT	8	33.77±7.50	11.02±1.25	11.85±6.00	1.68±0.58
Δ279-292	13	28.61±5.23	23.27±5.08	17.65±5.89	8.51±3.49
WT + Colchicine	9	30.48±3.93	23.34±3.76	7.09±4.77	47.66±20.94
Δ279-292 + Colchicine	10	36.25±5.92	30.10±4.78	11.88±2.33	28.80±8.96
WT + Paclitaxel	13	21.54±4.06	11.46±1.50	14.58±5.75	11.86±5.02
Δ279-292 + Paclitaxel	15	40.54±5.99	17.39±1.74	12.12±3.14	25.58±7.45
WT + Cytochalasin D	12	34.26±7.05	22.50±1.73	10.83±4.67	12.87±3.78

Table A4.2: The p-values corresponding to the mobile fraction and half time of recovery analyses of WT (and Δ279-292 where specified) rCx36 expressing N2a cells treated with colchicine, paclitaxel or cytochalasin D.

		Mobile Fraction	Significance	Half-Time of Recovery	Significance
	Plaque Lateral to Membrane	0.247	ns	0.190	ns
	Membrane	0.694	ns	0.223	ns
WT + Colchicine	Plaque Lateral	0.006	**	0.093	ns
	Plaque Lateral to Membrane	0.447	ns	0.200	ns
Δ279-292 +	Membrane	0.282	ns	0.565	ns
Colchicine	Plaque Lateral	0.290	ns	0.068	ns
	Plaque Lateral to Membrane	0.007	**	0.742	ns
	Membrane	0.133	ns	0.591	ns
WT + Paclitaxel	Plaque Lateral	0.839	ns	0.650	ns

	Plaque Lateral to Membrane	0.000	****	0.221	ns
Δ279-292 + Paclitaxel	Membrane	0.119	ns	0.558	ns
	Plaque Lateral	0.012	ns	0.137	ns
	Plaque Lateral to Membrane	0.000	***	0.178	ns
WT + Cytochalasin D	Membrane	0.964	ns	0.340	ns
	Plaque Lateral	0.000	****	0.438	ns

*Shaded areas represent the cross comparisons to the ROIs of the untreated counterpart (*refer to **Table A4.1***).

Table A4.3: Gap junction plaque area represented as the mean ± SEM, and corresponding p-values, of wild-type (and Δ279-292 where specified) rCx36 expressing N2a cells treated with colchicine, paclitaxel or cytochalasin D.

	GJP area (μm²)	n	p-value	Significance
WT + Colchicine	1.37±0.21	15	0.006986669	**
Δ279-292 + Colchicine	1.32±0.18	13	0.335340799	ns
WT + Paclitaxel	1.44±0.20	17	0.009155905	**
Δ279-292 + Paclitaxel	1.22±0.08	19	0.081437	ns
WT + Cytochalasin D	2.13±0.41	14	0.806818105	ns

*p-values is based on comparisons to the untreated counterpart (*refer to **Table A2.3***).

Table A5.1: The mobile fraction (%) and half-time of recovery (s) at the selected ROIs of wild-type and (point) mutant rCx36 expressing N2a cells represented as the mean ± SEM.

		Mobile Fraction (%)		Half-Time of Recovery (s)	
	n	Membrane	Plaque Lateral	Membrane	Plaque Lateral
WT	8	33.77±7.50	11.02±1.25	11.85±6.00	1.68±0.58
K279A	5	37.38±4.84	25.08±0.30	17.05±12.67	33.73±3.35
I280A	10	32.85±8.07	22.88±4.92	4.46±2.53	28.47±8.66
K281A	8	27.93±7.45	16.27±4.03	7.15±2.09	14.09±2.17
L282A	9	33.02±6.85	13.73±2.48	4.80±2.10	19.64±5.77
V284A	11	30.63±7.08	17.16±3.12	10.94±5.55	18.12±9.82
R285A	7	23.69±5.42	14.92±2.73	3.78±1.81	25.57±4.71
G286A	9	23.99±4.98	21.44±3.29	3.73±1.72	14.30±2.84

Table A5.2: The p-values corresponding to the mobile fraction and half time of recovery analyses of point mutant rCx36 expressing N2a cells.

		Mobile Fraction	Significance	Half-Time of Recovery	Significance
	Plaque Lateral to Membrane	0.097	ns	0.423	ns
	Membrane	0.733	ns	0.839	ns
K279A	Plaque Lateral	0.001	***	0.030	ns
	Plaque Lateral to Membrane	0.276	ns	0.065	ns
	Membrane	0.936	ns	0.099	ns
I280A	Plaque Lateral	0.042	ns	0.061	ns
	Plaque Lateral to Membrane	0.146	ns	0.160	ns
	Membrane	0.589	ns	0.205	ns
K281A	Plaque Lateral	0.223	ns	0.262	ns
	Plaque Lateral to Membrane	0.003	**	0.088	ns
	Membrane	0.942	ns	0.118	ns
L282A	Plaque Lateral	0.352	ns	0.126	ns
	Plaque Lateral to Membrane	0.051	ns	0.504	ns
	Membrane	0.769	ns	0.383	ns
V284A	Plaque Lateral	0.117	ns	0.284	ns
	Plaque Lateral to Membrane	0.121	ns	0.005	**
	Membrane	0.308	ns	0.140	ns
R285A	Plaque Lateral	0.185	ns	0.007	**
	Plaque Lateral to Membrane	0.664	ns	0.019	ns
	Membrane	0.285	ns	0.094	ns
G286A	Plaque Lateral	0.008	**	0.219	ns

*Shaded areas represent the cross comparisons to the WT rCx36 ROIs (*refer to **Table A5.1***).

Table A5.3: Gap junction plaque area represented as the mean ± SEM, and corresponding p-values, of point mutant rCx36 expressing N2a cells.

	GJP area (μm^2)	n	p-value	Significance
K279A	0.90±0.18	7	0.001822	**
I280A	1.67±0.26	19	0.079548	ns
K281A	1.06±0.15	9	0.00176	**

L282A	1.26±0.11	16	0.000668	***
V284A	1.38±0.26	14	0.012561	ns
R285A	1.60±0.30	12	0.079888	ns
G286A	1.13±0.19	10	0.00255	**

*p-value is based on comparisons to WT rCx36 (*refer to* ***Table A2.3***).

Table A6.1: The mobile fraction (%) and half-time of recovery (s) at the selected ROIs of N2a cells expressing CaM and wild-type rCx36 with ionomycin application (where specified) represented as the mean ± SEM.

		Mobile Fraction (%)		Half-Time of Recovery (s)	
	n	Membrane	Plaque Lateral	Membrane	Plaque Lateral
WT	8	33.77±7.50	11.02±1.25	11.85±6.00	1.68±0.58
WT+CaM	9	24.86±4.54	22.58±4.19	7.35±2.41	12.10±2.67
WT+CaM+Iono	9	39.91±7.94	7.31±1.14	10.49±3.09	3.09±2.22

Table A6.2: The p-values corresponding to the mobile fraction and half time of recovery analyses of N2a cells expressing CaM and wild-type rCx36 with ionomycin application (where specified).

		Mobile Fraction	Significance	Half-Time of Recovery	Significance
Cx36 + CaM	Plaque Lateral to Membrane	0.739075	ns	0.264598	ns
	Membrane	0.313134	ns	0.189661	ns
	Plaque Lateral	0.017337	ns	0.436955	ns
Cx36 + CaM + Ionomycin	Plaque Lateral to Membrane	6.46E-06	****	0.736209	ns
	Membrane	0.119227	ns	0.43527	ns
	Plaque Lateral	0.001272	**	0.928627	ns

* Text in red denotes the cross comparisons to the rCx36 (wild-type) ROIs whereas the text in blue denotes cross comparisons to the rCx36 (wild-type) + CaM ROIs (*refer to* ***Table A6.1***).

Table A6.3: Gap junction plaque area represented as the mean ± SEM, and corresponding p-values, of point mutant rCx36 expressing N2a cells.

	GJP area (μm²)	n	p-value	Significance
WT+CaM	1.72±0.20	35	0.075103	ns
WT+CaM+Ionomycin	0.74±0.20	14	0.609691	ns

* Text in red denotes the cross comparisons to the rCx36 (wild-type) ROIs whereas the text in blue denotes cross comparisons to the rCx36 (wild-type) + CaM ROIs (*refer to* ***Table A2.3*** *for WT*).

APPENDIX D: PREDICTED PROTEIN CANDIDATES OF RCX36

The potential interaction candidates identified for rCx36 in N2a cells via mass-spectrometry of BioID elution fraction.

Partner Protein	ID
Membrane-associated progesterone receptor component 2	[PGRC2_MOUSE]
60S ribosomal protein L17	[RL17_MOUSE]
60S ribosomal protein L29	[RL29_MOUSE]
ATP synthase subunit alpha, mitochondrial	[ATPA_MOUSE]
Alpha-enolase	[ENOA_MOUSE]
cAMP-dependent protein kinase type I-alpha regulatory subunit	[KAP0_MOUSE]
Lamina-associated polypeptide 2, isoforms beta/delta/epsilon/gamma	[LAP2B_MOUSE]
Mitochondrial ribonuclease P protein 1	[MRRP1_MOUSE]
Tubulin beta-3 chain	**[TBB3_MOUSE]**
T-complex protein 1 subunit beta	[TCPB_MOUSE]
WW domain-containing oxidoreductase	[WWOX_MOUSE]
Neutral amino acid transporter B(0)	[AAAT_MOUSE]
Cytoskeleton-associated protein 4	[CKAP4_MOUSE]
Importin subunit alpha-1	[IMA1_MOUSE]
Sequestosome-1	[SQSTM_MOUSE]
T-complex protein 1 subunit alpha	[TCPA_MOUSE]
Netrin receptor UNC5B	[UNC5B_MOUSE]
Calnexin	[CALX_MOUSE]
Putative pre-mRNA-splicing factor ATP-dependent RNA helicase DHX15	[DHX15_MOUSE]
Elongation factor 2	[EF2_MOUSE]
Golgi resident protein GCP60	[GCP60_MOUSE]
Heterogeneous nuclear ribonucleoprotein M	[HNRPM_MOUSE]
Heat shock protein HSP 90-beta	[HS90B_MOUSE]
Ribosomal RNA processing protein 1 homolog B	[RRP1B_MOUSE]
AP-3 complex subunit delta-1	[AP3D1_MOUSE]
Sarcoplasmic/endoplasmic reticulum calcium ATPase 2	[AT2A2_MOUSE]
Lysine-rich nucleolar protein 1	[KNOP1_MOUSE]
ATP-dependent RNA helicase DDX24	[DDX24_MOUSE]
G-protein coupled receptor-associated sorting protein 1	[GASP1_MOUSE]
E3 SUMO-protein ligase RanBP2	[RBP2_MOUSE]
Ribosome-binding protein 1	[RRBP1_MOUSE]
RRP12-like protein	[RRP12_MOUSE]
Bifunctional glutamate/proline--tRNA ligase	[SYEP_MOUSE]
Small subunit processome component 20 homolog	[UTP20_MOUSE]

APPENDIX E: PREDICTED SHORT LINEAR MOTIFS OF THE RCX36 PROTEIN

A Eukaryotic Linear Motif (ELM) search was conducted on the full length rCx36 protein sequence to identify possible binding motifs within all cell compartments. Output generated indicated a possible actin binding domain within the cytoplasmic loop (aa: 167-184), denoted as the protein sequence "DCLEVKELAPHPSGLRTA."

APPENDIX F: PREDICTED RCX36 PROTEIN MODELS

Structural models of rCx36 were generated by I-TASSER and ordered from highest to the lowest C-score. The C-scores were as follows: (A) -2.20, (B) -2.24 (C) -2.79 (D) -2.95 (E) -3.21 (Roy, Kucukural, & Zhang, 2010; Yang et al., 2014; Zhang, 2008).